



KADIR HAS UNIVERSITY
SCHOOL OF GRADUATE STUDIES
PROGRAM OF COMPUTATIONAL BIOLOGY AND BIOINFORMATICS

**DESIGNING OF SELECTIVE AND POTENT INHIBITORS
AGAINST HISTONE DEACETYLASE ENZYMES (HDAC6
AND HDAC10) VIA IN SILICO SCREENING AND
MOLECULAR MODELING TECHNIQUES FOR THE
TREATMENT OF CANCER**

NAZ MINA MERT

MASTER'S THESIS

ISTANBUL, JULY, 2021



Naz Mina Mert

M.Sc.Thesis

2021



**Designing of Selective and Potent Inhibitors against Histone
Deacetylase Enzymes (HDAC6 and HDAC10) via *in silico*
Screening and Molecular Modeling Techniques for the
Treatment of Cancer**

NAZ MINA MERT

MASTER'S THESIS

Submitted to the School of Graduate Studies of Kadir Has University in partial
fulfillment of the requirements for the degree of Master's in the Program of
Computational Biology and Bioinformatics

ISTANBUL, JULY, 2021

DECLARATION OF RESEARCH ETHICS

I, NAZ MINA MERT, hereby declare that;

- this Master's Thesis is my own original work and that due references have been appropriately provided on all supporting literature and resources;
- this Master's Thesis contains no material that has been submitted or accepted for a degree or diploma in any other educational institution;
- I have followed "Kadir Has University Academic Ethics Principles" prepared in accordance with the "The Council of Higher Education's Ethical Conduct Principles"

In addition, I understand that any false claim in respect of this work will result in disciplinary action in accordance with University regulations.

Furthermore, both printed and electronic copies of my work will be kept in Kadir Has Information Center under the following condition as indicated below;

- the full content of my thesis will be accessible from everywhere by all means.

NAZ MINA MERT

27/07/2021

KADIR HAS UNIVERSITY
SCHOOL OF GRADUATE STUDIES

ACCEPTANCE AND APPROVAL

This work entitled **DESIGNING OF SELECTIVE AND POTENT INHIBITORS AGAINST HISTONE DEACETYLASE ENZYMES (HDAC6 AND HDAC10) VIA IN SILICO SCREENING AND MOLECULAR MODELING TECHNIQUES FOR THE TREATMENT OF CANCER** prepared by **NAZ MINA MERT** has been judged to be successful at the defense exam held on 27/07/2021 and accepted by our jury as **M.Sc.THESIS**.

APPROVED BY:

(Prof. Dr. Kemal Yelekçi) (Advisor) (Kadir Has University) _____

(Prof. Dr. Demet Akdoğan) (Kadir Has University) _____

(Prof. Dr. Safiye Erdem) (Marmara University) _____

I certify that the above signatures belong to the faculty members named above.

Prof. Dr. Mehmet Timur Aydemir
Director of the School of Graduate Studies
DATE OF APPROVAL: (27/07/2021)

TABLE OF CONTENTS

ABSTRACT	i
ÖZET	iii
ACKNOWLEDGEMENTS	v
LIST OF TABLES	viii
LIST OF FIGURES	ix
LIST OF ABBREVIATIONS	xiii
INTRODUCTION	1
Aim and Objectives	7
2. LITERATURE REVIEW	7
2.1 Classification of Histone Deacetylases	7
2.2 Role of HDACs in Cancer Pathogenesis	8
2.3 Role of HDACs in Other Diseases	8
2.4 Histone Deacetylases Class 2b Subfamily	9
2.4.1 Histone Deacetylase 6	10
2.4.2 Histone Deacetylase 10	15
2.5 HDACs Class2b Inhibitors for Cancer Therapy	16
2.6 Computer-Aided Drug Design	23
2.6.1 Virtual screening	24
2.6.2 Molecular docking	24
2.6.3 Drug-likeness and ADMET prediction	26
2.6.4 Molecular dynamics simulation	27
3. MATERIALS AND METHODS	30
3.1 Preparation of Class 2b Enzymes	30
3.1.1 Protein Structure Determination of Class 2b HDACs.....	31
3.1.2 Sequence Alignment and Structural Superimposition of Class 2b HDACs	32
3.2 Structure-Based Drug Design for Isoform-selective Inhibitors by Virtual Screening	34
3.2.1 Compound libraries for virtual screening	34
3.2.2 Ligand set-up protocol	35
3.2.3 Structure-based virtual screening	36

3.2.4 Drug-likeness and ADMET prediction	39
3.2.5 Molecular dynamics simulation	40
4. RESULTS	42
4.1 Sequence Alignment and Structural Analysis of Class 2b HDACs	42
4.2 Molecular Docking and Binding Affinity Analysis	43
4.3 Drug-Likeness and ADMET Prediction Analysis.....	58
4.4 Molecular Dynamics Simulation Analysis	61
5. DISCUSSION	777
6. CONCLUSIONS	799
REFERENCES.....	811
CURRICULUM VITAE	99

**DESIGNING OF SELECTIVE AND POTENT INHIBITORS AGAINST
HISTONE DEACETYLASE ENZYMES (HDAC6 AND HDAC10) VIA IN
SILICO SCREENING AND MOLECULAR MODELING TECHNIQUES FOR
THE TREATMENT OF CANCER**

ABSTRACT

HDACs are the class of enzymes that are involved in the process of cancer development by removing the acetyl groups from histone protein, inducing chromatin condensation and in this way regulating the expression of tumor suppressor genes. HDACs grouped into four classes based on their homology to their respective yeast orthologous. Class I, II and IV HDACs contain zinc as a cofactor in their active site, whereas class III HDACs are NAD⁺-dependent enzymes known as sirtuins. Class I, II and IV HDACs are shown to be promising anticancer targets in drug development. Especially, hydroxamic acid derivatives show significant potential for inhibiting histone deacetylases efficiently in many cancer types. But, the selectivity of these inhibitors for various HDAC isoenzymes and cancer types keeps its mystery in current researches. The overexpression of HDAC isoforms is not same in all cancer types; in which the Class I and Iib HDAC isoforms are seemed to be overexpressed in cutaneous and hematologic cancer cells on the contrary to normal organ and endothelial cells. Thence, the selective inhibition of the Class Iib HDACs became quite outstanding targets in cancer chemotherapies. Class Iib HDACs are studied *in silico* studies aiming to discover lead compounds that could have the potential to be a drug candidate. The X-ray crystal structure of Class Iib HDAC6 was retrieved from protein data bank (PDB) and prepared for further screening and docking processes by certain docking programs like AutoDock 4.2, AutoDockVina, and GOLD. Likewise, the crystal 3D structure of the Class Iib HDAC10 was obtained from our group's previous homology modeling studies because the X-ray crystal structure of HDAC10 has not resolved yet. By structure-based virtual screening, numerous small molecule databanks such as cancer-like compound database libraries and ZINC database, potential drug candidates against HDAC6 and HDAC10 is determined. The top inhibitors having good binding affinity

and selectivity were subjected to structure-based *in silico* absorption, distribution, metabolism, elimination and toxicity (ADMET) prediction that show their drug-likeness properties. Moreover, molecular dynamics (MD) simulations are applied to their docking complexes to observe the stability of the ligand's binding modes. Based on this, promising novel and selective inhibitor candidates will be purchased along with the enzymes and their experimental biological activities will be tested as an anticancer drug. The compounds showing the highest inhibition activity are aimed to be used in cancer cell lines for further researches in drug discovery and drug development.

Keywords: Class IIb HDACs, HDAC6, HDAC10, cancer, drug, *in silico* screening, docking, HDAC inhibitors.



KANSER TEDAVİSİ İÇİN SİLİKO TARAMA VE MOLEKÜLER MODELLEME
TEKNİKLERİ İLE HİSTON DEACETİLİZ ENZİMLERİNE (HDAC6 VE HDAC10)
KARŞI SEÇİCİ VE ETKİLİ İNHİBİTÖRLERİN TASARLANMASI

ÖZET

HDAC'lar, histon proteininden asetil gruplarını kopartarak, kromatin yoğunlaşmasını indükleyerek kanser gelişimi sürecinde tümör baskılayıcı genlerin ekspresyonunu düzenlemede rol alan enzim sınıfıdır. HDAC enzimleri, ilgili maya ortologlarına karşı gelen homolojilerine göre dört sınıfa ayrılmıştır. Sınıf I, II ve IV HDAC'ler aktif bölgelerinde kofaktör olarak çinko içerirken, sınıf III HDAC'lar sirtuinler olarak bilinen kofaktör olarak da NAD⁺ bulunduran enzimlerdir. Yapılan çalışmalardan Sınıf I, II ve IV HDAC'ların kanser karşıtı ilaç geliştirmede umut vadeci hedefler olduğu belirlenmiştir. Özellikle hidrokisamik asit türevleri, birçok kanser türünde histon deasetilazları etkili bir şekilde inhibe etmek için önemli bir potansiyel göstermektedir. Ancak bu inhibitörlerin çeşitli HDAC izoenzimleri ve kanser türleri için seçiciliği, güncel araştırmalarda gizemini korumaktadır. HDAC izoformlarının aşırı ekspresyonu tüm kanser türlerinde aynı değildir; Sınıf I ve IIb HDAC izoformlarının, normal organ ve endotel hücrelerinin aksine kutanöz ve hematolojik kanser hücrelerinde aşırı eksprese edildiği görülmektedir. Bu nedenle, Sınıf IIb HDAC'lerin seçici inhibisyonu, kanser kemoterapilerinde oldukça göze çarpan hedefler haline gelmiştir. Sınıf IIb HDAC'lar, ilaç adayı olma potansiyeline sahip olabilecek öncü bileşikler keşfetmeyi amaçlayan yapı temelli *in silico* çalışmalarda incelenmiştir. Sınıf IIb HDAC6'nın X-ışını kristal yapısı, protein veri bankasından (PDB) alınmıştır ve AutoDock 4.2, AutoDockVina ve GOLD gibi belirli doking programları tarafından daha ileri tarama ve doking işlemleri için hazırlanmıştır. Benzer şekilde, Sınıf IIb HDAC10'un kristal 3D yapısı, HDAC10'un X-ışını kristal yapısı henüz çözülmediği için grubumuzun önceki homoloji modelleme çalışmalarından elde edilmiştir. Kanser benzeri bileşik veri tabanı kütüphaneleri ve ZINC veri tabanı gibi çok sayıda küçük molekül veri bankası taranarak, HDAC6 ve HDAC10'a karşı potansiyel ilaç adayları belirlenmiştir. İyi bağlanma afinitesine ve seçiciliğe sahip olan en iyi inhibitörler, ilaç benzeri özelliklerini

gösteren yapı bazlı siliko absorpsiyon, dağılım, metabolizma, eliminasyon ve toksisite (ADMET) tahminine tabi tutulmuştur. Ayrıca, ligandın bağlanma modlarının stabilitesini gözlemlemek için moleküler dinamik (MD) simülasyonları doking komplekslerine uygulanmıştır. Buna dayanarak, enzimlerle birlikte ümit vadeden yeni ve seçici inhibitör adayları satın alınacak ve deneysel biyolojik aktivitelerine göre antikanser ilacı olarak test edilecektir. En yüksek inhibisyon aktivitesi gösteren bileşiklerin, ilaç keşfi ve ilaç geliştirmede daha ileri araştırmalar elde edebilmek adına kanser hücre hatlarında kullanılması amaçlanmaktadır.

Anahtar Sözcükler: Sınıf IIb HDAC'lar, HDAC6, HDAC10, kanser, ilaç, *in siliko* tarama, doking, HDAC inhibitörleri.



ACKNOWLEDGEMENTS

First of all, my sincere gratitude to my supervisor, **Professor Dr. Kemal Yelekçi** for introducing me to this field, giving me all the courage and support to pursue my project research, and providing a networking opportunity for me to thrive, such as with the **Health Institutes of Turkey (TUSEB)**. I would also like to acknowledge **TUSEB** for providing me academic support (January 2020-date, Project Number: 4084). Indeed, I would like to express my deepest appreciation to my dearest supervisor, Professor **Dr. Kemal Yelekçi**, for being not just my supervisor but also as a caring father, who always inspired me by his work, his passion for his work, and kindness. He offered me tremendous academic support towards the satisfactory and timely completion of this dissertation.

I am deeply grateful to my parents **Ahmet Hamdi Mert and Nejla Mert** for the unconditional support, and incredible love they have offered me throughout my life.

My sincere thanks to my sisters **Almira Malhun Mert and Ayşe Ala Mert** for being such supportive and encouraging for my dreams in my whole life.

Also, I am so grateful to my aunts, **Nuray Mert and Mine Mert** for their constructive advice, guidance, and unconditional love in my whole life.

I would also like to thank my friends, **Anas Al-Obaidi, Ammar Dawoud Elmezayen and Abdullahi Ibrahim Uba** for providing support and friendship throughout my academic life. I am so thankful to them for being patient and understanding.

My endless gratefulness to my special cat **Pamuk Prens** for being an adorable and cutest member of my family.

I would like to thank all **my teachers and colleagues** at the **Department of Bioinformatics and Genetics** of **Kadir Has University** for their help and support during my studies.

I dedicate this thesis to my precious deceased grandfathers **Necmettin Mert and Gngr Saęlam** whom I will always feel their support and incredible love for me throughout my whole life.





To my beloved family and my cat,

LIST OF TABLES

Table 2. 1 Localization, structural property, and functionality of Class IIb histone deacetylases in humans.	10
Table 2. 2 List of 10 known HDAC-selective and Pan-HDAC inhibitors.....	17
Table 2. 3 Structures of 10 known HDAC6 and Pan-HDAC inhibitors	18
Table 3. 1 Conserved amino acid residues of the catalytic active site of HDAC6 and HDAC10. (* indicates the “Gatekeeper” amino acid at the catalytic pocket of HDAC10).....	33
Table 3. 2 Cancer-like compound libraries used for virtual screening for HDAC6 and HDAC10.	34
Table 3. 4 Grid mapping parameters used for AutoDock Vina and QuickVina for HDAC6 and HDAC10.	37
Table 3. 5 Grid mapping parameters used for AutoDock 4.2 for HDAC6 and HDAC10.	38
Table 4. 1 Sequence similarity and identity analysis of class 2b HDACs in percentages.....	42
Table 4. 2 Sequence alignment and structural superimposition analysis of class 2b HDACs. RMSD values are shown above the diagonal in Orange, and the number of overlapping residues is shown below the diagonal in Purple.	42
Table 4. 3 Calculated binding energy of the hit compounds by AutoDock 4.2 against HDAC6 and HDAC10. HDAC6 - selective compounds are in pink color, HDAC10 – selective compounds are in blue.	44
Table 4. 4 Calculated binding energy (ΔG) and inhibition constant (K_i) of the 5-selected known HDAC6-selective and 5-selected known HDAC10-selective inhibitors compared with 7- potential selective lead compounds (highlighted in bold) identified through structure-based virtual screening (exceptional K_i values indicated as picoMolar (pM)).	45
Table 4. 5 Drug-likeness and ADMET properties of 36 hit compounds of cancer-like libraries using AdmetSAR and SwissADME.	58
Table 4. 6 Drug-likeness and ADMET properties of 18 hit compounds of ZINC library using AdmetSAR and SwissADME.....	60

LIST OF FIGURES

Figure 1. 1 Chromatin structure made up of nucleosomes showing the reversible dynamic nature of histone acetylation (HAT) and histone deacetylation (HDAC) modifications (Eslaminejad et al., 2013).....	3
Figure 1. 2 Proposed mechanism of acetyllysine hydrolysis forming lysine and acetate catalyzed by HDACs (A. Ganesan, 2019).	4
Figure 2. 1 Schematic representation and functional domains of human HDAC6. The only HDAC with two tandem catalytic domains, deacetylase domains (CD1 and CD2 including Zn ⁺² catalytic activity. Tubulin, Hsp90, and cortactin are HDAC6 substrates in the Zn ⁺² catalytic region. The nuclear export signal (NES) prevents the accumulation of the protein in the nucleus and the Ser-Glu-containing tetrapeptide (SE14) region ensures a stable anchorage of the enzyme in the cytoplasm. The nuclear localization signal (NLS) translocates HDAC6 into the nucleus. The linker (dynein motor binding, DMB) between both CATs can bind to dynein and the high-affinity ubiquitin-binding zinc finger domain (ZnF-UBP) (Pulya et al., 2020).....	11
Figure 2. 2 Deacetylase-dependent and -independent functions of HDAC6 showing substrates, interacting partners, and others. HDAC6 plays a role in the recruitment of partner proteins (Yingxiu Li et al., 2013).	13
Figure 2. 3 Domain composition of human HDAC10 consisting of deacetylase domain and leucine-rich domain (S. Y. Park & Kim, 2020).....	15
Figure 2. 4 The representation of the 3D structure of human HDAC6 CD2 with its selective-inhibitor Tubacin.....	21
Figure 2. 5 Representation of the 3D-modeled structure of human HDAC10 CD2 with its unique “Gatekeeper” residue highlighted at the entrance of the catalytic pocket.....	22
Figure 2. 6 Representative workflows for computer-aided drug design (Macalino et al., 2015).	23
Figure 2. 7 A typical force field (FF) model. Energy dependencies are related to (a) stretching or compressing a bonded pair of atoms (modeled by a simple spring) (b) Increasing or decreasing the bond angle (modeled by a simple spring) (c) dihedral angle rotations (modeled by a sinusoidal function) (d) Van der Waals interactions (modeled by Lennard-Jones potential) and (e) Electrostatic interactions (modeled by Coulomb’s	

law). (a-c) are caused by interactions between atoms that are chemically bonded to one another while (c-e) are caused by interactions between atoms that are not bonded (Aminpour et al., 2019).....28

Figure 3. 1 Ramachandran plots of HDAC6 and HDAC10.....31

Figure 3. 2 Sequence alignment of human HDAC6 CD2 and human HDAC10 CD2. Identity is represented with **dark blue**, similarity in **light blue**, and difference in white. The overall sequence identity is calculated as 52.1% and the sequence similarity as 69.1%.32

Figure 3. 3 Sequence alignment of hydrophobicity and charges of amino acid residues for human HDAC6 CD2 and human HDAC10 CD2. Hydrophobic residues are indicated as **yellow**, amphiphilic residues as **grey**, hydrophobic neutral residues as **green**, slightly basic residues as **light blue**, basic residues as **dark blue**, slightly acidic residues as **pink**, acidic residues as **red** and other residues as white..... 32

Figure 3. 4 Structural alignment and superimposition of class 2b HDACs' catalytic domain 2. HDAC6 CD2 is represented in claret red and HDAC10 CD2 is represented in dark green.....33

Figure 3. 1 Virtual screening workflow for the identification of potential lead compounds to design HDAC6-selective and HDAC10-selective inhibitors through cancer-like compound libraries.....38

Figure 3. 2 Virtual screening workflow for the identification of potential lead compounds to design HDAC6-selective and HDAC10-selective inhibitors through ZINC compound library.....39

Figure 4. 1 Binding modes of known HDAC6 inhibitors with human HDAC6 (5EDU); Tubacin (a), Tubastatin A (b), Nexturastat A (c), Belinostat (d).....47

Figure 4. 2 Binding modes of known HDAC10 inhibitors with human HDAC10 homology model; Rocilinostat (a), Quisinostat (b), Citarinostat (c), Abexinostat (d)....49

Figure 4. 1 3D (upper) and 2D (lower) representations of the interaction between **HDAC6 and Asinex_imm_3320**; the types of nonbonded interactions are indicated as respective colors in the 2D scheme.....51

Figure 4. 2 3D (upper) and 2D (lower) representations of the interaction between **HDAC6 and Nih4_13387**; the types of nonbonded interactions are indicated as respective colors in the 2D scheme.....52

Figure 4. 3 3D (upper) and 2D (lower) representations of the interaction between HDAC6 and Enzo_190 ; the types of nonbonded interactions are indicated as respective colors in the 2D scheme.....	53
Figure 4. 6 3D (upper) and 2D (lower) representations of the interaction between HDAC6 and ZINC000103531486 ; the types of nonbonded interactions are indicated as respective colors in the 2D scheme.....	54
Figure 4. 7 3D (upper) and 2D (lower) representations of the interaction between HDAC10 and Asinex_imm_2279 ; the types of nonbonded interactions are indicated as respective colors in the 2D scheme.....	55
Figure 4. 8 3D (upper) and 2D (lower) representations of the interaction between HDAC10 and Targeted_onc_758 ; the types of nonbonded interactions are indicated as respective colors in the 2D scheme.....	55
Figure 4.9 3D (upper) and 2D (lower) representations of the interaction between HDAC10 and ZINC000245284480 ; the types of nonbonded interactions are indicated as respective colors in the 2D scheme.....	57
Figure 4.10 Benchmarking of the binding modes of docked (a) and simulated (b) complexes of HDAC6 and Asinex_imm3320 through their 2D and 3D schemes with100 ns MD simulation.....	62
Figure 4.11 Benchmarking of the binding modes of docked (a) and simulated (b) complexes of HDAC6 and Nih4_13387 through their 2D and 3D schemes with100 ns MD simulation.....	63
Figure 4.12 Benchmarking of the binding modes of docked (a) and simulated (b) complexes of HDAC6 and Enzo_190 through their 2D and 3D schemes with100 ns MD simulation.....	64
Figure 4.13 Benchmarking of the binding modes of docked (a) and simulated (b) complexes of HDAC6 and ZINC000103531486 through their 2D and 3D schemes with100 ns MD simulation.....	65
Figure 4.14 Benchmarking of the binding modes of docked (a) and simulated (b) complexes of HDAC10 and Asinex_imm2279 through their 2D and 3D schemes with100 ns MD simulation.....	66

Figure 4.15 Benchmarking of the binding modes of docked (a) and simulated (b) complexes of HDAC10 and Targeted_onc758 through their 2D and 3D schemes with 100 ns MD simulation.....	67
Figure 4.16 Benchmarking of the binding modes of docked (a) and simulated (b) complexes of HDAC10 and ZINC000245284480 through their 2D and 3D schemes with 100 ns MD simulation.....	68
Figure 4. 17 100 ns-MD simulation of Root-mean-squared deviation (RMSD), Root-mean-squared fluctuation (RMSF) and Radius of Gyration (Rg) profiles of free form of HDAC6 and HDAC10 and their complexes. RMSD graphs of HDAC6_free and with their complexes (a). RMSD graphs of HDAC10_free and with their complexes(b). RMSF graphs of HDAC6_free and with their complexes (c). RMSF graphs of HDAC10_free and with their complexes (d). RG graphs of HDAC6_free and with their complexes (e). RG graphs of HDAC10_free and with their complexes (f).	72

LIST OF ABBREVIATIONS

AC: Acetyl Groups
ACETYL-COA: Acetyl-Coenzyme A
ADMET: Absorption, Distribution, Metabolism, Elimination and Toxicity
ADT: AutoDockTool
AMBER: Assisted Model Building with Energy Refinement
AML: Acute Myeloid Leukemia
AR: Androgen Receptor
BRCA-1: Breast Cancer 1 Dependent
Caco-2: Human Epithelial Colorectal Adenocarcinoma
CADD: Computer-Aided Drug Design
CD1: Catalytic Domain 1
CD2: Catalytic Domain 2
CHARMM: Chemistry at Harvard Macromolecular Mechanics
CGenFF: CHARMM general Force Field
CNS: Central Nervous System
CTCL: Cutaneous T-cell lymphoma
DDH: Asp-Asp-His residues
DMB: Dynein Motor Binding
DNA: DeoxyriboNucleic Acid
EA: Evolutionary algorithm
ER- α : Estrogen receptor-alpha
ES: Embryonic stem cells
FDA: US Food and Drug Administration
GA: Genetic Algorithm
GROMOS: GRONingen MOlecular Simulation
GSK-3 β : Glycogen synthase kinase 3 beta
H2A: Histone 2A
H2B: Histone 2B
H3: Histone 3
H4: Histone 4

HATs: Histone Acetyltransferases
Hda1: Yeast histone deacetylases 1
HBA: Hydrogen Bond Acceptor
HBD: Hydrogen Bond Donor
HDAC: Histone Deacetylases
HDACi: Histone deacetylase inhibitors
HDLP: Histone deacetylase like protein
HIF-1 α : Hypoxia-inducible factor 1 alpha
HIV: Human Immunodeficiency Virus
HL: Hodgkin's Lymphoma
HSF-1: Heat-Shock Factor 1
HSP90: Heat Shock Protein 90
KU70: DNA repair protein
LBDD: Ligand-based drug design
LNC-RNA: Long non-coding RNA
LRD: Leucine-rich domain
MC: Monte Carlo
MD: Molecular Dynamics
miRNA: microRNA
MyoD: Myogenic Determination Factor
MlogP: Moriguchi model of octanol-H₂O partition coefficient, log P
MM: Multiple Myeloma
NAD⁺: Nicotinamide Adenine Dinucleotide
NAMD: Nanoscale Molecular Dynamics
NES: Nuclear Export Signal
NLS: Nuclear Localization Signal
NME: New molecular entities
NMR: Nuclear Magnetic Resonance
PDAC: Polyamine deacetylase activity
PDB: Protein data bank
PD-1: Program death receptor 1
PD-L1: Program death receptor ligand 1

P²³(E,A)CE²⁶: The “PEACE” motif
P2D6: Cytochrome inhibition gene
PTCL: Peripheral T-cell Lymphoma
QSAR: Quantitative Structure–Activity Relationship
Rg: Radius of gyration
RMSD: Root-Mean-Squared Deviation
RMSF: Root-Mean-Squared Fluctuations
RNA: Ribonucleic Acid
Ruleof5 (RO5): Computational filter for oral absorption identical to the Lipinski’s “Rule of Five”
Rpd3: Yeast histone deacetylases 1
SAHA: Suberoylanilide Hydroxamic Acid
SBDD: Structure-based drug design
SBVS: Structure-based virtual screening
SE14: Serine-glutamate containing tetradecapeptide repeat
siRNA: Small interfering RNA
Sirt: Sirtuin proteins
SMA: Spinal muscular atrophy
Smad: Contraction of Sma and Mad (Mothers against decapentaplegic)
Stat: Signal transducer and activator of transcription
S+logP: Simulation Plus Model of octanol-H₂O partition coefficient, log P
TPSA: Topological Polar Surface Area
TSA: Trichostatin A
Tubacin: Tubulin Acetylation Inducer
ZBG: Zinc-binding group
ZnF-UBP: Zinc finger ubiquitin-binding protease.

as Prednisone, Methylprednisolone and Dexamethasone. In addition, other chemotherapy drugs consisting of Vorinostat and Romidepsin act slightly different manner that do not accord with other categories.

The other way for treating cancer pathogenesis is targeted therapy which is different than traditional chemotherapy methods. A specific substance that the cancer cells have which is a protein or a receptor is targeted specifically by the drug to prevent normal cells to be affected by the drug itself. In hormone therapy, drugs are applied to retard the growth of specific cancer types such as prostate or breast cancer by enabling the body from producing the hormone (Rau et al., 2005). Kruger et al. (2019) reviewed in their study that recent clinical and translational medicine focused on the importance and methods of cellular combinatorial immunotherapy drugs used to change a person's immune system by supporting a patient's immune system to recognize and attack the aberrant cancer cells. Although novel concepts from biological therapies are introduced for cancer treatment to reduce low tumor specificity and high toxicity, still there is a huge effort for individualized treatments to alleviate side effects (Schirmacher, 2019).

In the human body, epigenetic mechanisms are highly crucial to maintain regular growth, development, and gene expression. Any abnormal genetic alterations or mutations in the genes leading to misfunctions in the regulation of epigenetic mechanisms result in cancer formation (Chen et al., 2014). Post-translational modifications such as methylation, acetylation, phosphorylation, and ubiquitination occur through long N-terminal tails of core histones (Gallinari et al., 2007; Jaenisch & Bird, 2003). A nucleosome consists of 147 bp of DNA are wrapped around a histone octamer (H3, H4, H2A, and H2B) which is composed of two copies of each histone, and core histones are substantial for chromatin assembly and compaction. The structural condition of chromatin and its domains manages both gene expression and DNA replication. Epigenetic modifications have a turn-on/off-like mechanism for regulating gene expression and they are also responsible for chemical modifications of DNA and histones. However, these modifications do not end up with a change in DNA sequence (Mariño-Ramírez et al., 2005). The reversible process of histone acetylation

and histone deacetylation is carried out by the enzymes histone acetyltransferases (HATs) and histone deacetylases (HDACs), in order (Icardi et al., 2012).

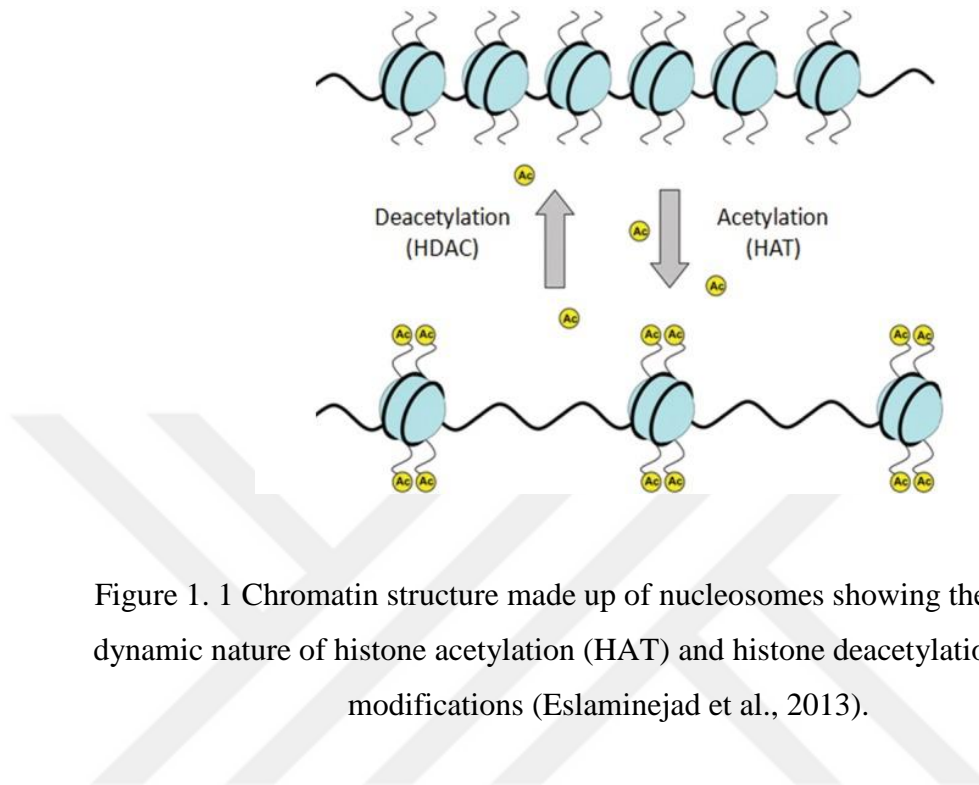


Figure 1. 1 Chromatin structure made up of nucleosomes showing the reversible dynamic nature of histone acetylation (HAT) and histone deacetylation (HDAC) modifications (Eslaminejad et al., 2013).

Histone deacetylases are essential for both regulating fundamental cellular activities like cell proliferation, survival, differentiation, and development by binding to transcription factors and for being a key target for today's cancer therapeutics (Kagohara et al., 2018; Kaplan, 2012; Li et al., 2020). Histone acetyltransferase (HATs) adds acetyl groups (Ac) from lysine residue onto histone tails which relaxes and opens the nucleosome structure allowing the transcription factors to reach DNA and start gene transcription. On the contrary, histone deacetylase (HDACs) remove Ac groups from the epsilon amino group of a lysine residue of histone tails causing chromatin structure to become compact and transcriptionally repressed status (Figure 1.1). Lysine acetylation needs “writers” and “erasers” in which writers are acetyltransferases that use acetyl-CoA as a co-substrate and erasers are deacetylases that catalyze the hydrolysis of acetyl-lysine to produce lysine and acetate (Quispe-Tintaya, 2017a)(Figure 1.2).

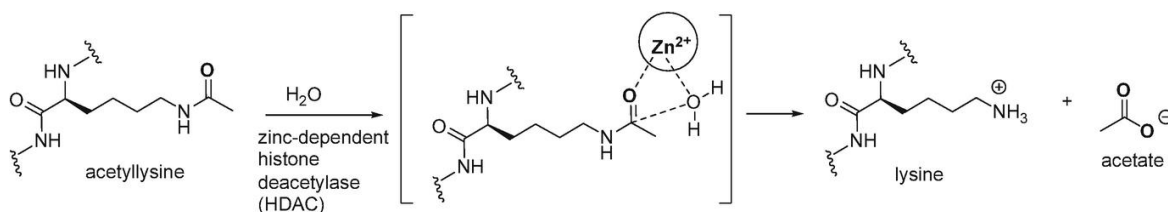


Figure 1. 2 Proposed mechanism of acetyllysine hydrolysis forming lysine and acetate catalyzed by HDACs (A. Ganesan, 2019).

So, histone acetylation changes the chromatin structure serving as docking sites for protein complexes that reshape nucleosomes (Smith & Workman, 2009). As DNA is negatively charged, histones bind to DNA through positively charged lysine in the amino-terminal tail of histones, thus neutralizing the environment. Modification in the lysine residue regulates the chemical interaction between the DNA and histones. Effectuation of “charge-relay system” takes place with the removal of an acetyl group from the substrate which includes two histidine residues, two aspartic acid residues, and one tyrosine residue in the pocket (Omotuyi & Olusanya, 2015; Porter & Christianson, 2019).

Moreover, a various number of nonhistone proteins are targets for HDACs and known as HDAC substrates such as heat shock proteins (HSP90), α -tubulin, β -catenin, transcription factors (p53, NF- κ B), MyoD, estrogen receptor (ER α), androgen receptor (AR), signaling mediators (Stat3, Smad7), DNA repair proteins (Ku70) and hypoxia-inducible factors (HIF-1 α) and some more. These nonhistone deacetylations by HDACs are crucial for further cellular processes elucidating the development and progression of cancer (Cheng et al., 2019; D. H. Kim et al., 2003; Peng & Seto, 2011; Quispe-Tintaya, 2017b).

HDACs are important targets for many diseases such as neurodegenerative diseases, human immunodeficiency virus (HIV), cardiac diseases, inflammatory diseases, cancer, and many others. Since there are some constraints for the present HDAC inhibitors like drug-tissue specific actions and some effects are unproficiently understood, a limited number of drugs are accepted for cancer treatment. Vorinostat (SAHA) (Grant et al.,

2007), Belinostat (Porwal et al., 2016), Romidepsin (Bertino & Otterson, 2011) and Panobinostat (Laubach et al., 2015) are the four drugs that have passed all the clinical phases and have been approved by The Food and Drug Administration for the treatment of cancer until today. Vorinostat (SAHA) is approved for the treatment of refractory and relapsed cutaneous T-Cell Lymphoma, Belinostat for the treatment of refractory peripheral T-Cell Lymphoma, Romidepsin also for peripheral T-Cell Lymphoma and Panobinostat for multiple myeloma.

HDAC inhibitors are divided into 4 major groups based on their individual chemical structures shown below;

- Hydroxamic acids: TSA (Trichostatin A) and Vorinostat (SAHA).
- Benzamides: Entinostat (MS-275), Tacedinaline (CI-994) and Chidamide (CS-055).
- Short Chain Fatty Acids: Butyric acid and Valproic acid.
- Cyclic Tetrapeptides: CHAP31 and Romidepsin (FK-228).

According to their specificity for HDACs, Romidepsin is a natural cyclic peptide product that inhibits HDAC1 and 2 selectively. SAHA, Trichostatin A (TSA), Belinostat, Panobinostat, and Resminostat are hydroxamic acid-based pan-HDAC inhibitors, but Romidepsin and Entinostat are selective for HDAC1,2 and 3. Tubacin specifically inhibits HDAC6. Valproic acid and butyric acid are known to be aliphatic acids that have low potency for HDAC inhibition. Hydroxamic acid-based compounds are discovered extensively in clinical and pre-clinical studies as anti-cancer agents. Abexinostat, Pracinostat, Resminostat, Givinostat, Quisinostat, Panobinostat, and CUDC-101 are some novel hydroxamic acid-based HDAC inhibitors that are still being studied in different clinical stages (Delcuve et al., 2013; Estiu et al., 2008; Jinhua Tang & Zhuan, 2013; Jung, 2001; H. J. Kim & Bae, 2011; Milazzo et al., 2020; M. J. Morris & Monteggia, 2013; J. Park et al., 2017; Yadav et al., 2019; L. Zhang et al., 2018) (Except from Belinostat and Vorinostat) .

A Zinc ion (Zn^{+2}) is needed as a cofactor and it is charged with stabilizing the acetyl-lysine and also, coordinated by three residues Asp-Asp-His (DDH) inside the pocket. Common HDAC inhibitors are Zn^{+2} -dependent class I and class II HDACs and bind to Zn^{+2} -containing the catalytic domain of HDACs specifically (Youxuan Li & Woster, 2015). Hydroxamic acid is the most common zinc-binding group (ZBG) because of its high affinity to zinc ions. HDAC inhibitors are most commonly characterized by three specific parts – a zinc chelating group, a linker and a cap group. The ZBG enables the binding of the catalytic metal group to the active site of the HDAC enzyme. The linker group embraces the entire area of the pocket and connects to the cap group which blocks the active site by covering the surface of HDACs.

The key amino acid residues which catalyze the action are highly conserved in between all HDACs and this brings specificity to HDACs for their working mechanism among other species and structures. There are lots of efforts to discover therapeutically effective HDAC inhibitors still in various stages of clinical development. Rational drug design techniques in computational drug design have been playing a remarkable role in revealing potential inhibitors having diverse chemistry and characteristics.

In this thesis, human class2b HDACs are put under the scope of designing potential isoform-selective inhibitors for both HDAC6 and HDAC10 by using rational drug design techniques. Potential lead compounds are obtained as anticancer therapeutic agents for further optimization. In this research, the crystal structure of human HDAC6 catalytic domain 2 (CD2) was retrieved from protein data bank (PDB) (PDB ID; 5EDU, release date 27-07-2016) (Hai & Christianson, 2016) and the homology model of human HDAC10 (Ibrahim Uba & Yelekçi, 2019a) is used which is modeled based on the newly-released X-ray crystal structure of *Danio rerio* (Zebrafish) HDAC10 (PDB ID; 5TD7, release date 24-05-2017)(Hai et al., 2017). With this improvement, class2b HDACs which are closest relatives sharing common evolutionary origin take notice of today's researches by being crucial targets for drug design.

Aim and Objectives

In this study, the main objectives are conducted as follows:

- i. Hit identification of isoform-selective HDAC6 and HDAC10 inhibitors by structure-based virtual screening via the cancer-specific library.
- ii. Searching for isoform-selective HDAC6 and HDAC10 inhibitors by structure-based virtual screening with ZINC library.

2. LITERATURE REVIEW

2.1 Classification of Histone Deacetylases

The first structural information about HDACs superfamily is achieved from the crystal structure of a histone deacetylase-like protein (HDLP) which has an unknown functionality. HDACs are enzymes that catalyze the biological reaction of removing the acetyl group from the acetyl-lysine residue to promote gene expression in cells. Until now, eighteen mammalian histone deacetylases are identified and divided into four different categories based on their sequence homology. Class I HDACs (HDAC1,2,3 and 8), class II HDACs (HDAC5,6,7,9 and 10), class III HDACs (Sirtuins- SIRT1, SIRT2, SIRT3, SIRT4, SIRT5, SIRT6 and SIRT7 which requires NAD^+ for their enzymatic activity), and HDAC IV (HDAC11) are the members of HDAC superfamily. Except for sirtuins, all other HDACs need a Zn^{+2} cofactor for their activity (Elmallah & Micheau, 2019). Class I HDACs are considered to be yeast Rpd3-like and localized in the nucleus, class II HDACs are known as yeast Had-1 like shuttling between the cytoplasm and nucleus (Uba & Yelekçi, 2018). Nevertheless, class III HDACs (sirtuins) share similar homology with yeast Sir2 and are localized in nucleus (SIRT1, SIRT6, and SIRT7), cytoplasm (SIRT2), and mitochondria (SIRT3, SIRT4, and SIRT5). Only HDAC11 which belongs to class IV HDACs is both found in the nucleus and the cytoplasm and has no similarity with yeast histone deacetylases (Abbass et al., 2019). HDAC10 and HDAC11 are declared to have no substantial activity, but HDAC 1,2,3 and 6 are known to have a variety of different substrate and inhibitor specificities despite their well-conserved structure of the binding pocket.

2.2 Role of HDACs in Cancer Pathogenesis

To date, HDACs are involved in various types of cancer. Aberrant expression and regulation of HDACs promote directly cell proliferation and cancer progression. In class I HDACs, high or low expression of HDACs reveals the formation of gastric, pancreatic, breast, lung, and prostate cancer. In particular, overexpression of HDAC 1,2 and 3 are linked to colorectal cancer; overexpression of HDAC 1 is associated with breast and lung cancer. The overexpression of HDAC2 is correlated with gastric, uterine, cutaneous T cell lymphoma (CTCL), and Hodgkin's lymphoma (HL), overexpression of HDAC3 reported in lung, colon, and ovarian cancers. Moreover, HDAC8 is linked to childhood neuroblastoma. In class IIa HDACs; overexpression of HDAC4 leads to breast cancer, overexpression of HDAC5 is seen in hepatocellular carcinoma and medulloblastoma, overexpression of HDAC7 is reported in pancreatic and colon cancer, high expression of HDAC9 is associated with medulloblastoma. Class IIb HDACs; HDAC6 is correlated with hematological tumors, whereas HDAC10 is linked with cervical and chronic lymphocytic leukemia in cells. Class III HDACs (Sirtuins) are also related to the progression of certain cancer types such as myeloid leukemia, prostate, gastric, and breast cancer. Ultimately, the only member of class IV HDACs which is HDAC11's overexpression is involved in Hodgkin's lymphoma but still, the role of HDAC11 in cancer pathogenesis is not well understood (Benedetti et al., 2015; Yixuan Li & Seto, 2016; Singh et al., 2018).

2.3 Role of HDACs in Other Diseases

To date, HDACs are known as promising targets for many diseases such as cancer, metabolic disorders, interstitial fibrosis, neurological disorders, autoimmune and inflammatory diseases. Overexpression of class I HDACs (HDAC1,2,3) is associated with the nodal spread and is a prognostic marker for gastric cancer. HDAC1 and HDAC2 are together found in repressive complexes, but HDAC3 is found in distinct complexes. Increased expression of HDAC6 which is a class II HDAC is associated with aberrant cell growth, thus generation of tumors leading to breast cancer. HDAC4 is quite enriched in the brain and skeleton. Silencing HDAC4 annihilates the expression of SMA transcript and also regulates vascular inflammatory responses and enhances

hypertension. Tang et al. suggest that HDAC4 is a crucial target for myofibroblastic differentiation and also HDAC1 and HDAC2 regulates the proliferation of renal interstitial fibroblasts. Recently, investigations suggested that HDAC4, HDAC5, and HDAC9 have significant roles in regulating the production of insulin in cells (Jinhua Tang & Zhuan, 2013). HDAC5 and HDAC9 present in high amounts in muscles, brain, and heart. HDAC7 serves in the apoptosis of T-cells (Moradzadeh et al., 2015) and is also expressed in the endothelial cells and thymocytes (Haberland et al., 2009). HDAC8 can be considered an unusual isoform as its association with other nuclear proteins is independent. In addition to this, it has been acting as a potential target for numerous cancers and CNS disorders, and still being a hot topic for researchers as it is highly crucial for therapeutic diseases having available isoform-selective inhibitors today (Kashyap & Kakkar, 2020). Finally, HDAC10 and HDAC11 can be considered as the least studied HDAC isoforms among others just because their structure and function are barely understood (Seto & Yoshida, 2014).

2.4 Histone Deacetylases Class 2b Subfamily

Class IIb histone deacetylases consist of only two isoforms which are HDAC6 and HDAC10. In mammalian cells, these enzymes are mostly localized in the cytoplasm, so that non-histone proteins are known to be their actual physiological target. HDAC6 and to a minor extent HDAC10 show promising therapeutic potential (D. Wang, 2009).

Table 2. 1 Localization, structural property, and functionality of Class IIb histone deacetylases in humans.

	Class	Localization	Tissue Expression	Catalytic Domain	Amino acids number	Activity in cancer
HDAC6	Hda1-like	Nucleus & Cytoplasm (Mainly Cytoplasm)	Tissue-specific	Two	1215	Overexpressed in breast cancer
HDAC10	Hda1-like	Nucleus & Cytoplasm (Mainly Cytoplasm)	Tissue-specific	One	669	Metastasis suppressor for Cervical cancer

The structure of HDAC6 is unconventional due to its two independent catalytic domains and it is the largest HDAC isoform with 1215 amino acids identified in humans. On the other hand, although HDAC6 and HDAC10 enzymes are evolutionarily the closest and have structural homology with each other among other HDACs, the crystal structure of HDAC10 is not elucidated yet and has only one functional catalytic domain (Kazantsev & Thompson, 2008).

2.4.1 Histone Deacetylase 6

To date, 66 various X-ray crystal structures of HDAC6 from *Homo sapiens* (human) and *Danio rerio* (zebrafish) have been identified and listed in PDB. In this thesis, CD2 of human HDAC6 with Trichostatin A is retrieved and studied extensively for further discovery of protein-ligand interactions and isoform-selective inhibitors.

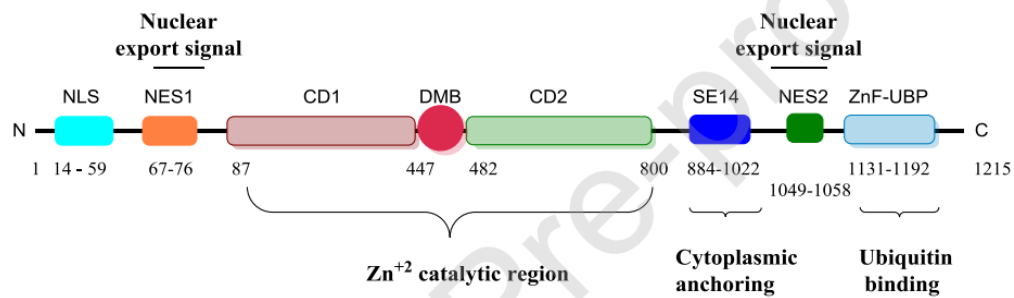


Figure 2. 1 Schematic representation and functional domains of human HDAC6. The only HDAC with two tandem catalytic domains, deacetylase domains (CD1 and CD2 including Zn⁺² catalytic activity). Tubulin, Hsp90, and cortactin are HDAC6 substrates in the Zn⁺² catalytic region. The nuclear export signal (NES) prevents the accumulation of the protein in the nucleus and the Ser-Glu-containing tetrapeptide (SE14) region ensures a stable anchorage of the enzyme in the cytoplasm. The nuclear localization signal (NLS) translocates HDAC6 into the nucleus. The linker (dynein motor binding, DMB) between both CATs can bind to dynein and the high-affinity ubiquitin-binding zinc finger domain (ZnF-UBP) (Pulya et al., 2020).

HDAC6 is an isoform of HDACs superfamily with its specific structural and physiological characteristics. The structure of HDAC6 is more complex compared with other isoforms because it has two tandem catalytic domains and they function in several biological processes (Miyake et al., 2016). HDAC6 is encoded in chromosome X p11.22-23 gene region. HDAC6 is an IIb HDAC isoenzyme sharing similar sequence homology with yeast Hda1 protein and it is tissue-specific (Gregoretta et al., 2004). It is highly expressed in the liver, kidney, heart, and pancreas. Even though HDAC6 shuttles between the nucleus and cytoplasm, it mainly resides in the cytoplasm and is considered as the largest HDAC isoform having 1215 amino acid residues. HDAC6 consists of two functional catalytic domains: CD1 and CD2. They are known to be highly conserved catalytic domains; thus, this makes HDAC6 structurally unique in comparison with other HDAC isoforms. CD2 shows more activity over CD1 and it shares more similarity with other HDAC isoforms. Moreover, HDAC6 has a wider and shallower binding pocket surface in comparison with its orthologues. If we look at the domain organization, structurally we see that HDAC6 enzyme starts with N-terminal, nuclear

localization signal (NLS), nuclear export signal (NES), CD1, CD2, Ser-Glu containing tetrapeptide (SE14), a zinc finger ubiquitin-binding domain (ZnF-UBD or BUZ) and ends with C-terminal, respectively (Y. Liu et al., 2012). NES and SE14 are responsible for cytoplasmic localization of HDAC6 and NLS direct shuttling between cytoplasm and nucleus. CD1 and CD2 together constitute the Zn^{+2} catalytic region and there exists a dynein motor binding region in both catalytic regions. The zinc finger binding domain is unique to HDAC6 containing conserved cysteine-rich and histidine-rich regions leading ubiquitination process (Ferreira De Freitas et al., 2018; Thaler & Mercurio, 2014).

HDAC6 plays a crucial role in regulating cell migration, cytoskeleton dynamics, angiogenesis, transcription, immune response, cell proliferation, cell death, stress response pathways, and degradation of misfolded proteins. HDAC6 does not interact with histone proteins *in vivo*, yet targets non-histone cytoplasmic substrates. HDAC6 is the only isoform that deacetylates the α -tubulin in microtubules so that controls the microtubule stability and cell motility (Haberland et al., 2009; Zilberman et al., 2009). On this basis, tubulin deacetylase activity in the cell only occurs in CD2 since CD1 activity is not clear yet. HDAC 6 targets not only α -tubulin but also deacetylates chaperone protein (Hsp90) and cortactin and many others still in the ongoing investigational phases. This means that it has a critical role in clearing the misfolded proteins and aggregates in the cytoplasm by autophagy. Inhibiting HDAC6 results in hyperacetylation of Hsp90 and alleviates the chaperone association with its neighboring proteins.

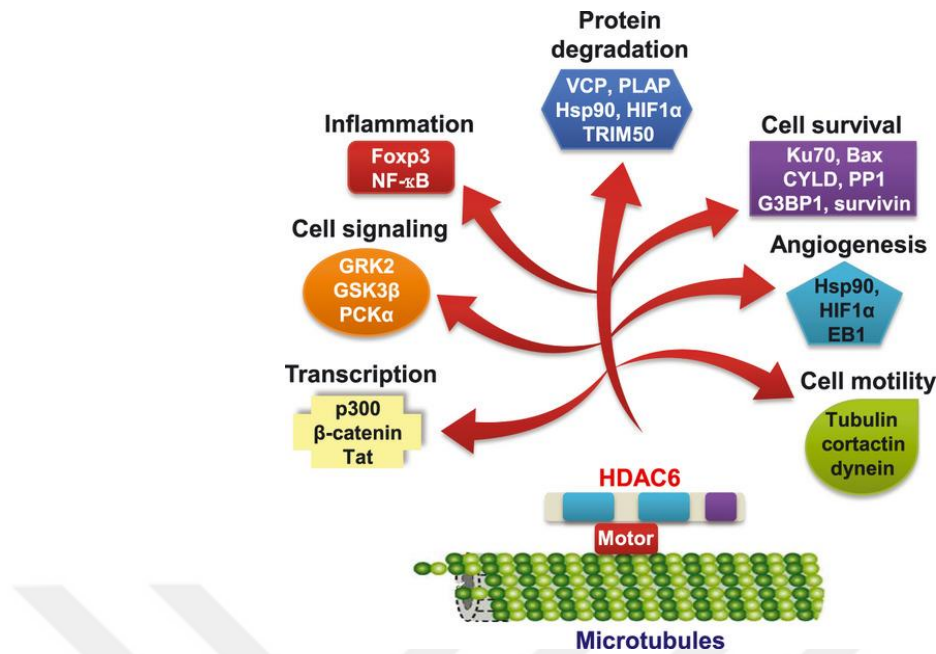


Figure 2. 2 Deacetylase-dependent and -independent functions of HDAC6 showing substrates, interacting partners, and others. HDAC6 plays a role in the recruitment of partner proteins (Yingxiu Li et al., 2013).

Furthermore, HDAC6 is associated with neurodegenerative diseases such as Alzheimer's disease and Parkinson's disease (Simões-Pires et al., 2013). Mazzocchi et al. (2020) mentioned in their review that HDAC6 is the main focus as a neural therapeutic target for clearing the aggregated proteins in the brain. In this case, HDAC6 plays a protective role by wiping away all the detrimental aggregates and reduces oxidative stress. Inhibiting HDAC6 procures α -tubulin acetylation and keeping it stable (LoPresti, 2020). In this way, HDAC6 acts as a neuroprotective enzyme by assisting microtubule stabilization, axonal transport, and mitochondrial transport, but in some cases its effects are neurotoxic. For instance, tau proteins (a microtubule-binding protein) are today's evolving research topic that plays a huge role in Alzheimer's disease. Deacetylation of tau proteins by HDAC6 promotes tauopathy by enhancing aggregation and toxicity (Janke & Montagnac, 2017; Thomas & D'Mello, 2018). Noack et al. (2014) supported in their work by testing with mice brain that knockdown of HDAC6 enhances pathological hyperphosphorylated tau, hence HDAC6 has a critical

role in tau aggregates formation which contributes to neurodegenerative diseases. Also, in Alzheimer's disease, overexpression of HDAC6 prevents mitochondrial transport in neurons in a glycogen synthase (GSK)3 β -dependent way.

HDAC6 is a potential target for tumorigenesis as well due to its involvement in various cellular processes (Cosenza & Pozzi, 2018). HDAC6 is considered a great drug target because its inhibition does not create a toxic environment like other HDACs (Butler et al., 2010). Whilst pan-HDAC inhibitors show more activity in anti-tumor pathways, they end up with toxicities because they have limited specificity. Ubiquitination and deubiquitylation of HDAC6 are so important for the progression and metastasis of tumors. Ubiquitin-HDAC6 deacetylation alters gene transcription which leads a change in protein expression and continually condensation of chromosomes (P. Yang, 2013). Additively, HDAC6 draws attention by its role in breast, gastric, ovarian and esophageal cancer as well. In fact, J. R. Liu et al. (2019) showed that in glioblastoma, a deadly brain cancer type, HDAC6 is overexpressed and glioma cell proliferation can be suppressed with siRNA-mediated inhibition of HDAC6. HDAC6 is overexpressed in germ cell tissues, spermatogenic cells, and other somatic tissues. Thus, X. Zhang et al. (2017) tested highly expressed HDAC6 in embryonic stem cells (ES) and DNA damage and resulted in reduced DNA damage and triggered DNA repair. Some significant agents like program death receptor-1 (PD-1) and program death receptor ligand-1 (PD-L1) receptor are upregulated by HDAC6 and show notably positive results in pre-clinical trials and this demonstrates how effectual HDAC6 in cancer immunotherapy. HDAC6 also appears in the STAT3-PD-L1 pathway participating in antitumor immunity for the treatment of melanoma and lung cancer (Pulya et al., 2020). Thus, highly expressed HDAC6 induces the migration of lung cancerous cells through the PKA/Epac/ERK-dependent pathway (Pulya et al., 2020). Besides, overexpression of HDAC6 has been identified in several cancer cell lines and tested in mouse tumor models to identify effective cancer therapies (Sakamoto & Aldana-Masangkay, 2011). To sum up, HDAC6 along with its specific structure and function will be a hot topic for researchers to reveal more about carcinogenesis in the future.

2.4.2 Histone Deacetylase 10



Figure 2. 3 Domain composition of human HDAC10 consisting of deacetylase domain and leucine-rich domain (S. Y. Park & Kim, 2020).

HDAC10 is the second class IIb enzyme that is evolutionarily related to HDAC6 and its chromosomal location is 22q13.31-33. Although the human HDAC10 structure is not revealed yet, the structure of *Danio rerio* (zebrafish) is available as 5TD7 in the PDB data bank. HDAC6 and HDAC10 both contain a unique second catalytic domain whereas the second catalytic domain of HDAC10 doesn't have any known function. HDAC10 contains 669 amino acid residues and widely expressed in mammalian cells and human tissues (Tong et al., 2002). It is highly expressed in the kidney, liver, pancreas, and spleen in humans. HDAC6 and HDAC10 both have subcellular localization with class IIa HDACs but they are separated from class IIa HDACs through having two catalytic domains (Seto & Yoshida, 2014). From figure 2.4, HDAC10 contains an N-terminal, active deacetylase domain (DAC domain), and catalytically inactive leucine-rich domain (LRD domain) respectively. LRD is described as a putative domain and is responsible for cytoplasmic enrichment. One unique property of LRD is that it doesn't show any sequence similarity to any known proteins. HDAC10 just as HDAC6 shuttles between the nucleus and cytoplasm but its primarily localized in the cytoplasm. Although very little is known about the substrate information and the role of HDAC10, it functions in polyamine metabolism by performing a robust polyamine deacetylase (PDAC) activity. On the other hand, it has poor lysine-deacetylase activity in cells. It is found that HDAC10 has a transcriptional repressor role and it is involved in homologous recombination, melanogenesis, and autophagy-mediated cell survival (Guardiola & Yao, 2002; Oehme et al., 2013). In addition, De Ruijter et al. (2003) indicate that interaction of HDAC10 with HDAC1,2,3,4,5 and 7 but not with HDAC6

shows that it functions like a recruiter rather than a deacetylase. The only amino acid, Glu272, named as the “gatekeeper” chooses its substrate selectively in the catalytic region. Surprisingly, if Glu272 (HDAC10 numbering) is missing at the site deacetylation of acetylated lysine substrates cannot be catalyzed (Géraldy et al., 2019). Moreover, another unique feature of HDAC10 is the 3_{10} helix with consensus sequence $p^{23}(E, A)CE^{26}$ (the “PEACE” motif) that restricts the active region ensuring the binding of long and shallow polyamines (Herbst-Gervasoni et al., 2020).

Various studies elucidated that HDAC10 is a potential drug target for cancer. There has been no isoform-specific HDAC10 inhibitor is identified yet, but HDAC10 is a promising biological target for chemotherapy through cancer cell lines. Uba & Yelekçi (2020) performed the first molecular dynamics study by building hHDAC10 using zHDAC10 as a template. Recently, Géraldy et al. (2019) conducted two assays; Tubastatin A showed even more potency to bind HDAC10 rather than HDAC6, and the other is the hHDAC10 homology model revealed that the gatekeeper (Glu272) and hydrogen between a cap group nitrogen demonstrated a potent binding. Inhibition of HDAC10 shows significant anti-tumor impacts in neuroblastoma patients (Ridinger et al., 2018). Meanwhile, Islam et al. (2017) investigated that inhibition of HDAC10 may enhance the platinum-based therapy response in BRCA1-deficient ovarian carcinoma patients. Herewith, HDAC10 is an emerging anti-tumor target for several cancer types to quest in future researches.

2.5 HDACs Class2b Inhibitors for Cancer Therapy

In recent years, HDAC inhibitors exhibited great progress as a therapeutic potential for the treatment of cancer because high expression of HDACs was found in various types of cancers. These include some malignancies such as solid and hematological tumors (Abbass et al., 2019). Also, HDACs’ involvement to enhance the proliferation, migration, invasion, and angiogenesis of tumor cells supported that HDACs play a vital role in tumorigenesis (F. Yang et al., 2019). Although the therapeutic avails of isoform-selective HDACi are not clinically proved yet, many researchers indicate that isoform-selective HDAC inhibitors show better index (Clawson, 2016). Present HDAC

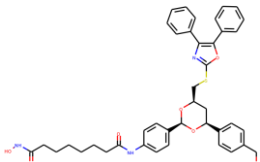
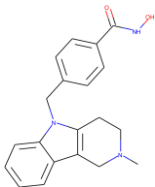
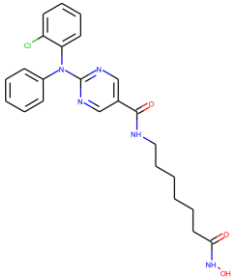
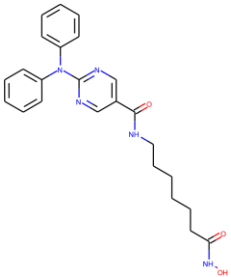
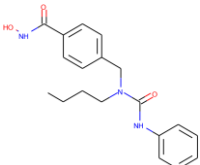
inhibitors which inhibit all HDAC isoforms are mostly pan-inhibitors having several side effects as well such as diarrhea, vomiting, and fatigue (Saraswati et al., 2020).

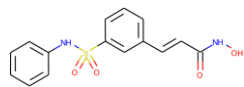
Table 2. 2 List of 10 known HDAC-selective and Pan-HDAC inhibitors.

#	Name of known inhibitor	Phases	Inhibitor selectivity
1	Tubacin	Not in trials	Hdac6
2	Tubastatin A	Not in trials	Hdac6
3	Citarinostat	I	Hdac6
4	Rocilinostat	II	Hdac6
5	Nexturastat A	Not in trials	Hdac6
6	Belinostat	FDA approved	Class I
7	Quisinostat	II	Pan-Hdac
8	Pracinostat	III	Pan-Hdac
9	Abexinostat	III	Class 1 and 2
10	CUDC-101	I	Class 1 and 2

According to their structural features, HDACi is divided into five classes: hydroxamic acid-based derivatives, cyclic peptides, benzamides, short-chain fatty acids, electrophilic ketones. Many natural and synthetic compounds are still in clinical trials, especially most of the compounds are hydroxamide analogs (Abend & Kehat, 2015; Prachayasittikul et al., 2017). Vorinostat, Belinostat, Romidepsin, and Panobinostat are four drugs that are approved by Food and Drug Administration (FDA) to cure cutaneous T-cell lymphoma (Hassell, 2019). The last HDACi is Chiamide which is a benzamide approved only in China FDA for the treatment of cutaneous and peripheral T-cell lymphoma (PTCL, CTCL), multiple myeloma (MM), and acute myeloid leukemia (AML) (Tang et al., 2014).

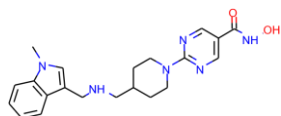
Table 2. 3 Structures of 10 known HDAC6 and Pan-HDAC inhibitors

Compound Structure	Compound Name	ChEMBL ID
	Tubacin	ChEMBL356769
	Tubastatin A	ChEMBL2018302
	Citarinostat (ACY-241)	ChEMBL3693786
	Rocilinostat (ACY-1215)	ChEMBL2364628
	Nexturastat A	ChEMBL2179618



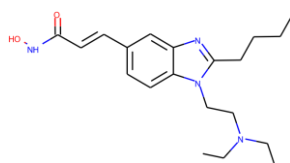
Belinostat

ChEMBL408513



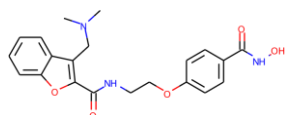
Quisinostat

ChEMBL2105763



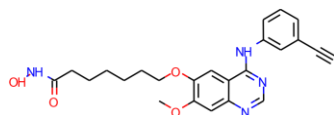
Pracinostat

ChEMBL1851943



Abexinostat

ChEMBL2103863



CUDC-101

ChEMBL598797

The general pharmacophore model of HDAC inhibitors obtains a specificity and selectivity as long as there is a change in cap group, the linker, or the ZBG in HDAC isoform (Mottamal et al., 2015). Many advances in HDAC6-selective inhibitors have been made until today, such as Tubastatin A (TSA), Tubacin, Ricolinostat (ACY-1215), CAY10603, Nexturastat A, HPOB, Citarinostat, and ACY-775. These inhibitors exhibit HDAC6-selectivity ranging from 10- to greater than 1000-fold relative to the other HDACs. Only Ricolinostat and Citarinostat are still in clinical trials. Tubacin, shown in Figure 2.2, is identified as the first compound holding a T-shaped unique structure and selectively inhibits HDAC6 (P. Yang, 2013). That's why, Tubacin and its derivatives are generating a promising anticancer potential (Dawood et al., 2020). In addition to these, Tubastatin A is a selective HDAC6 compound almost 8-fold from HDAC10 (Herbst-Gervasoni et al., 2020). HBOP revealed that the cap group of inhibitors is gathered around the L1 loop and only the hydroxy of hydroxamate group of HPOB collaborates with a zinc ion. From this achievement, it is proposed that bulky and short aromatic linker groups but big and rigid hydrophobic cap groups are more preferred while investigating HDAC6-selective inhibitors (Porter et al., 2017; F. Yang et al., 2019).

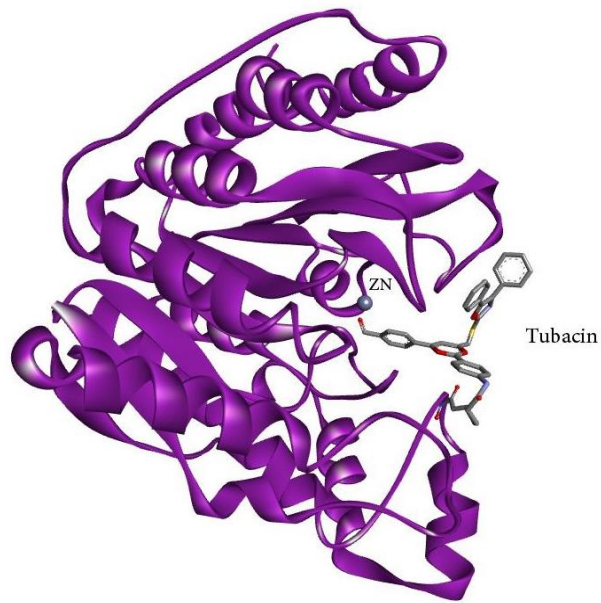


Figure 2. 4 The representation of the 3D structure of human HDAC6 CD2 with its selective-inhibitor Tubacin.

For HDAC10, there has been no isoform-specific inhibitor is identified yet. However, HDAC10 is believed to be a remarkable anticancer target due to its role in chemo-resistant cell lines and unprecedented structure. Herbst-Gervasoni et al. (2020) revealed that the electrostatic “gatekeeper” residue contributes to selectivity.

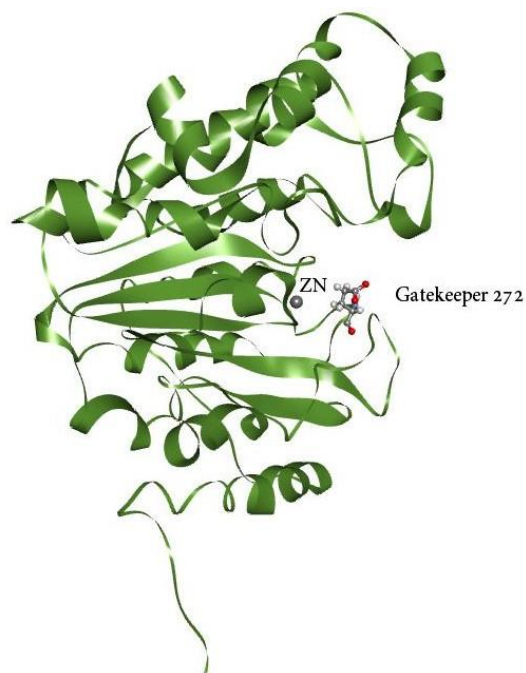


Figure 2. 5 Representation of the 3D-modeled structure of human HDAC10 CD2 with its unique “Gatekeeper” residue highlighted at the entrance of the catalytic pocket.

In conclusion, various *in vitro*, *in vivo*, and *in silico* studies are conducted for searching potential HDACi using different methods. Because of the pleiotropic nature of HDACs, they are identified with certain limitations (Hull et al., 2016). However, potential limitations in selective HDAC inhibitor search, *in silico* approaches constitute a great way in the identification of novel and hit lead HDAC inhibitors today.

2.6 Computer-Aided Drug Design

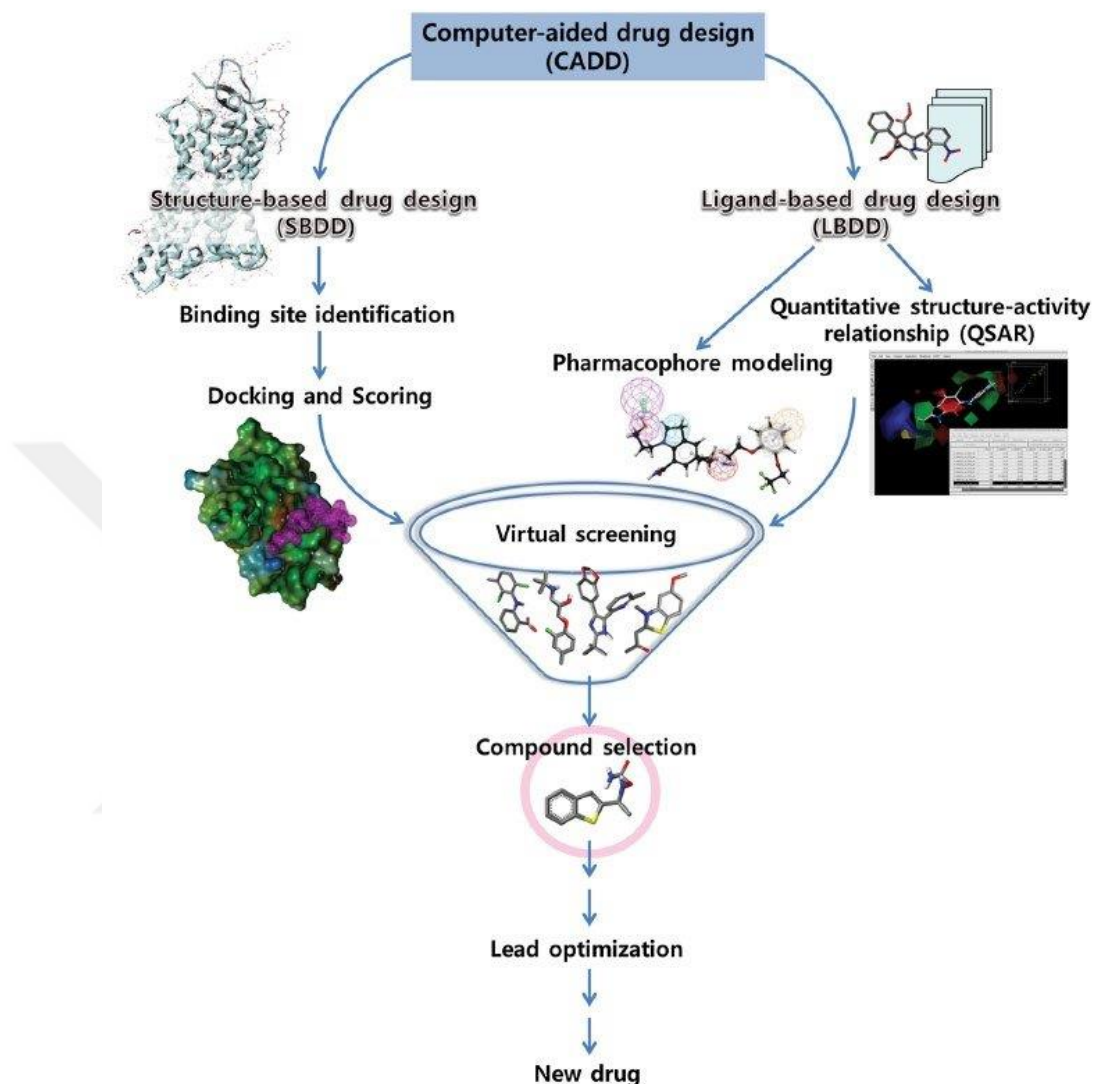


Figure 2. 6 Representative workflow for computer-aided drug design (Macalino et al., 2015).

Computer-aided drug design (CADD) has reached the most preferred approach for the development of new epigenetic inhibitors lately. Also, CADD plays a significant role in medicinal chemistry to develop highly selective, more potent, and less toxic molecules for the treatment of diseases like cancer. With the help of CADD large chemical libraries is easily accessible, low cost, and time-saving as well (Surabhi, 2018).

2.6.1 Virtual screening

Virtual screening (VS) is a computational approach to identify potential compounds that can bind to a drug target such as a receptor or an enzyme. VS can be divided into two: structure-based drug design (SBDD) and ligand-based drug design (LBDD). SBDD uses the knowledge of the target protein structure obtained from X-ray crystallography or NMR to calculate the binding energy. On the other hand, in LBDD 3D structure of the target protein is not identified but the knowledge of ligands binding the target is known. In this way, ligands can be used to build a pharmacophore model having all the structural characters to bind its target's active site. Additively, the quantitative structure-activity relationship (QSARs) method is used in LBDD to quantify the relationship between chemical structures of compounds (Badalà et al., 2008; Neves et al., 2018). In the discovery of new drug molecules and 3D structures of targets, SBDD has emerged as a promising tool for the drug industry. With the help of SBDD new drug targets are identified as well such as MicroRNAs (miRNAs), long non-coding RNAs (LncRNAs), and novel drug targets. SBDD helped researchers computationally visualize the binding modes of ligands to their targets, predicting the significant binding site residues as well. Still, there are some disadvantages of SBDD like the high false-positive rate of virtual screening, scoring functions that estimate inaccurate target flexibility while docking and calculating target-ligand complex binding free energy. However, new techniques are rising to increase the efficiency of SBDD to enhance the success rate of SBDD today (Batool et al., 2019; X. Wang et al., 2018).

2.6.2 Molecular docking

In SBDD, molecular docking is accepted as a popular technique to predict the best conformation/orientation and the binding site of ligands to the target's active site with high accuracy. Molecular docking ensures the identification of binding modes of the ligand and intermolecular interactions formed between the ligand and its target. The net predicted binding energy (ΔG_{bind}) is calculated with the sum of certain parameters, hydrogen bond (ΔG_{hbond}), electrostatic (ΔG_{elec}), torsional free energy (ΔG_{tor}), dispersion and repulsion (ΔG_{vdw}), desolvation (ΔG_{desolv}), total internal energy (ΔG_{total}) and

unbound system's energy (ΔG_{unb}) (Dar & Mir, 2017). The binding energies can be calculated with scoring functions which dictate a score to each predicted pose (Salmaso & Moro, 2018). Scoring functions can be named as force-field-based, empirical, and knowledge-based scoring functions. The earliest docking methods are based on Fischer's "lock-and-key" theory proposing that ligands fit into their receptor-like lock and key (Meng, X. Y., Zhang, H. X., Mezei, M., & Cui, 2011). Then, Koshland carries this theory a step further by claiming that the receptor's active site changes with new interactions so that both protein and ligand should be considered flexible while docking. Thus, results eventuate with more accuracy rather than rigid docking.

Molecular docking approaches comprise of two approaches: simulation and shape complementary approaches. In the simulation approach, the ligand performs various conformations until it reaches the minimum energy state. This method seems to be more advantageous due to accurate molecular recognition among ligand and target but takes a lot of time to estimate each conformer releasing huge energy. In the shape complementary approach, the molecular surface of both ligand and target is represented in terms of matching surface illustration such as estimating hydrophobicity. This approach is faster and applies a quick scan to numerous amounts of ligands in a very short time. Docking algorithms can be classified into systematic search techniques such as exhaustive search, fragment-based search and conformational ensemble, stochastic methods like Monte Carlo (MC) methods and evolutionary algorithms (EA), and finally simulation methods such as molecular dynamics (MD) (Alejandra Hernandez-Santoyo, Aldo Yair Tenorio-Barajas, Victor Altuzar, 2016; Anna E. Lohning, Stephan M. Levonis, 2017).

Many molecular docking programs using these algorithms are available today, some of them are DOCK, GOLD, FlexX, Glide, AutoDock, AutoDock Vina, Cdocker, and rDock. AutoDock and GOLD use random/stochastic algorithms, DOCK, FlexX, and Glide use systematic algorithms, and DOCK, Glide, and AutoDock also use simulation methods as well. In addition, software programs such as DOCK, GOLD, and AutoDock uses force-field-based scoring functions considering hydrogen bonds, solvations, and entropy. Some examples of empirical scoring functions are GlideScore and ChemScore

in which the sum of empirical energy parameters (Van der Waals, electrophilic, hydrogen bond, desolvation, entropy, and hydrophobicity) is optimized to form a score of binding affinity. Drugscore is an example of a knowledge-based scoring function that supposes that ligand and target connect statistically with favorable interactions. Finally, new scoring functions are in progress based on machine learning techniques and tools for scoring binding energy and affinity. In this dissertation, AutoDock 4.2 (G. M. Morris et al., 2009), AutoDock Vina (Trott & Olson, 2010), and GOLD (Jones et al., 1997) were introduced to estimate protein-ligand binding free energies.

2.6.3 Drug-likeness and ADMET prediction

Absorption, Distribution, Metabolism, Excretion, and toxicity (ADMET) properties are very crucial filtration criteria for numerous new molecular entities (NMEs) as drug candidates in the process of drug discovery and development (Guan et al., 2019). ADME is related to pharmacokinetics to designate whether a drug molecule will achieve the target protein in the body and the time it spends in the bloodstream (Dong et al., 2018). Blood-brain-barrier penetration, human intestinal absorption, aqueous solubility, hepatotoxicity, cytochrome P2D6 inhibition, and plasma protein binding are the mathematical predictive ADMET pharmacokinetics parameters (Pal et al., 2019). During the early stage of drug discovery, Christopher Lipinski defined the relationship between pharmacokinetics and physicochemical parameters. He and his co-workers defined that orally active compounds depict physicochemical properties with a high probability to be an oral drug which indicates “drug-likeness”. Then, the concept of “drug-likeness” was associated with oral bioavailability and the well-known “Rule of Five” (RO5) is proposed by them in 1997 (Ntie-Kang et al., 2019).

Rule of Five proposes that:

1. Molecular weight (MW) less than 500 Da,
2. Computed logarithm of octanol/water partition coefficient (LogP) less than 5,
3. Number of hydrogen bond acceptors (HBAs) less than 10 and
4. Number of hydrogen bond donors (HBDs) less than 5.

A molecule is considered orally inactive only if it violates if two or more of the four rules according to the Rule of Five. Today, ADMET processes are applied in the early stage of drug discovery to reduce clinical trial failures. Evaluating ADMET properties in the early stage saves money and time since clinical trial failures occur mostly due to ADMET issues, not the lack of efficacy of compounds. Still, *in silico* strategies are being developed by medicinal chemists to reduce the risk of toxicity of drugs.

2.6.4 Molecular dynamics simulation

Molecular dynamics simulations (MDs) predict the spatial position and motion of each atom in a protein at every point in time by interatomic interactions. Ligand-protein complex docking techniques have been combined with MD simulations to have an accurate model. MD simulation is used in many experimental techniques such as X-ray crystallography and nuclear magnetic resonance (NMR) as well. MD simulations are applied to allow the change in the conformation of the receptor in the binding of the docking process. MD simulations rely on a force field which are the forces composed of chemical interactions. Along with the MD simulation, motions of all the atoms are modeled calculating the force of each atom by the numerical solution of classical Newtonian dynamics equation. Particularly, in every step, after calculating the forces on each atom, recursively calculates velocity on each atom as well. The trajectory is a 3D clip that defines the whole atomic-level configuration of the system at every point during a simulated time interval at a microscopic level (Allen, 2004). Force field involves both non-bonded and bonded interactions. Bonded interactions include bond angles and torsional dihedral angles, whilst Van der Waals interactions and charged electrostatic interactions build non-bonded interactions (Patodia, 2014).

The forces acting on each atomic system is shown with an equation as:

$$E_{tot} = \underbrace{\sum_{bonds} K_r (r - r_{eq})^2 + \sum_{angles} K_\theta (\theta - r\theta_{eq})^2 + \sum_{dihedrals} \frac{V_n}{2} [1 + \cos(n\phi - \gamma)]}_{\text{Bonded}} + \underbrace{\sum_{i < j} \left[\frac{A_{ij}}{R_{ij}^{12}} - \frac{B_{ij}}{R_{ij}^6} + \frac{q_i q_j}{\epsilon R_{ij}} \right]}_{\text{Non-bonded}}$$

Figure 2. 7 A typical force field (FF) model. Energy dependencies are related to (a) stretching or compressing a bonded pair of atoms (modeled by a simple spring) (b) Increasing or decreasing the bond angle (modeled by a simple spring) (c) dihedral angle rotations (modeled by a sinusoidal function) (d) Van der Waals interactions (modeled by Lennard-Jones potential) and (e) Electrostatic interactions (modeled by Coulomb's law). (a-c) are caused by interactions between atoms that are chemically bonded to one another while (c-e) are caused by interactions between atoms that are not bonded (Aminpour et al., 2019).

In Figure 2.7, bonds, angles and dihedrals form the bonded energies and the rest constitutes non-bonded energies.

E_{Bond} : Oscillations of the bond length of equilibrium

E_{Angles} : Oscillations of three atoms' bond angles in an equilibrium

$E_{\text{Dihedrals}}$: Torsional rotation of four atoms around a central bond

$E_{\text{non-bond}}$: Non-bonded energies (electrostatics and Lenard-Jones)

Various force fields are mostly used in MD, including AMBER, CHARMM, and GROMOS. These force fields use only different parameters but in general, give the same results. The most popular MD simulation software programs are AMBER, CHARMM, GROMACS, and NAMD (Hospital et al., 2015) CHARMM (Chemistry at HARvard Macromolecular Mechanics). AMBER and CHARMM have their force fields

with their name, however, GROMACS import AMBER, CHARMM, or GROMOS force field to run MD. NAMD (Nanoscale Molecular Dynamics) (Phillips et al., 2005) is designed to simulate large molecules to continue with parallel machines. It is highly compatible with other MD programs and NAMD has the same input, output, and force field formats as CHARMM (Durrant JD, 2011; Hollingsworth & Dror, 2018). CHARMM (Jo et al., 2008) and its force field are used in this thesis in the search for HDAC6 and HDAC10 isoform-selective inhibitors.



3. MATERIALS AND METHODS

3.1 Preparation of Class 2b Enzymes

The X-ray crystallographic structure of human HDAC6 (5EDU) catalytic domain 2 was downloaded from the PDB website (<https://www.rcsb.org/>). The catalytic domain of the HDAC6 is bound to Trichostatin A (TSA) inhibitor with a resolution of 2.79 Å (Hai & Christianson, 2016). The 3D structural model of human HDAC10 was obtained from (Ibrahim Uba & Yelekçi, 2019b) recent research. Water molecules, native ligands, and salt ions were removed from HDAC6 using BIOVIA DS 4.5 (BIOVIA, 2017). Then, the native ligand (TSA) redocked to the HDAC6 to see if the RMSD value which is found to be less than 2.0 Å is properly calculated with respect to the reference ligand. HDAC6 and HDAC10 enzymes were prepared with the protokol “Prepare Protein” in BIOVIA DS 4.5. This protocol adds hydrogen atoms to the protein with an optimum pH of 7.4 and removes the co-crystallized ligands from the protein structure. In addition, 10 known inhibitors were downloaded from the ChEMBL website (<https://www.ebi.ac.uk/chembl/>) and docked with HDAC6 to see whether their binding affinity is consistent with their experimental K_i or IC_{50} values from the literature. The details are described under the molecular docking subsection.

3.1.1 Protein Structure Determination of Class 2b HDACs

Ramachandran plot for HDAC6 and HDAC10 is drawn by using BIOVIA DS 4.5 and the energetically allowed conformations are depicted in Figure 3.1.

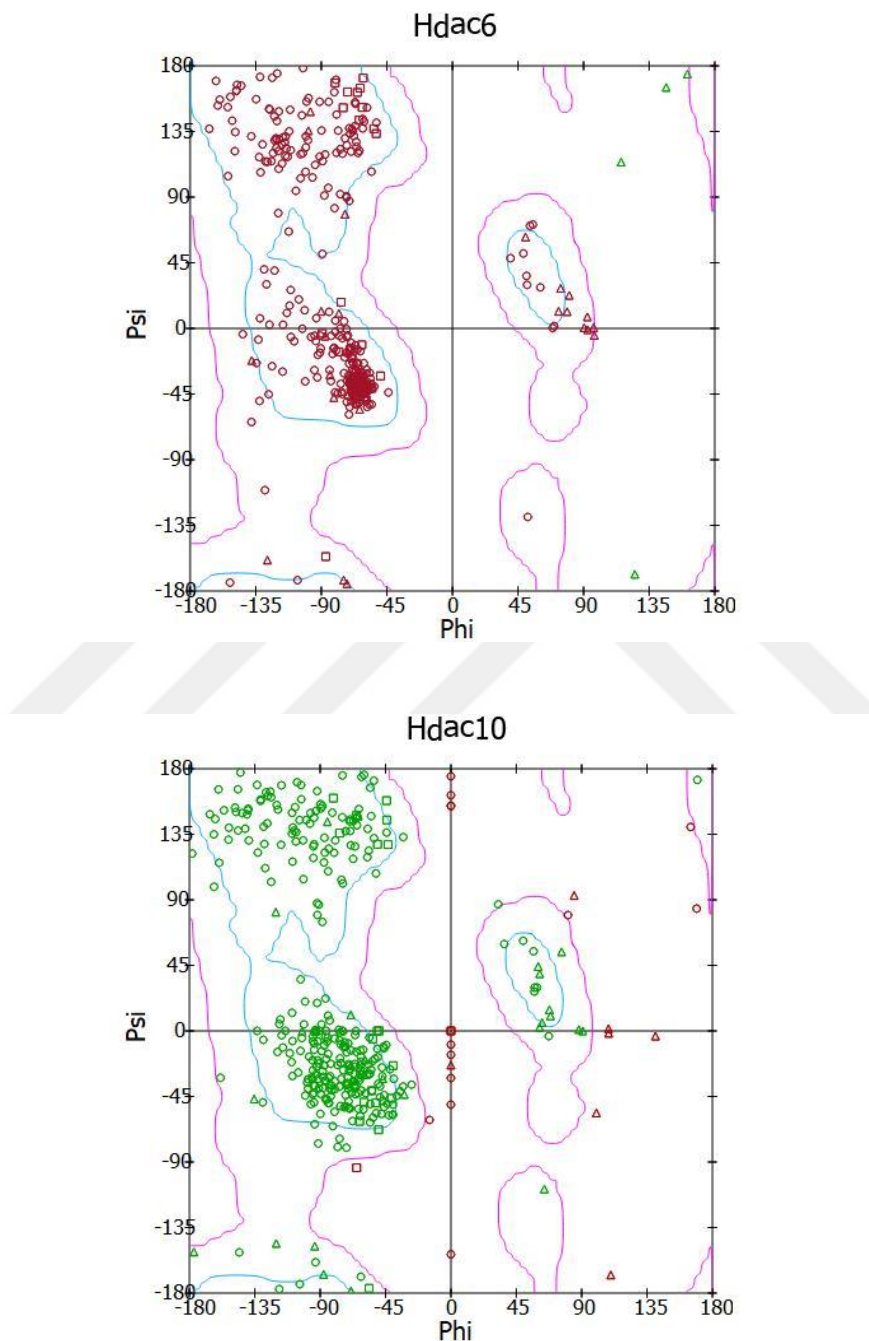


Figure 3. 3 Ramachandran plots of HDAC6 and HDAC10.

3.1.2 Sequence Alignment and Structural Superimposition of Class 2b HDACs

The amino acid sequence of HDAC10 CD2 was aligned to the amino acid sequence of HDAC6 CD2 using BIOVIA DS 4.5 (Figure 3.2), sequence alignment of hydrophobicity plus charge similarity is distributed (Figure 3.3) and 3D structures of HDAC6 and HDAC10 are superimposed (Figure 3.4). Also, the conserved amino acid residues of HDAC6 and HDAC10's catalytic pocket were aligned and shown in Table 3.1.

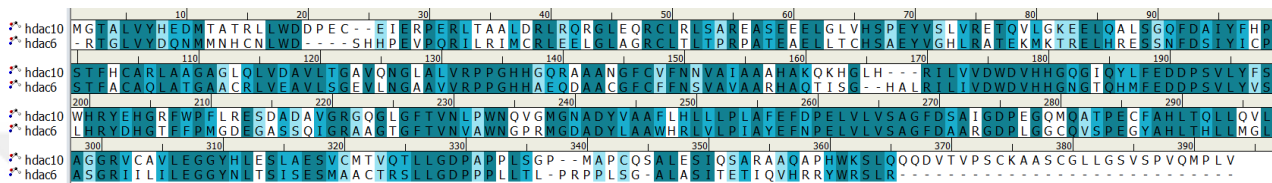


Figure 3.4 Sequence alignment of human HDAC6 CD2 and human HDAC10 CD2.

Identity is represented with **dark blue**, similarity in **light blue**, and difference in white.

The overall sequence identity is calculated as 52.1% and the sequence similarity as

69.1%.

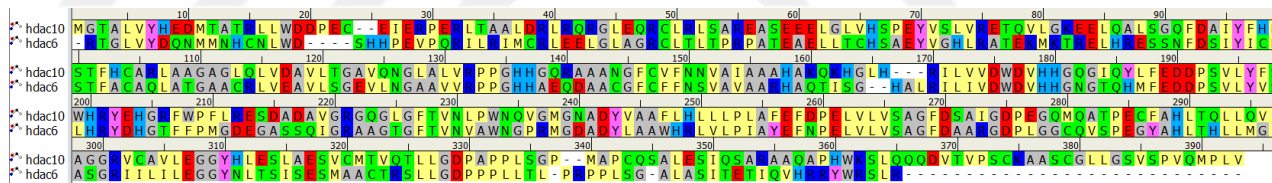


Figure 3.5 Sequence alignment of hydrophobicity and charges of amino acid residues

for human HDAC6 CD2 and human HDAC10 CD2. Hydrophobic residues are

indicated as **yellow**, amphiphilic residues as **grey**, hydrophobic neutral residues as

green, slightly basic residues as **light blue**, basic residues as **dark blue**, slightly acidic

residues as **pink**, acidic residues as **red** and other residues as white.

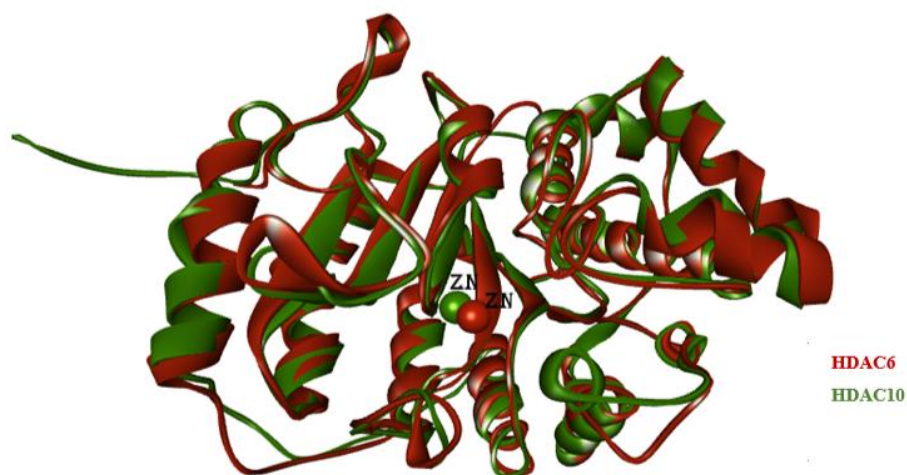


Figure 3. 6 Structural alignments and superimposition of class 2b HDACs' catalytic domain 2. HDAC6 CD2 is represented in claret red and HDAC10 CD2 is represented in dark green.

Table 3. 1 Conserved amino acid residues of the catalytic active site of HDAC6 and HDAC10. (* indicates the "Gatekeeper" amino acid at the catalytic pocket of HDAC10).

HDAC6	HDAC10
HIS610	HIS134
HIS611	HIS135
HIS651	HIS174
ASP649	ASP 172
VAL650	VAL173
ASP742	ASP265
GLY781	GLY303
TYR782	TYR305
	GLU272*

3.2 Structure-Based Drug Design for Isoform-selective Inhibitors by Virtual Screening

As mentioned before, structure-based virtual screening (SBVS) is one of the most useful and robust *in silico* techniques for drug design lately. In this study, AutoDock Vina (Trott & Olson, 2010) (<http://vina.scripps.edu/>) is used due to its higher speed to other docking programs. Two different compound libraries (Cancer-like compounds library and ZINC database) with a huge number of datasets are used and screened by AutoDock Vina, QuickVina, AutoDock 4.2, and GOLD in different stages of screening which is described in the next sections. AutoDock Vina gives accurate and quick results by using a hybrid scoring function including knowledge-based and empirical scoring functions (Trott & Olson, 2010). QuickVina 2.0 (<https://qvina.github.io/>) (Alhossary et al., 2015) also uses the same hybrid scoring function with AutoDock Vina. AutoDock 4.2 was used as well due to its reliable and accurate calculations. GOLD software was also used due to its high speed of screening and reliability. ChemPLP is known as an empirical scoring function of GOLD software which was used amongst other scoring functions because of its accurate pose prediction (Jones et al., 1997). The criteria of the selection of compounds was determined according to the 10 known inhibitors retrieved from ChEMBL website which will be covered in the coming subsections in detail.

3.2.1 Compound libraries for virtual screening

Table 3. 2 Cancer-like compound libraries used for virtual screening for HDAC6 and HDAC10.

Name of the Libraries	Number of Compounds
NCI (National Cancer Institute)	Approved Oncology Drugs Set (147 comp.) Natural Products Set V (390 Comp.) AIDS Anti-Viral (42.000 Comp.)
Asinex	Asinex Targeted Oncology Library (6.728 Comp.) Asinex Immuno-Oncology Library (11.346 Comp.)
SelleckChem	Anti-Cancer Library (1.966 Comp.) Drug Repurposing Library (2830 Comp.)

	Preclinical and Clinical Compound Library (2.578 Comp.) Anti-Cancer Metabolism Compound Library (198 Comp.) Histone Modification Compound Library (112 Comp.) Epigenetics Compound Library (470 Comp.) Natural Compound Library (2.054 Comp.) FDA Approved Drug Library (2.573 Comp.)
Hypha	HDAC Active&Inactive Comp. (530 Comp.)
ChemBridge	Molecule Library (10.000 Comp.)
DrugCentral	Molecule Library (17.000 Comp.)
Enzo	FDA Approved (2.000 Comp.)
Molport	Molecule Library (40.000 Comp.)
Art-Chem	Molecule Library (187.554 Comp.)
NIH	NIH Molecule Library (345.189 Comp.)

The names of the libraries and their corresponding number of compounds are given as a list in Table 3.2 above. The cancer-like compound libraries consist of 1.205.135 compounds in total. In addition to this library, a total of 1.050.000 compounds were downloaded from the ZINC15 database (<https://zinc15.docking.org/>) (Sterling & Irwin, 2015) for further screening with HDAC6. The ZINC15 dataset contains 3D tranches of drug-like compounds with a molecular weight ranging from 200 to 500 MW and a LogP value from -1 to 5. The compounds downloaded from the ZINC15 library were ready for screening and obtained in SDF file format as well.

3.2.2 Ligand set-up protocol

The cancer-like compound libraries consisting of 1.205.135 compounds were prepared by the “Prepare Ligands” protocol by BIOVIA DS 4.5 at pH 7.4, all the ionizable groups were properly protonated, 3D geometries were optimized and files were saved as SDF file format. 1.050.000 compounds from the ZINC15 database were already downloaded as prepared and in SDF format.

3.2.3 Structure-based virtual screening

Due to the lack of known inhibitors of HDAC10, the datasets of 10 HDAC6 and pan-HDAC known inhibitors are retrieved from the ChEMBL website with calculated K_i values. The known inhibitors were prepared by the protocol “Prepare Ligands” in BIOVIA DS 4.5 tool and docked to HDAC6 by AutoDock 4.2 (G. M. Morris et al., 2009). Gasteiger partial charges were added to all atoms and the files were saved as PDBQT. Then, grid parameter files (GPFs) and docking parameter files (DPFs) were created in the docking process. The size of the grid box was set accordingly with AutoDock Tools (ADT) and the center was arranged with the zinc ion located in the active site. Grid box parameters of HDAC6 were ($x=17.16$, $y=-44.58$, $z=102.75$) covering the whole active site and grid box dimensions were set to 55_55_55 Å with the spacing of 0.375 angstroms. 10 runs applied to each ligand with medium (2.500.000) evaluations and Lamarckian genetic algorithm (LA). According to the docking results, calculated K_i values were so close to the experimental K_i values so that the criteria for virtual screening of compounds were decided based on the average molecular weight of known ligands which is 300 to 500.

In this study, virtual screening of two different libraries and divergent docking tools were used. For HDAC10, grid center parameters were arranged as ($x=49.039$, $y=-2.958$, $z=115.225$), size of the grid box was set to 20_20_20 Å, run as 10, and docking energy evaluations as 2.500.000 (medium) for each ligand conformational search. The Lamarckian genetic algorithm was performed to generate docking input files as well. For HDAC6, the grid mapping parameters mentioned above were used for screening.

Firstly, 1.205.135 compounds from cancer-like compound libraries were reduced to ~50.000 compounds by docking with QuickVina 2.0 (Alhossary et al., 2015) screened against both HDAC6 and HDAC10 in which the exhaustiveness was set to 10. The compounds showing the least binding affinities were eliminated. Then, ~50.000 compounds were docked with AutoDock 4.2 and were reduced into 100 molecules. Compounds having ΔG values lower than 10 were eliminated. 36 compounds showing good selectivity were detected to search for their ADMET properties. Among 100 compounds screened for both HDAC6 and HDAC10, 5 compounds in total (3 for

HDAC6 - selective and 2 for HDAC10 - selective) were chosen for both enzymes to carry out molecular dynamics simulation.

Table 3. 3 Grid mapping parameters used for AutoDock Vina and QuickVina for HDAC6 and HDAC10.

Centre (Å)	HDAC6	HDAC10
X	17.16	49.039
Y	-44.58	-2.958
Z	102.75	115.225
Dimension (Å)		
X	20	20
Y	20	20
Z	20	20

Secondly, 1,050,000 compounds from ZINC library with molecular weights between 300 to 500 were selected. HDAC6 enzyme was uploaded to GOLD software in PDB format, all hydrogens were added and each protein was saved as MOL2 files. The coordinates were set for HDAC6 accordingly as shown in Table 3.4 above. GOLD ran with 10 Genetic Algorithm (GA) and all atoms were selected within 10 Å and with default parameters. Then, compounds were uploaded as SDF file format. According to the ChemPLP scores, the top 2,000 ligands showing the best affinities were selected to be filtered with Lipinski rule of five and later on screened by AutoDock Vina. The top 100 compounds showing good binding affinity was passed the criteria for further docking. Then, grid map files and grid parameter files were prepared using AutoDockTools4 and AutoGrid4. Later, docking parameters for HDAC6 were used as mentioned in Table 3.5 below. Finally, all 100 compounds were docked with AutoDock 4.2 for HDAC6 and cross-docked with HDAC10 to search for the highest binding affinity for HDAC10 as well. 86 compounds for HDAC6 and 28 compounds for HDAC10 were satisfied the criteria of $\Delta G \geq 10$. In total, 18 compounds showing good selectivity were detected to search for their ADMET properties. Then, the best 2 compounds showing the greatest binding affinity and enzyme selectivity (1 for HDAC6 and 1 for HDAC10) were chosen. At last, molecular dynamics simulation was performed for these top compounds of both enzymes.

Table 3. 4 Grid mapping parameters used for AutoDock 4.2 for HDAC6 and HDAC10.

Centre (Å)	HDAC6	HDAC10
X	17.16	49.039
Y	-44.58	-2.958
Z	102.75	115.225
Dimension (Å)		
X	55	55
Y	55	55
Z	55	55

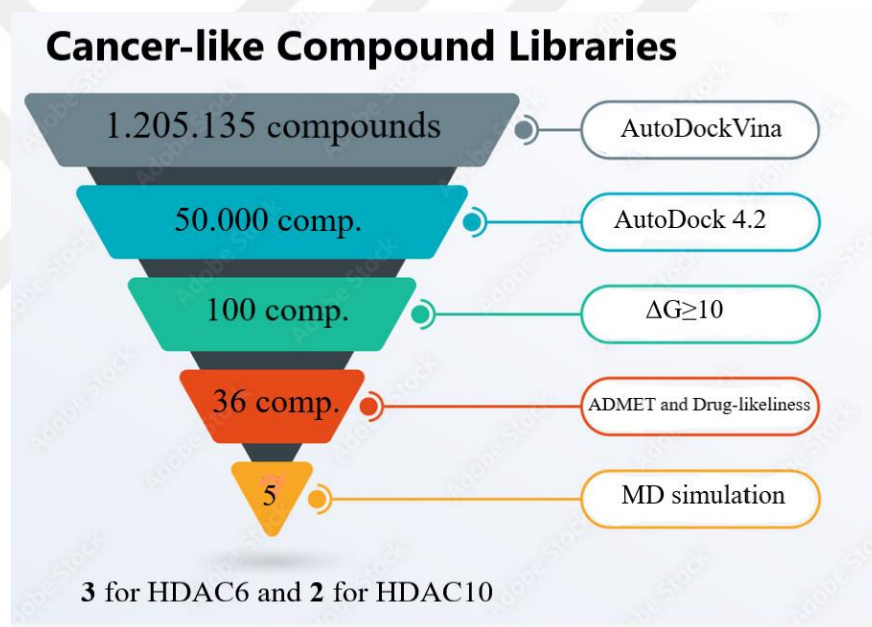


Figure 3. 7 Virtual screening workflow for the identification of potential lead compounds to design HDAC6-selective and HDAC10-selective inhibitors through cancer-like compound libraries.

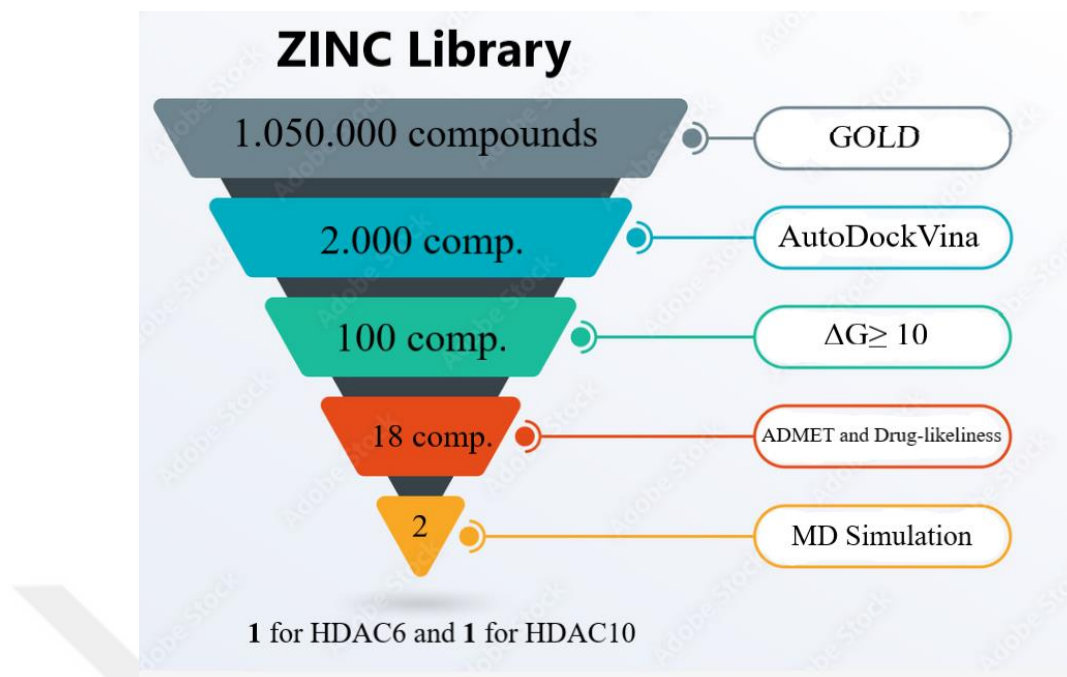


Figure 3. 8 Virtual screening workflow for the identification of potential lead compounds to design HDAC6-selective and HDAC10-selective inhibitors through ZINC compound library.

3.2.4 Drug-likeness and ADMET prediction

ADMET properties consist of the prediction of absorption, distribution, metabolism, excretion, and toxicity which are the key parameters to query for drug discovery. ADMET properties of novel compound candidates were predicted by severe *in silico* techniques for decades and still, it is so crucial to question these properties *in vitro* and *in vivo* as well. In this study, AdmetSAR and SwissADME are the web servers that were used to predict the Lipinski Rule of 5 and other physiochemical properties of drug-like compounds. So, Lipinski rule of 5 proposes that a drug-like compound should obey that: the octanol-water partition coefficient (LogP) value must be less than 5 (for the Moriguchi model, MLogP < 4.15) (Ikuo Moriguchi et al., 1992; Lipinski et al., 2001), the molecular weight must be lower than 500 Dalton, the sum of hydrogen bond acceptors (including N and O atoms) must not exceed 10 and the sum of hydrogen bond

donors must not exceed 5. SwissADME (<http://www.swissadme.ch/>) was used to predict these Lipinski Rule of 5, MlogP value, and topological surface area (TPSA). The other ADMET properties were detected using the AdmetSAR server (<http://lmmd.ecust.edu.cn/admetSar1>) which includes aqueous solubility (logS), Caco-2 cell permeability, and human intestinal absorption (HIA+). All the 36 compounds from cancer-like libraries and 18 compounds from the ZINC library were saved in SMILES format and uploaded to the servers to estimate their drug-likeness and ADMET properties.

3.2.5 Molecular dynamics simulation

HDAC6 and the modeled HDAC10 enzymes are simulated with MD simulation to see the stability of the protein itself and the complex. MD simulation is performed with the Nanoscale Molecular Dynamics (NAMD) software (Phillips et al., 2005) and 11 systems are chosen, which are: HDAC6 alone and HDAC10 alone itself, HDAC6_TubastatinA(TSN) complex, HDAC6_Asinex_imm3320 complex, HDAC6_Nih4_13387 complex, HDAC6_Enzo190 complex, HDAC6_ZINC000103531486 complex, HDAC10_Rocilinostat complex, HDAC10_Asinex_imm2279 complex, HDAC10_Targeted_Onc758 complex and HDAC10_ZINC000245284480 complex. The proteins themselves and the complexes are prepared using CHARMM-GUI web server (<https://www.charmm-gui.org/>) (Lee et al., 2016), input files for NAMD were generated step by step using CHARMM36m force field and ligands are parameterized with CHARMM General Force Field (CGenFF) server (<https://cgenff.umaryland.edu/>). All ligand atom typing and the assignment of charges and parameters are performed using the CGenFF server. All systems were solvated with the TIP3 water module and neutralized by the K⁺ and Cl⁻ ions (KCl) with a concentration of 0.15 M by the Distance (systematic) method. First of all, the energy of the system was minimized for 10,000 steps (20ps) at the beginning of the MD simulation and equilibrated with a 2 ns run. The system's temperature was set to 303.15 K with the constant number of atoms, volume, and temperature (NVT) ensemble. Finally, unrestrained production simulation was performed for all the systems at the constant number of atoms, pressure, and temperature (NPT) ensemble with 100 ns. During the unrestrained production run, the time step was set to 2 fs and the

collection interval and the frames are collected every 5.000 steps. The stability of the enzyme-ligand complex binding mode and the enzymes-free binding affinities will be compared with each other and then, analyzed with Visual Molecular Dynamics (VMD) according to their root-mean-squared deviation (RMSD), root-mean-squared fluctuation (RMSF), the radius of gyration (Rg) and potential energy (PE) profiles with their MD trajectory files.



4. RESULTS

4.1 Sequence Alignment and Structural Analysis of Class 2b HDACs

After the sequence alignment of both HDAC6 and HDAC10, results show that class 2b HDACs have similar amino acid residues that exist in their catalytic channel with a sequence identity of 52.1% and sequence similarity of 69.1%. Structural superimposition of HDAC6 and HDAC10 gives an RMSD value of 0.994 which is a low value as expected. In addition, the number of overlapping residues calculated between class 2b HDACs is 349.

Table 4. 1 Sequence similarity and identity analysis of class 2b HDACs in percentages.

%	HDAC6		HDAC10	
	<i>Similarity</i>	<i>Identity</i>	<i>Similarity</i>	<i>Identity</i>
HDAC6			69.1	52.1
HDAC10	69.1	52.1		

Table 4. 2 Sequence alignment and structural superimposition analysis of class 2b HDACs. RMSD values are shown above the diagonal in Orange, and the number of overlapping residues is shown below the diagonal in Purple.

	HDAC6	HDAC10
HDAC6		0.994
HDAC10	349	

4.2 Molecular Docking and Binding Affinity Analysis

The calculated binding free energy of the best-ranked compounds with selectivity for HDAC6 and HDAC10 are given with their respective colors in Table 4.3. The estimated free energy of binding (ΔG) and inhibition constant (K_i) of the known compounds and the docked compounds are shown in Table 4.4 below. A total of nine compounds showed potential selectivity towards their targets HDAC6 and HDAC10 according to their calculated binding energy and estimated inhibition constant (K_i). Five compounds for HDAC6 and four compounds showed selectivity for HDAC10. Compounds Asinex_Imm3320, Nih4_13387, Enzo_190, and ZINC000103531486 showed the highest binding affinity and selectivity for HDAC6 whereas, Asinex_Imm2279, Targeted_Onc758, and ZINC000245284480 showed high selectivity for HDAC10. Asinex_Imm3320 was found to show ~300-fold high selectivity, the compound Nih4_13387 showed ~10-fold high selectivity, Enzo_190 showed ~35-fold high selectivity, and ZINC000261366012 showed ~1-fold high selectivity for HDAC6. Asinex_Imm2279 calculated to have the highest binding affinity among all the other potential compounds, with a binding energy of -17.73 kcal/mol and an inhibitory constant of 0.1 pM (0.0001 nM) showing ~10-fold high selectivity over HDAC6. The second-best compound, Targeted_Onc758 showed the second-highest affinity and selectivity for HDAC10, with a binding energy of -16.65 kcal/mol and an inhibitory constant of 0.62 pM (0.00062 nM) displaying ~20 to 200-fold high selectivity for HDAC10 as well. The compound ZINC000245284480 also showed a promising selectivity for HDAC10 ranging from ~ 60-fold compared to HDAC6.

Table 4. 3 Calculated binding energy of the hit compounds by AutoDock 4.2 against HDAC6 and HDAC10. HDAC6 - selective compounds are in pink color, HDAC10 – selective compounds are in blue.

#	Compound Name	HDAC6	HDAC10
		ΔG (kcal/mol)	ΔG (kcal/mol)
1	Belinostat	-9.44	-6.75
2	Rocilinostat	-7.99	-9.50
3	Asinex_Imm3320	-12.7	-9.73
4	Nih4_13387	-11.1	-8.8
5	Enzo_190	-10.96	-6.84
6	Asinex_Imm2279	-11.62	-17.73
7	Targeted_Onc758	-13.08	-16.65
8	ZINC000103531486	-14.21	-10.07
9	ZINC000245284480	-9.54	-11.58

Asinex_imm3320, Nih4_13387, and Enzo_190 compounds covered the HDAC6 active site quite smoothly. They all have an interaction with the key amino acid residues in the catalytic channel by several types of chemical interactions including salt bridge interaction, van der Waals interactions, hydrogen bonds, π -cation, π -sulfur interaction, alkyl, π -alkyl, amide- π stacked interactions, hydrogen bonds, van der Waals interactions, attractive charge, π - π stacked, π - π T-shaped and π -sigma. Compound Asinex_imm3320 interacted with the catalytic Zn^{2+} metal atom as a metal-acceptor through their carboxyl groups by covalent bonds (Figure 4.3). Also, the compound bonded to key residues HIS610, HIS 611, and TYR 782 with a conventional hydrogen bond, and additionally it has formed π - π stacked interactions with the PHE 620 and PHE 680 residues. Similarly, Nih4_13387 has formed π - π stacked interactions with PHE 620, HIS 651 and PHE 680 but also it has an additional π - π stacked interaction with the residue HIS 500 as well. Also, there is an extra conventional hydrogen bonding with the nitrogen atom in the benzene ring to SER 568 residue. Interestingly, Enzo_190 has two additional distinctive interactions through Zn^{2+} ion and HIS 610 forming attractive charges together. Also, π -alkyl interactions with PRO 501 and LEU 749, conventional hydrogen bond with SER 568 and π - π stacked and π - π T-shaped

interactions with the key amino acid residues which are HIS 500, HIS 651, PHE620, and PHE 680.

Moreover, the Asinex_imm2279 compound spanned the hallow catalytic part of the active site of HDAC10, where they interacted with most of the key amino acid residues in the pocket. It has formed conventional hydrogen bonds with GLU 22 and TYR 305 residues, and also a π -sigma bond with the nitrogen at the backbone of the molecule with TRP 203 residue. Lastly, the compound Targeted_Onc758 has shown two π - π T-shaped bonding with PHE 202 residue and one conventional hydrogen bonding with a nitrogen atom to the ARG 196 residue.

Table 4. 4 Calculated binding energy (ΔG) and inhibition constant (K_i) of the 5-selected known HDAC6-selective and 5-selected known HDAC10-selective inhibitors compared with 7- potential selective lead compounds (highlighted in bold) identified through structure-based virtual screening (exceptional K_i values indicated as picoMolar (pM)).

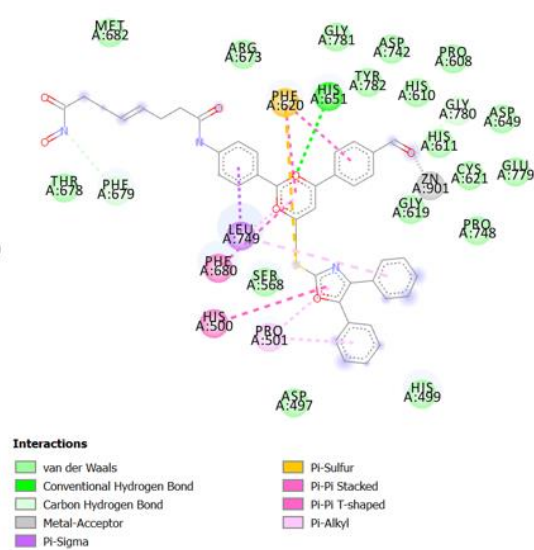
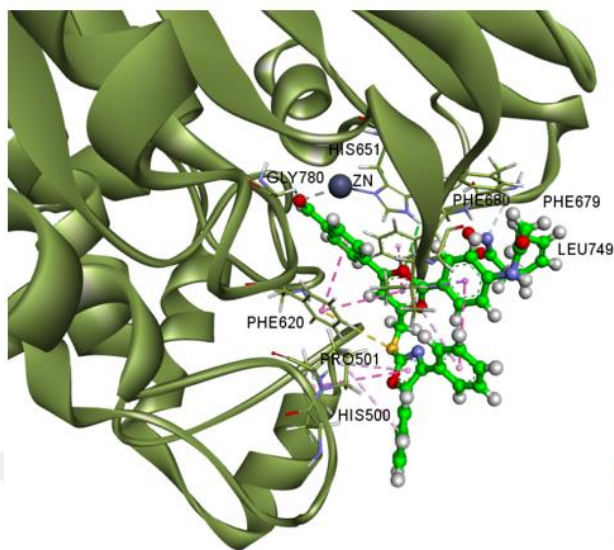
Compound Name	HDAC6		HDAC10	
	ΔG (kcal/mol)	K_i (nM)	ΔG (kcal/mol)	K_i (nM)
Tubacin	-10.17	35.36	-9.84	13.38
Tubastatin A	-10.50	20.27	-10.21	32.91
Citarinostat	-9.32	147.31	-9.81	64.61
Rocilinostat	-7.99	1390	-9.50	109.04
Nexturastat A	-9.19	183.18	-8.52	569.23

Belinostat	-9.44	119.44	-6.75	11.270
Quisinostat	-9.30	151.93	-9.80	65.36
Pracinostat	-9.43	121.47	-8.88	309.62
Abexinostat	-9.75	71.28	-9.20	181.30
CUDC_101	-9	253.96	-8.46	632.40
Asinex_Imm3320	-12.7	0.49	-9.73	193.5
Nih4_13387	-11.1	448.94	-8.8	3.083
Enzo_190	-10.96	9.24	-6.84	315.3
Asinex_imm2279	-11.62	1.43pM	-17.73	0.1pM
Targeted_Onc758	-13.08	260.26pM	-16.65	0.62pM
ZINC000103531486	-14.21	38.52pM	-10.07	0.03
ZINC000245284480	-9.54	199.8	-11.58	3.27

a) **Tubacin**

3D

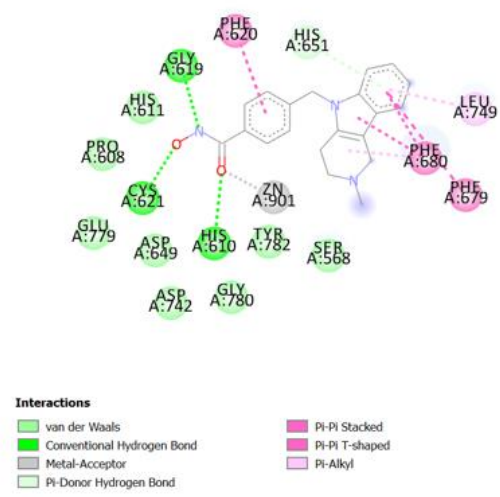
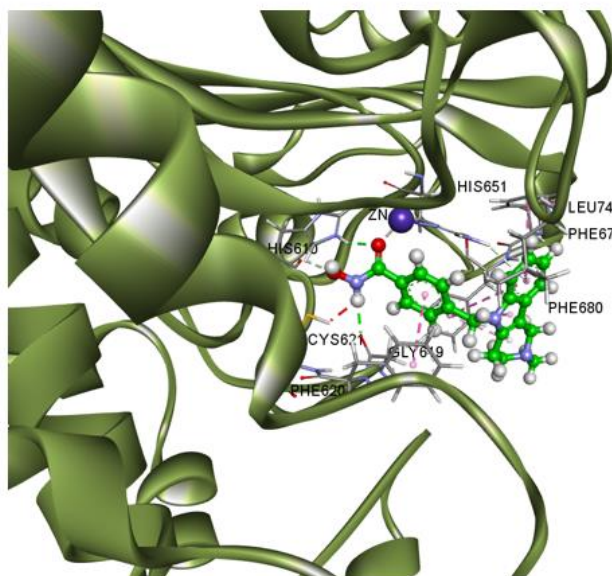
2D



b) **Tubastatin A**

3D

2D



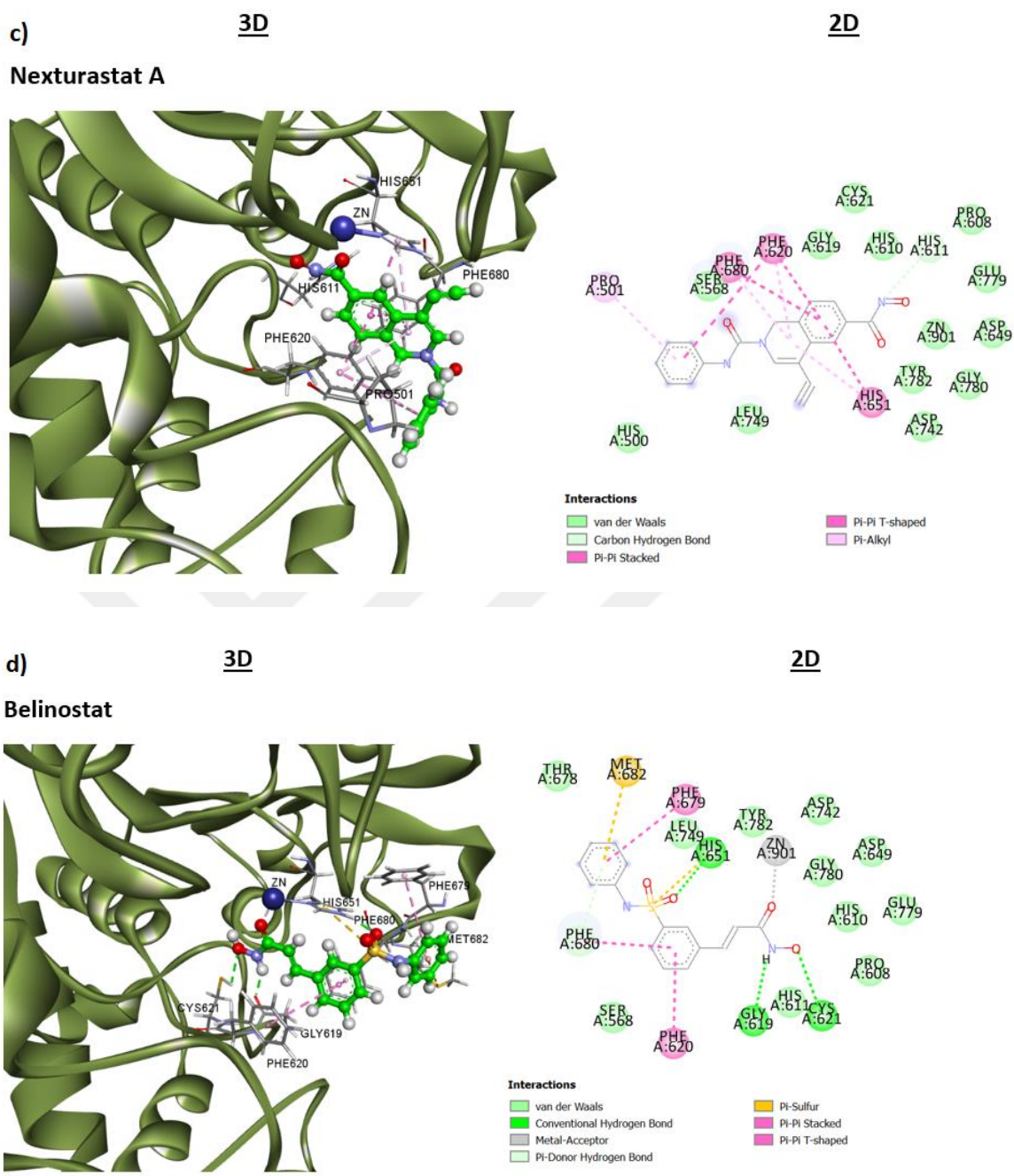


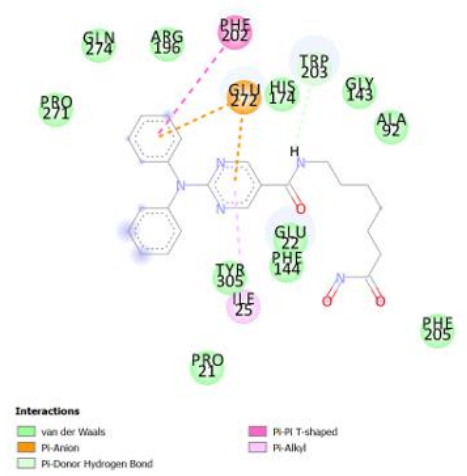
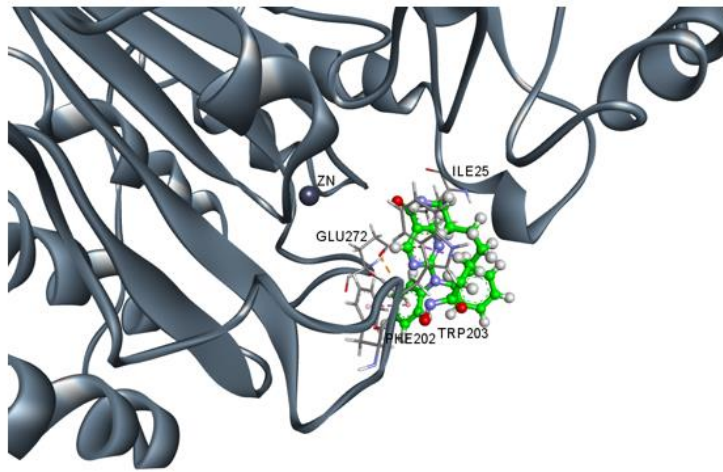
Figure 4. 4 Binding modes of known HDAC6 inhibitors with human HDAC6 (5EDU); Tubacin (a), Tubastatin A (b), Nexturastat A (c), Belinostat (d).

a)

3D

2D

Rocilinostat



b)

3D

2D

Quisinostat

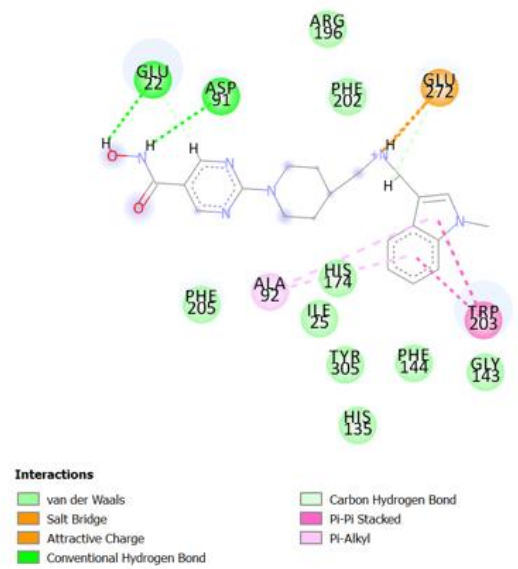
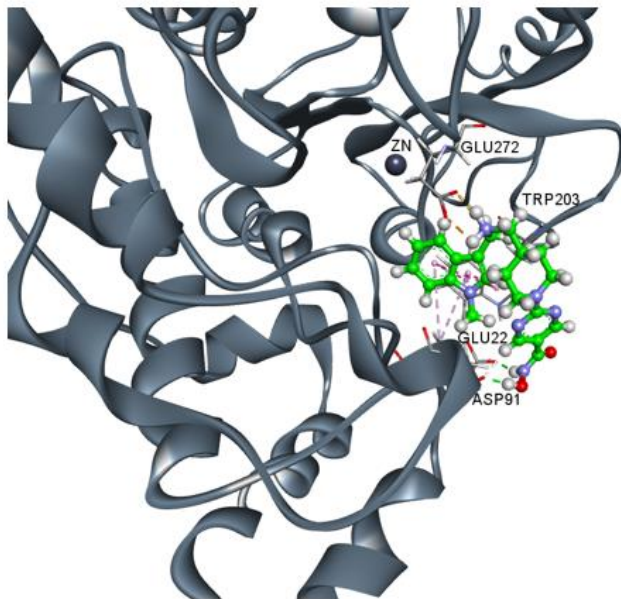




Figure 4. 5 Binding modes of known HDAC10 inhibitors with human HDAC10 homology model; Rocilinostat (a), Quisinostat (b), Citarinostat (c), Abexinostat (d).

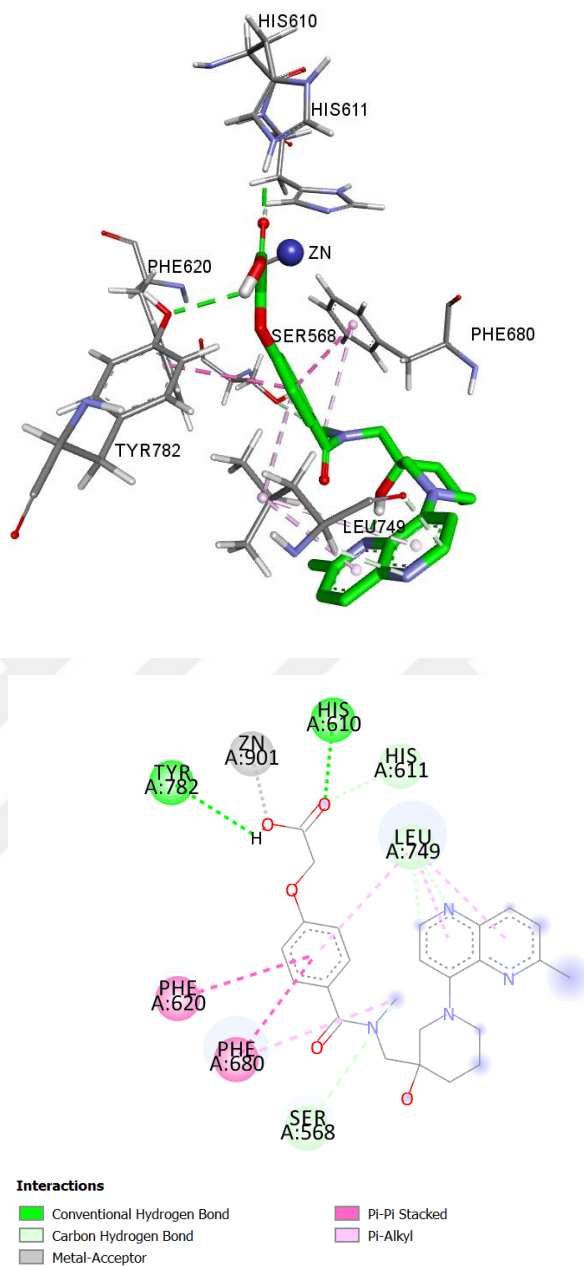


Figure 4. 6 3D (upper) and 2D (lower) representations of the interaction between **HDAC6** and **Asinex_imm_3320**; the types of nonbonded interactions are indicated as respective colors in the 2D scheme.

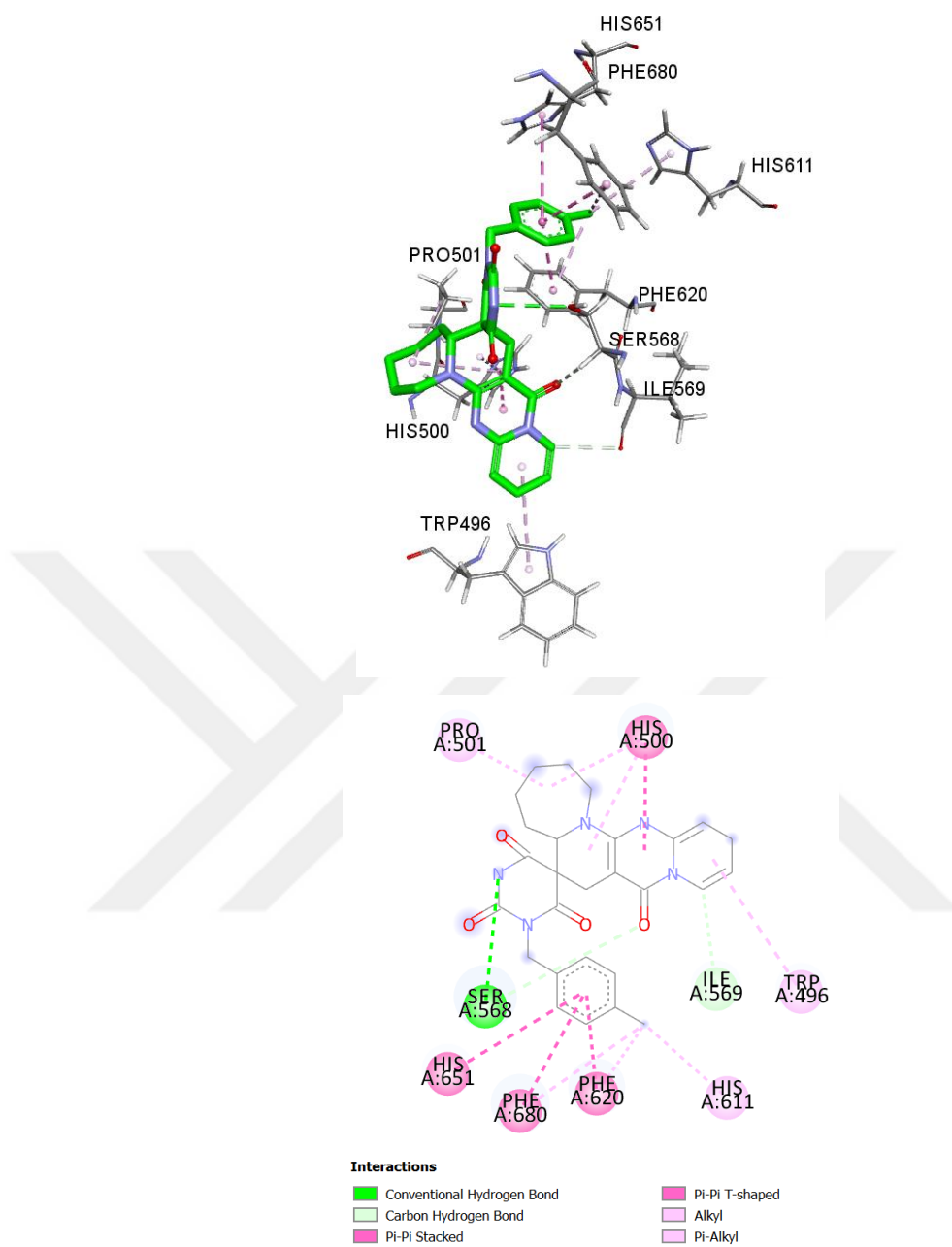


Figure 4. 7 3D (upper) and 2D (lower) representations of the interaction between **HDAC6** and **Nih4_13387**; the types of nonbonded interactions are indicated as respective colors in the 2D scheme.

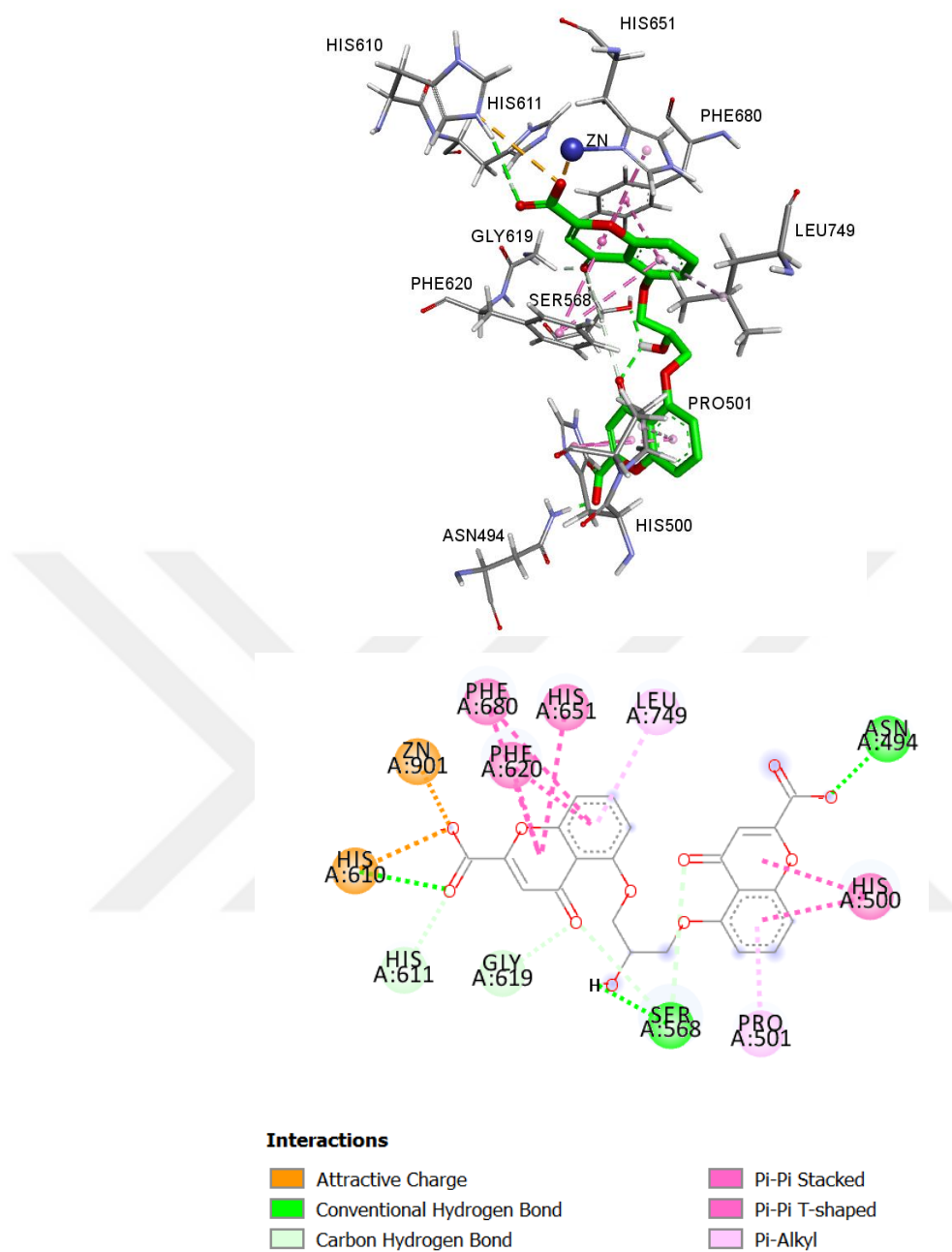


Figure 4. 8 3D (upper) and 2D (lower) representations of the interaction between **HDAC6 and Enzo_190**; the types of nonbonded interactions are indicated as respective colors in the 2D scheme.

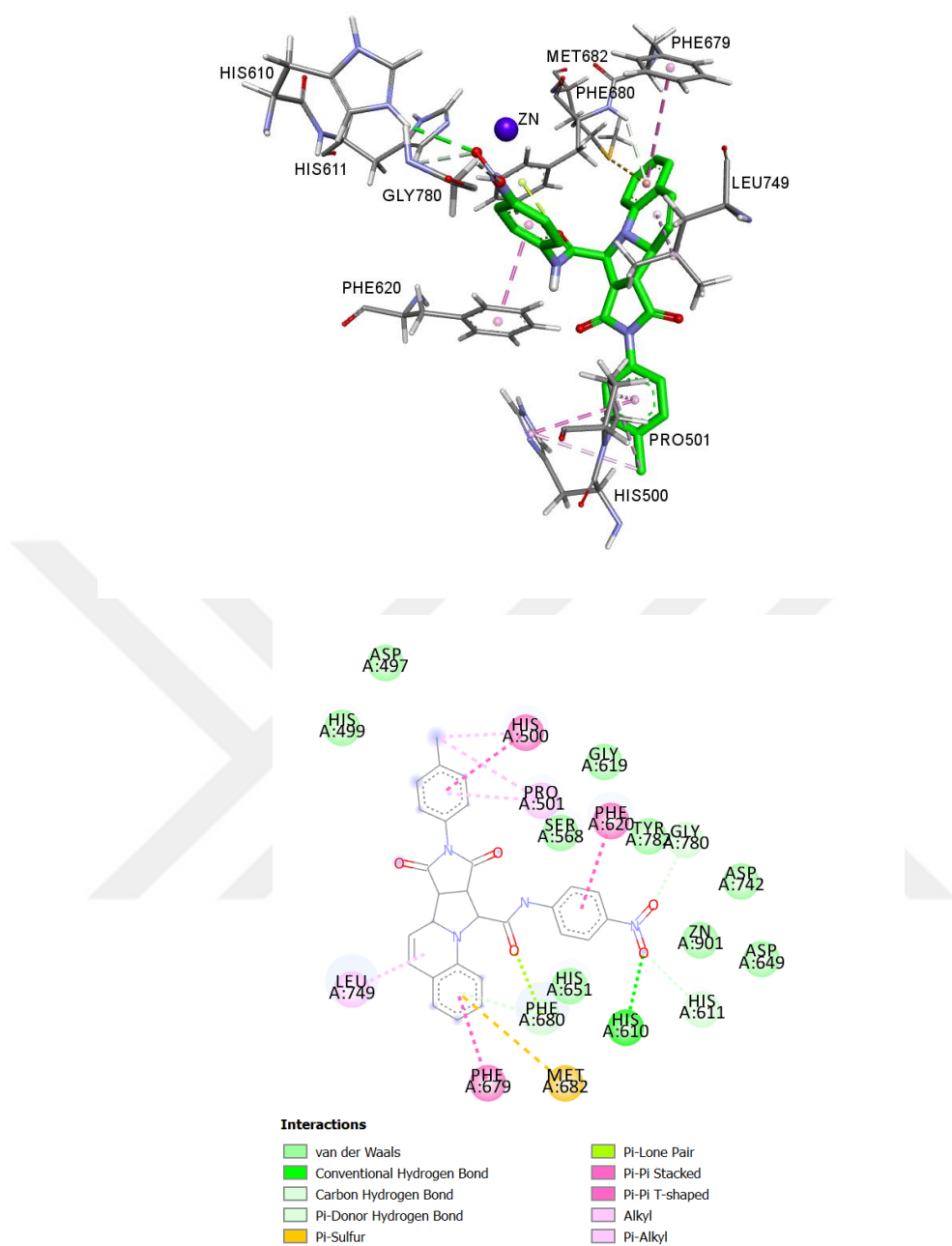


Figure 4. 6 3D (upper) and 2D (lower) representations of the interaction between HDAC6 and ZINC000103531486; the types of nonbonded interactions are indicated as respective colors in the 2D scheme.

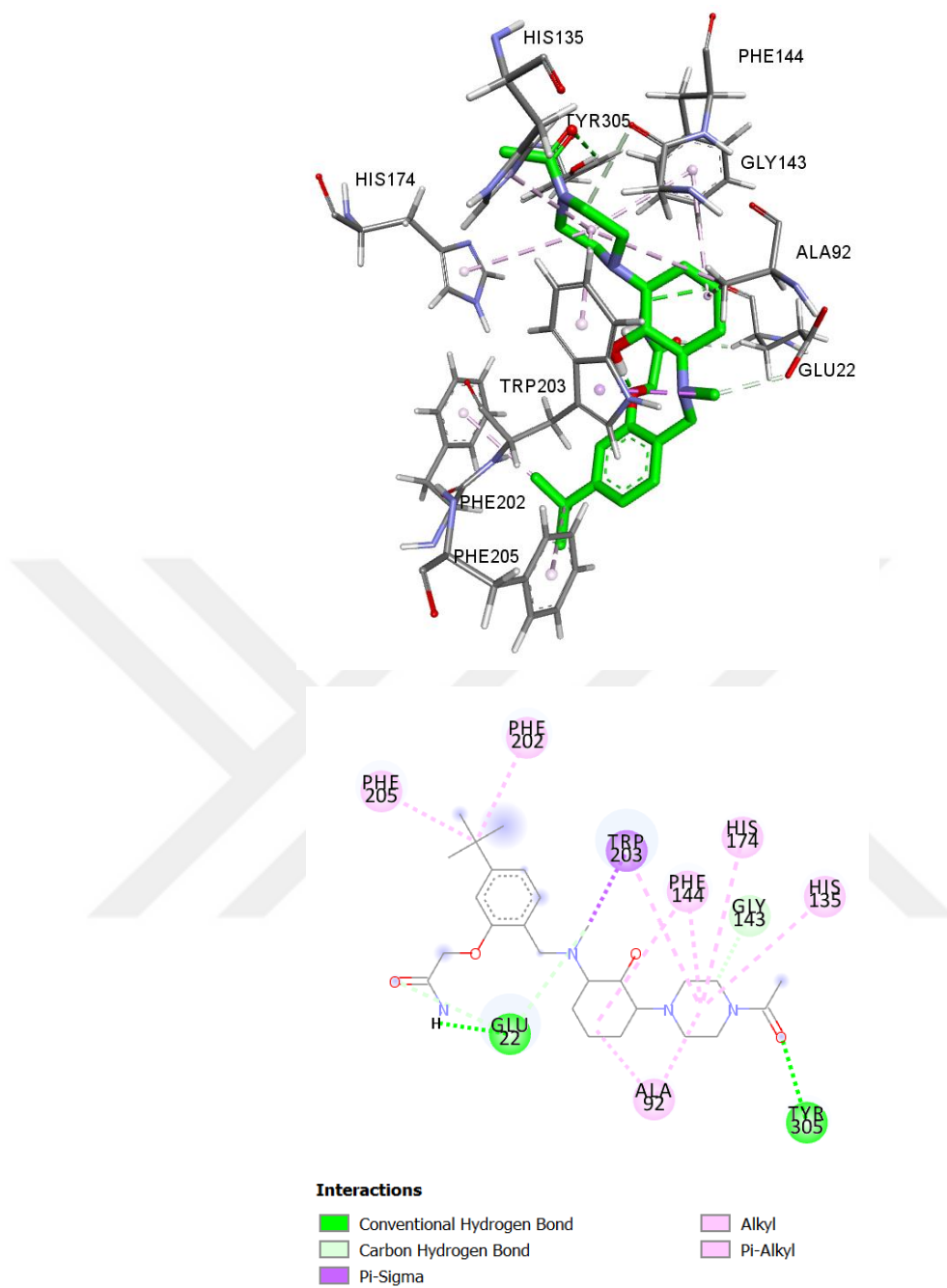


Figure 4. 7 3D (upper) and 2D (lower) representations of the interaction between **HDAC10** and **Asinex_imm_2279**; the types of nonbonded interactions are indicated as respective colors in the 2D scheme.

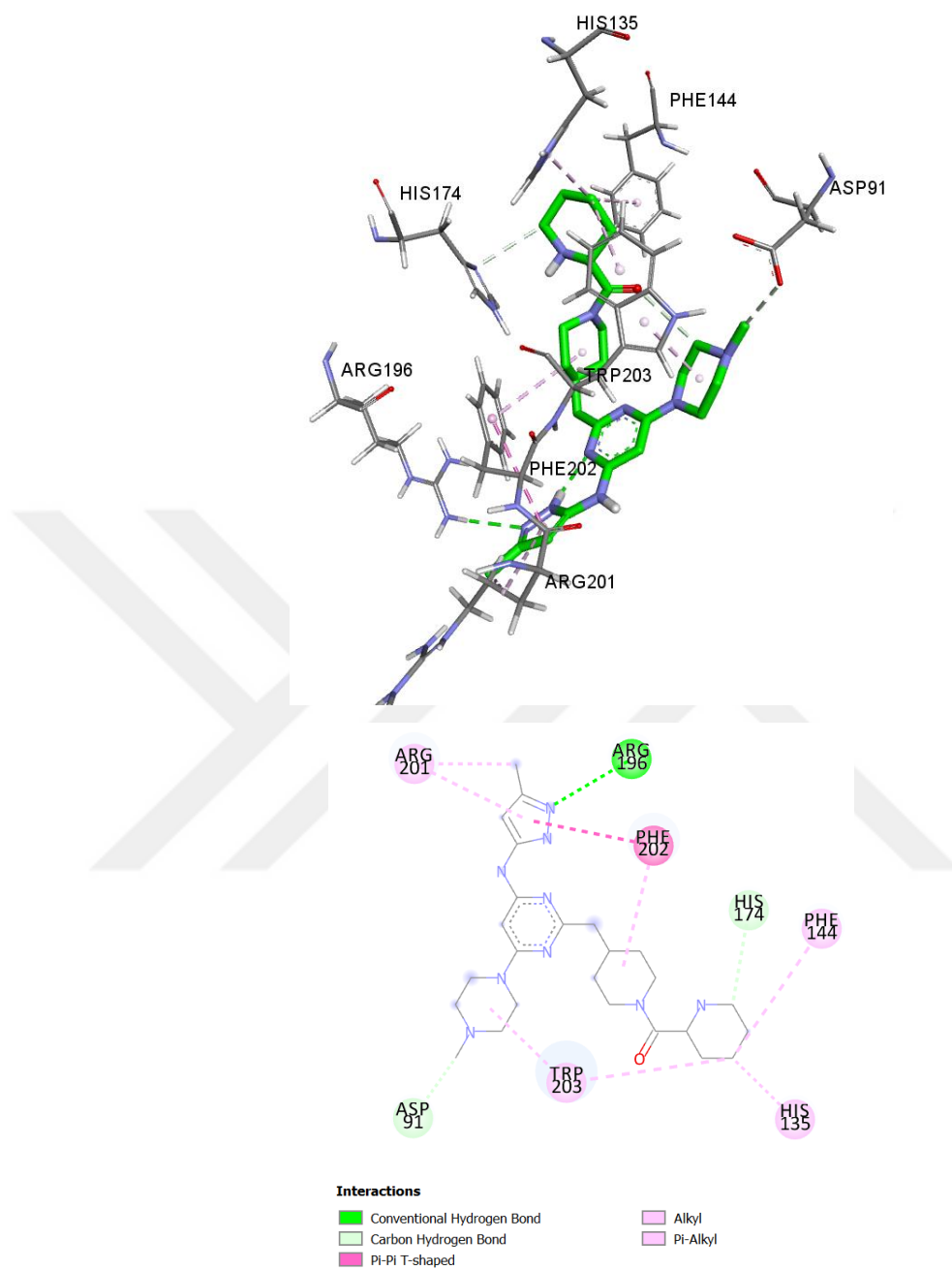


Figure 4. 8 3D (upper) and 2D (lower) representations of the interaction between **HDAC10** and **Targeted_onc_758**; the types of nonbonded interactions are indicated as respective colors in the 2D scheme.

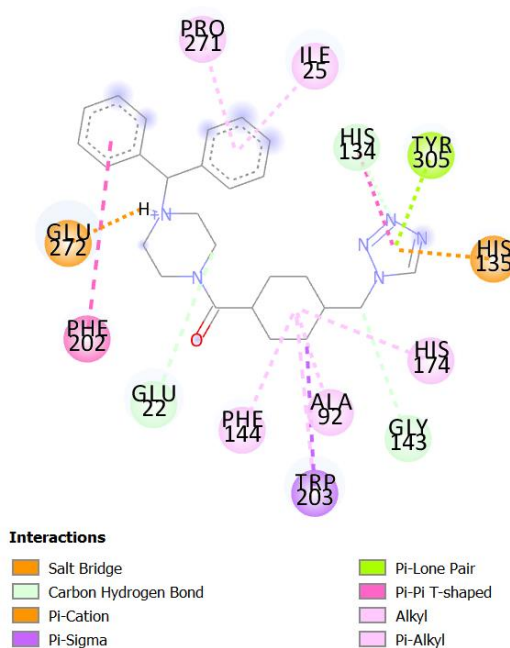
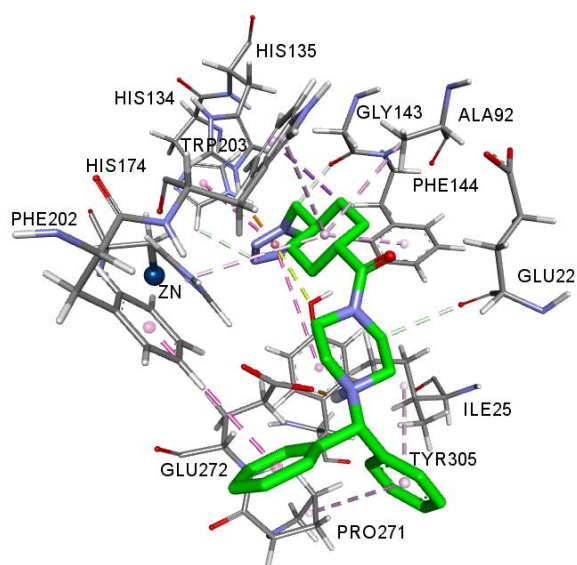


Figure 4. 9 3D (upper) and 2D (lower) representations of the interaction between **HDAC10** and **ZINC000245284480**; the types of nonbonded interactions are indicated as respective colors in the 2D scheme.

4.3 Drug-Likeliness and ADMET Prediction Analysis

The predicted drug-like and ADMET properties of the top 36 compounds from cancer-like libraries shown in Table 4.5 and 18 hit compounds from the ZINC library were depicted in Table 4.6 showing their physiochemical properties as well. AdmetSAR and SwissADME are the online servers that were used to predict these properties. All the 36 compounds from cancer-like libraries and 18 hit compounds from the ZINC library were obeyed the “Rule of 5” since the drug-like molecules can pass the rule with no more than one violation (Lipinski, 2004).

Table 4. 5 Drug-likeliness and ADMET properties of 36 hit compounds of cancer-like libraries using AdmetSAR and SwissADME.

	Compound Name	Lipinski RO_5	MlogP	Aq. Sol. (logS)	Mwt (Da)	HA	HD	TPSA (Å ²)	Caco-2 perm. (cm/s)	HIA+
1	Targeted_Onc756	0	1.23	-2.4295	481.64	6	3	105.31	0.1402	0.9935
2	DrugCentral 872	0	3.45	-4.2153	302.32	3	1	54.37	0.9325	0.9930
3	Enzo986	0	3.32	-2.1831	375.55	3	1	97.02	1.0191	0.9603
4	Asinex_imm3320	0	1.02	-3.4187	464.51	7	2	116.09	0.3738	0.6043
5	Asinex_imm5794	0	1.59	-3.0930	434.49	4	3	109.68	0.1776	0.9593
6	Targeted_Onc780	0	1.37	-2.6862	426.56	5	3	102.07	0.1989	0.9747
7	Art-Chem42614	0	2.93	-3.4890	383.4	3	3	98.8	0.7462	0.9950
8	Nih4_13387	0	2.1	-4.0150	485.53	5	1	104.09	0.9196	0.9811
9	Enzo190	1	-1.11	-2.9089	466.35	11	1	179.37	0.0720	0.7708
10	Nih5_8598	1	4.76	-3.8595	447.48	4	1	74.68	1.0680	0.9904
11	Nih3_29052	0	3.32	-3.9607	427.49	4	2	75.63	0.6695	0.9556
12	Nih3_14404	0	3.95	-3.6806	397.47	3	2	66.4	1.2458	0.9935
13	Nih3_20739	0	1.69	-3.3978	491.56	7	4	155.68	0.3940	0.9749
14	Nih4_35677	0	1.94	-3.4653	358.34	5	1	84.58	0.9443	1
15	Hypha128	0	2.03	-4.1283	486.61	4	3	99.87	0.6314	1
16	Nih5_8831	0	2.38	-4.1668	265.26	4	1	63.33	1.3515	1

17	Art-Chem1270	0	3.88	-4.4985	400.4	5	0	86.74	1.1891	0.9479
18	Nih5_5708	0	1.28	-3.0900	444.44	5	3	120.74	0.8091	0.9826
19	Nih3_52769	0	2.53	-3.7711	357.42	4	1	83.06	0.7684	1
20	Nih5_10577	0	1.39	-3.5610	361.37	6	2	110.31	0.4639	0.9941
21	Nih5_45964	0	4.11	-3.8890	415.27	4	1	72.19	0.7898	0.9695
22	Nih1_38075	0	1.84	-3.5795	469.55	5	1	112.24	0.4364	0.9617
23	Nih2_49030	0	3.07	-3.6420	479.48	8	1	138.11	0.6437	0.9947
24	Nih3_21656	0	2.3	-3.6924	343.4	4	1	83.06	0.7179	1
25	Asinex_imm2279	0	0.95	-3.0728	474.64	6	2	99.34	0.6080	0.7220
26	Targeted_Onc794	0	2.21	-2.3968	480.65	5	2	93.28	0.2446	0.9586
27	Targeted_Onc758	0	1.23	-2.3618	481.64	6	3	105.31	0.1762	0.9919
28	Asinex_imm4732	0	1.98	-3.3381	446.58	4	1	90.03	0.7164	0.9897
29	Hypha223	0	2.03	-4.1283	486.61	4	3	99.87	0.6314	0.9629
30	Hypha417	0	3.34	-3.0082	398.58	4	1	33.73	1.0838	0.9873
31	Art_Chem617	0	2.68	-3.7361	438.43	6	2	105.04	0.2720	0.9753
32	Nih2_22644	0	0.33	-2.5201	343.38	5	1	75.02	0.5231	0.8268
33	Nih7_43480	0	2.63	-3.3193	384.43	4	2	93.12	0.9074	0.9148
34	Nih2_42559	0	2.65	-3.6480	427.37	6	2	124.09	1.0121	1
35	Nih4_5941	0	2.95	-4.3208	458.85	6	2	105.04	0.4219	0.9642
36	Nih5_5902	0	3.81	-3.7956	496.49	6	2	95.94	0.8526	0.9271

MlogP: (Moriguchi model of octanol-water partition coefficient, LogP) ≤ 5 .

LogS: Aqueous Solubility > -5.7

MW: Molecular weight in ≤ 500 Da.

HA: Total number of H-bond acceptors, N and O ≤ 10 .

HD: Total number of H-bond donors, NH and OH ≤ 5 .

TPSA: Topological polar surface area $\leq 140 \text{ \AA}^2$

Caco-2 Permeability (LogPapp, cm/s, faster than 22 nm/s)

HIA+: Human intestinal absorption > 0.6

Table 4. 6 Drug-likeness and ADMET properties of 18 hit compounds of ZINC library using AdmetSAR and SwissADME.

	Compound Name	Lipinski RO_5	MlogP	Aq. Sol. (logS)	Mwt (Da)	HA	HD	TPSA (Å ²)	Caco-2 perm. (cm/s)	HIA+
1	ZINC000013655575	0	2.86	-3.8365	449.85	7	2	126.91	0.325	0.8426
2	ZINC000064979644	0	2.62	-4.1848	431.94	5	0	75.03	1.008	1
3	ZINC000013655575	0	2.86	-3.8746	449.85	7	2	126.91	0.3401	0.9646
4	ZINC000019712236	0	2.48	-3.3883	447.53	5	3	109	1.1262	1
5	ZINC000012882053	0	2.06	-3.7089	428.52	5	1	124.19	0.2658	0.9915
6	ZINC000101969184	0	-0.13	-1.998	445.58	4	1	68.35	0.5647	0.9308
7	ZINC000245232199	0	2.3	-3.7814	435.47	5	1	112.3	0.713	1
8	ZINC000245284480	0	-0.13	-1.998	445.58	4	1	68.35	0.5647	0.9308
9	ZINC000023075384	0	2.6	-3.4491	437.47	7	1	126.14	0.3791	1
10	ZINC000103531486	0	3.68	-3.8057	491.51	6	3	134.54	0.3489	0.9226
11	ZINC000261361753	0	2.83	-3.892	476.32	5	3	134.54	0.4175	0.8642
12	ZINC000001001148	0	2.06	-3.4029	480.47	5	1	119.3	0.5576	0.9973
13	ZINC000014745209	0	-0.43	-3.5277	470.58	3	1	58.2	1.0745	0.9931
14	ZINC000257288501	0	1.71	-3.061	453.48	7	2	105.53	0.6002	0.7519
15	ZINC000257333130	0	1.71	-3.061	453.48	7	2	105.53	0.6002	0.7519
16	ZINC000103531486	0	2.73	-3.4418	494.5	5	1	115.54	1.1473	1
17	ZINC000040156325	0	3	-3.7806	455.91	5	3	120.53	-0.1317	0.9901
18	ZINC000257209181	0	1.92	-3.017	467.51	7	1	94.53	0.9526	0.7153

MlogP: (Moriguchi model of octanol-water partition coefficient, LogP) ≤ 5.

LogS: Aqueous Solubility > -5.7

MW: Molecular weight in ≤ 500 Da.

HA: Total number of H-bond acceptors, N and O ≤ 10.

HD: Total number of H-bond donors, NH and OH ≤ 5.

TPSA: Topological polar surface area ≤ 140 Å²

Caco-2 Permeability (LogPapp, cm/s, faster than 22 nm/s)

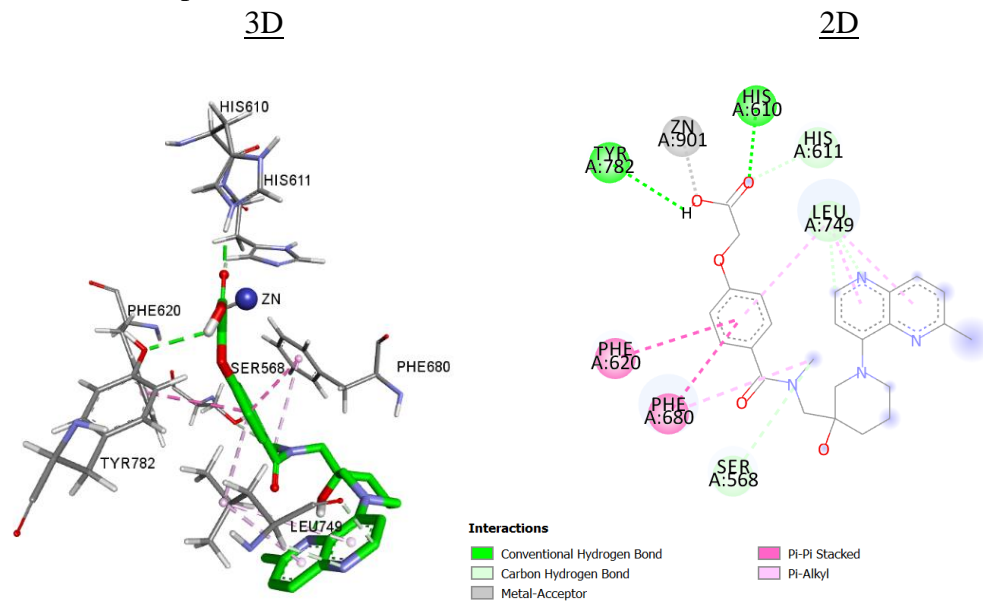
HIA+: Human intestinal absorption > 0.6

4.4 Molecular Dynamics Simulation Analysis

The structural stability of the free form of HDAC6 and HDAC10, with their known inhibitors and their complexes; HDAC6_Asinex_imm3320, HDAC6_Nih4_13387, HDAC6_Enzo190, HDAC6_ZINC000103531486, HDAC10_Asinex_imm2279, HDAC10_Targeted_Onc758, and HDAC10_ZINC000245284480 were analyzed to estimate their RMSD, RMSF, Rg and potential energy (PE) profiles along 100 ns MD simulations.

Binding modes of the docked and simulated complexes are shown in the Figures below. After 100ns simulation, the orientation of the HDAC6_Asinex_imm3320 complex remained almost same in the 3D space and the complex having bulky cap group stuck at the entrance to the channel and bound with zinc metal ion in the deep pocket with a strong metallic interaction with carboxyl group. The same carboxyl group ionized and interacted with HIS610 with a H-bond in the deep catalytic channel as shown in the 2D scheme. HDAC6 with Nih4_13387 showed the same 3D orientation with its docked complex, only it is observed that the SER 568 residue lost its interaction in the simulated complex. HDAC6 and Enzo_190 complex seemed to lost its pi-pi sigma interactions after the simulation and also showing a more relaxed binding mode to the enzyme. Instead of ASN 494, in the capping moiety carbonyl grouped found out to make an attractive charge with the ARG 673 residue at the entrance of the pocket. HDAC6 and ZINC000103531486 showed the same binding pose throughout the simulation, however we see that Pi-sulphur interactions with MET 682 group has disappeared with time. The interaction with GLU 22 via the nitrogen has lost within the simulation of HDAC10_Asinex_imm2279 causing a more relaxed orientation for the ligand. Similarly, the nitrogen atom on the imidazole ring of Targeted_onc758 compound with ARG 196 residue has faded away. Lastly, HDAC10 and ZINC000245284480 complex lost its some interactions showed in its 2D scheme and but still kept its 3D orientation as same with time forming some more Van der Waals interactions.

a) Docked Complex



b) Simulated Complex

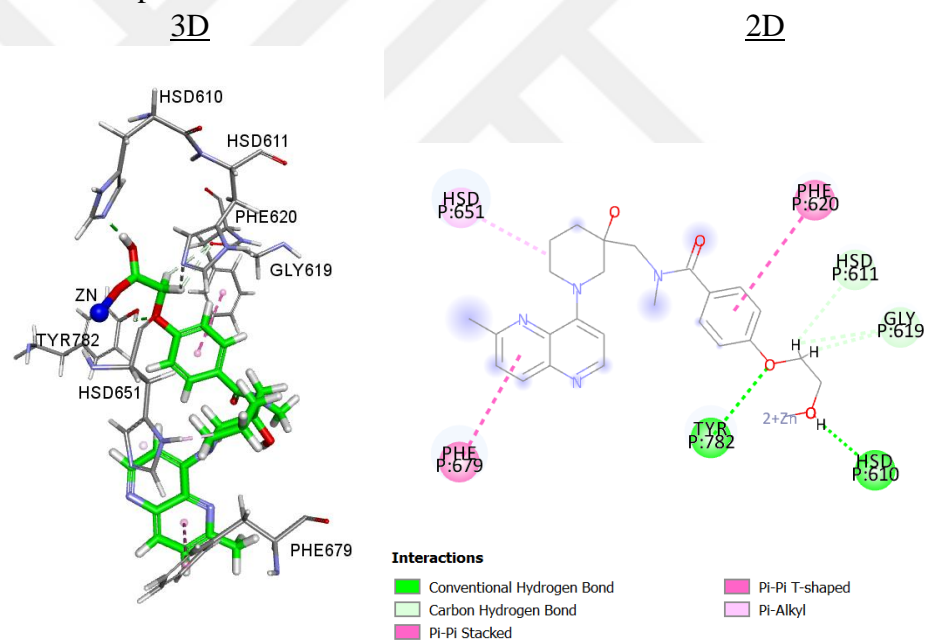
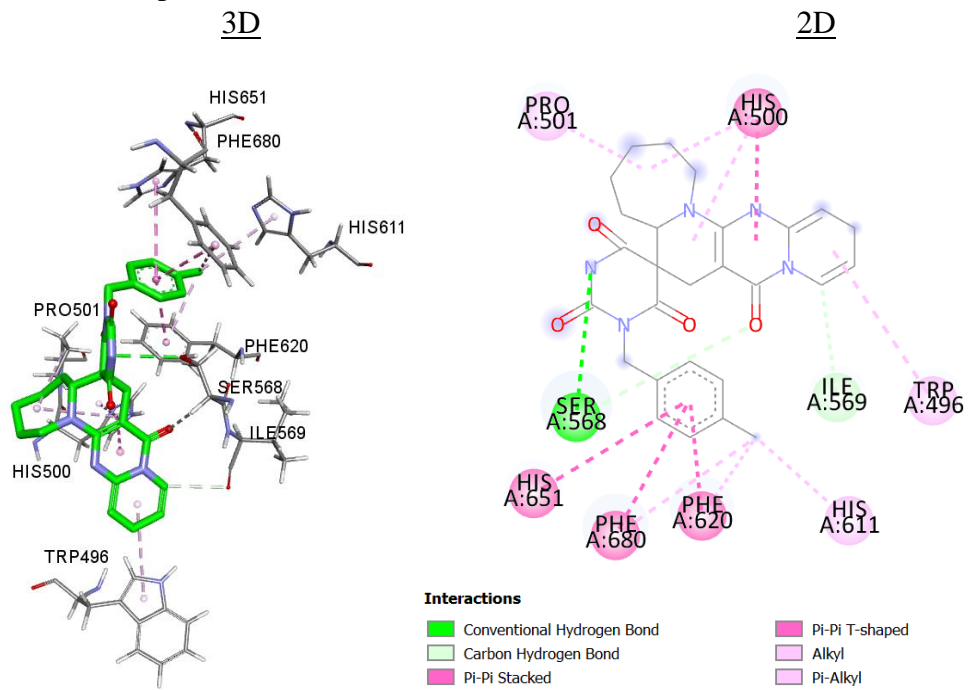


Figure 4.10 Benchmarking of the binding modes of docked (a) and simulated (b) complexes of **HDAC6** and **Asinex_imm3320** through their 2D and 3D schemes with 100 ns MD simulation.

a) Docked Complex



b) Simulated Complex

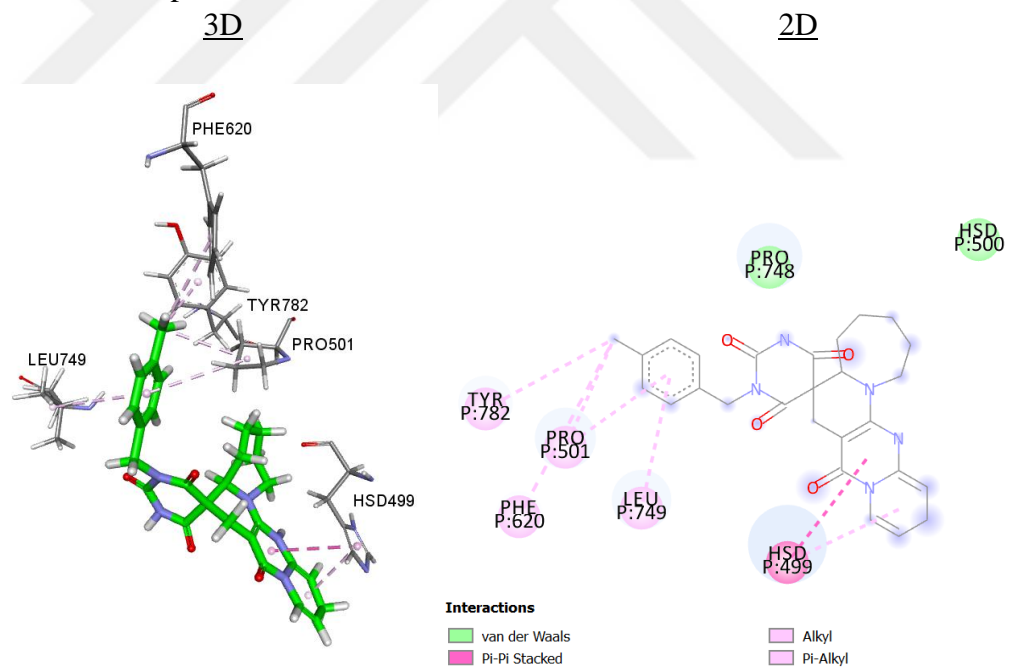
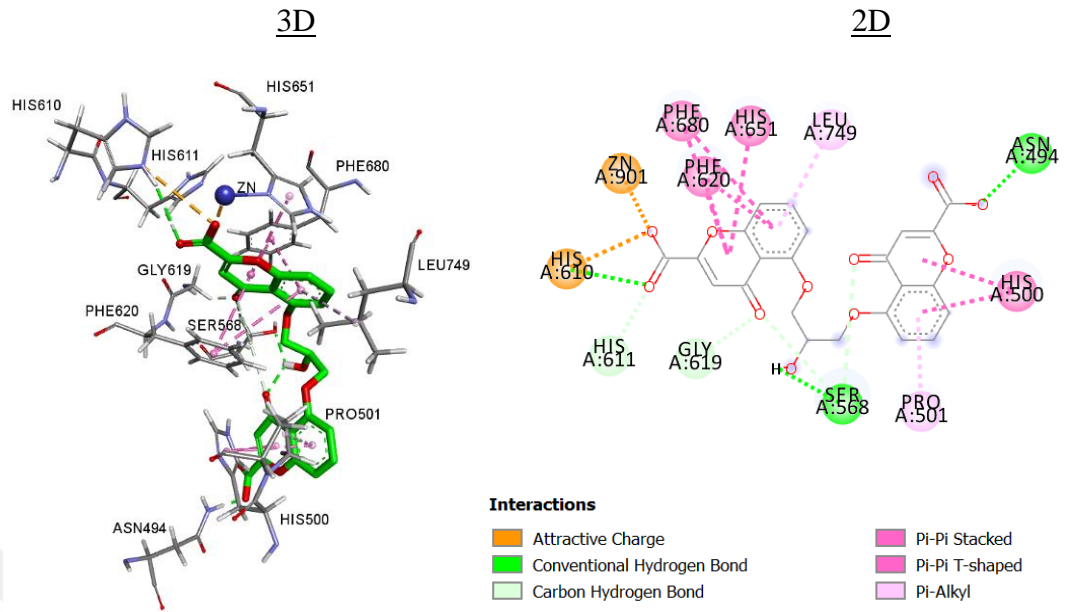


Figure 4.11 Benchmarking of the binding modes of docked (a) and simulated (b) complexes of **HDAC6** and **Nih4_13387** through their 2D and 3D schemes with 100 ns MD simulation.

a) Docked Complex



b) Simulated Complex

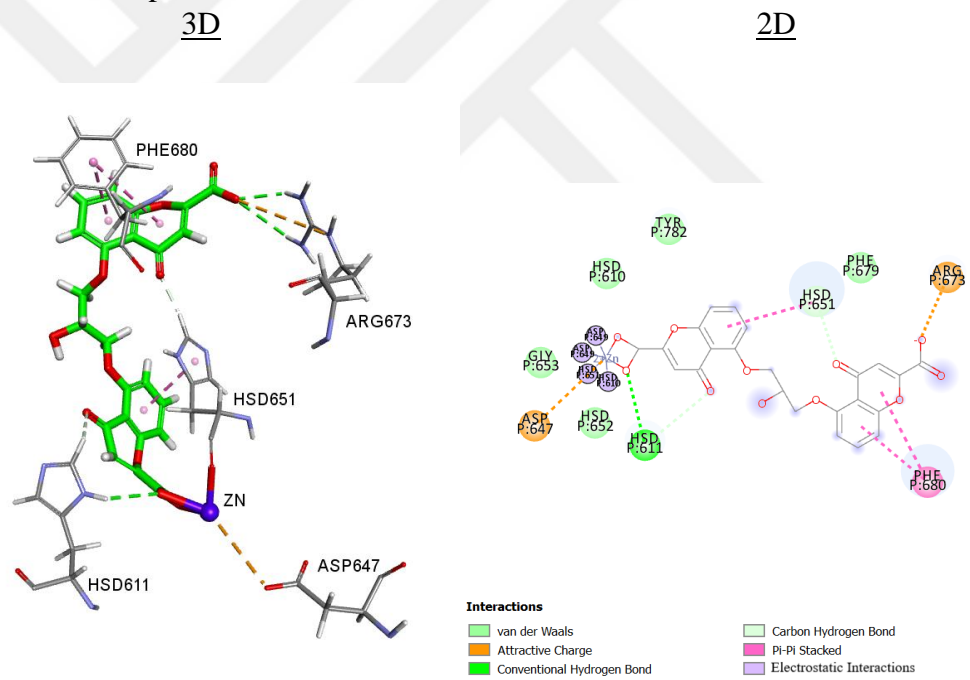
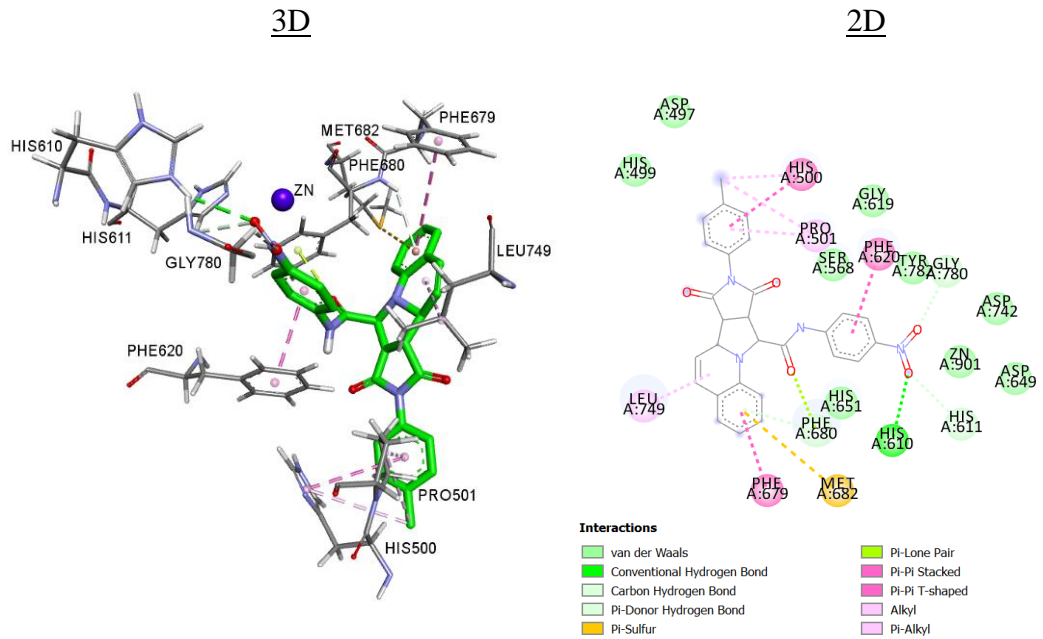


Figure 4.12 Benchmarking of the binding modes of docked (a) and simulated (b) complexes of **HDAC6** and **Enzo_190** through their 2D and 3D schemes with 100 ns MD simulation.

a) Docked Complex



b) Simulated Complex

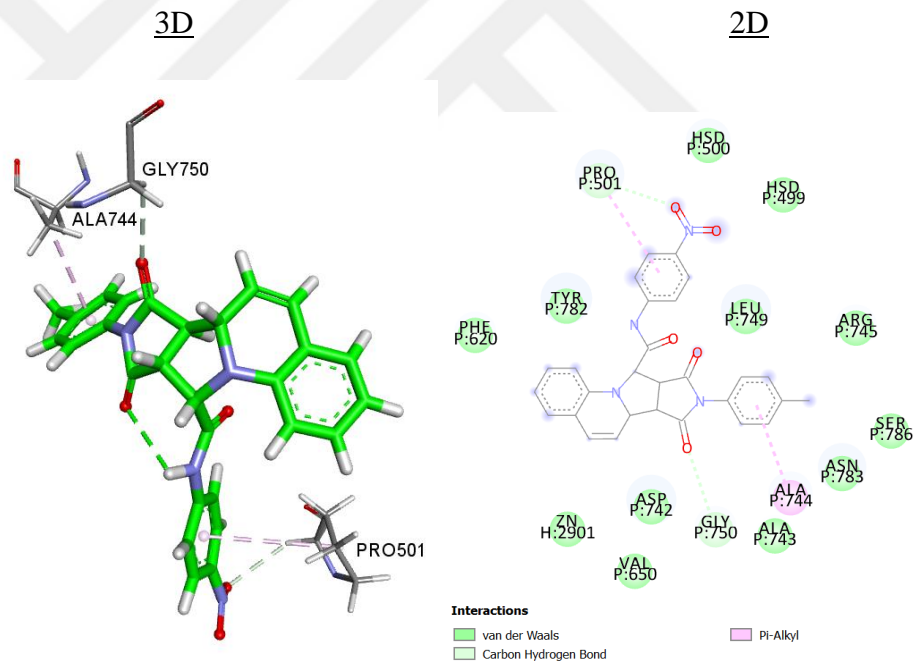
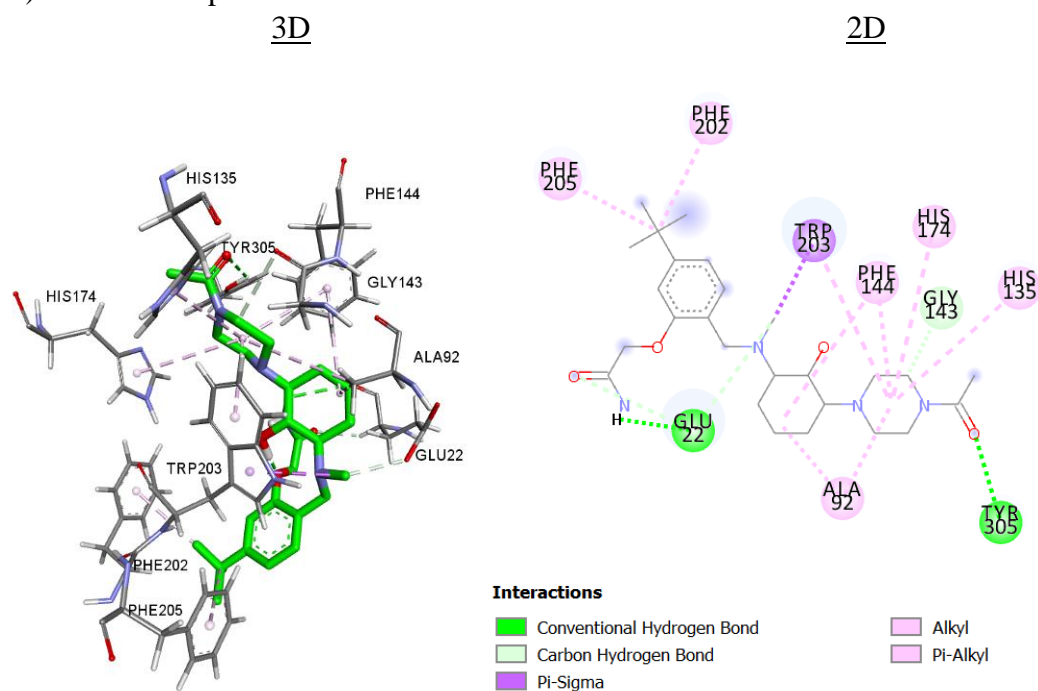


Figure 4.13 Benchmarking of the binding modes of docked (a) and simulated (b) complexes of **HDAC6** and **ZINC000103531486** through their 2D and 3D schemes with 100 ns MD simulation.

a) Docked Complex



b) Simulated Complex

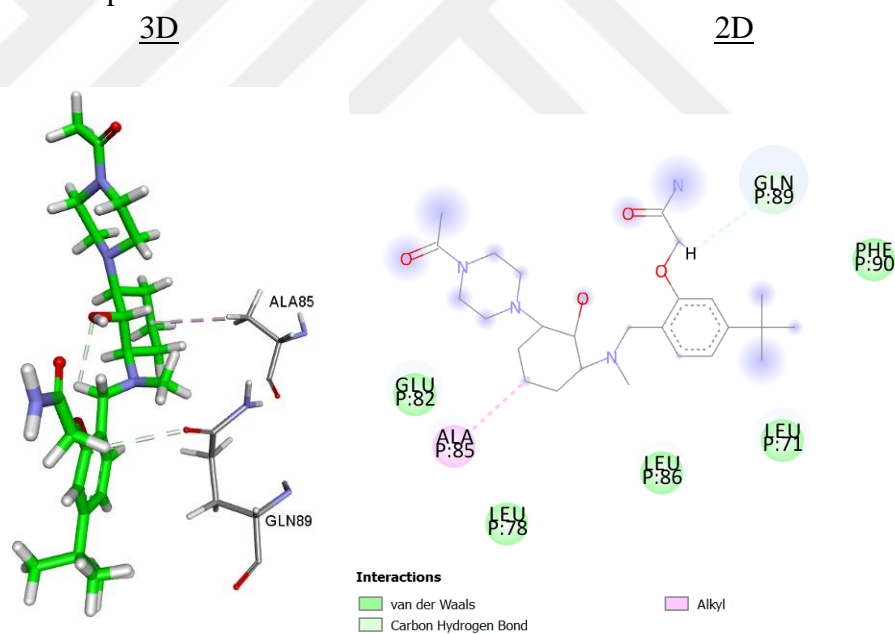
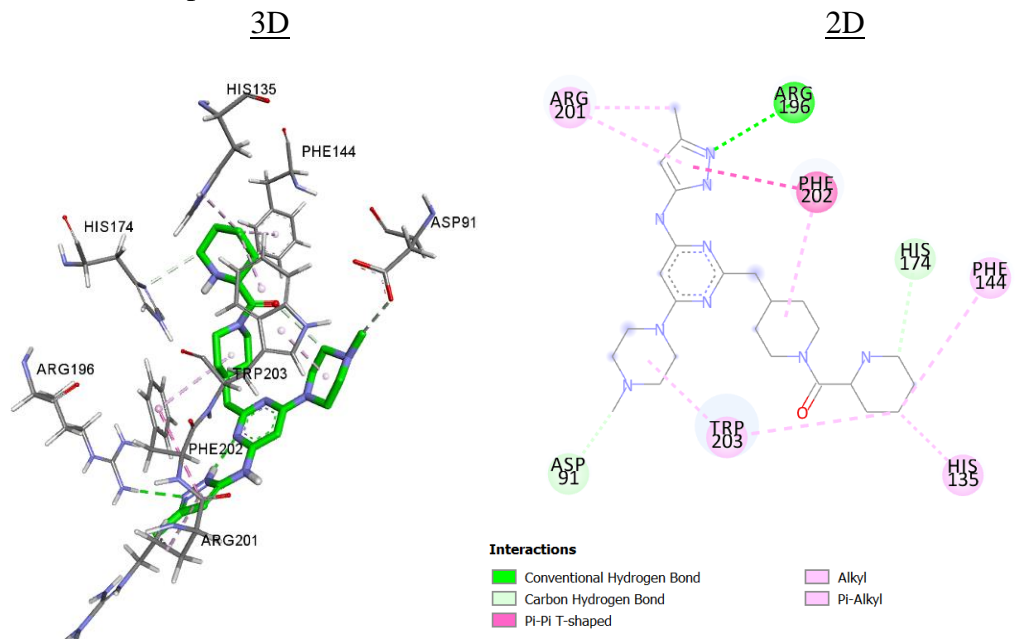


Figure 4.14 Benchmarking of the binding modes of docked (a) and simulated (b) complexes of **HDAC10 and Asinex_imm2279** through their 2D and 3D schemes with 100 ns MD simulation.

a) Docked Complex



b) Simulated Complex

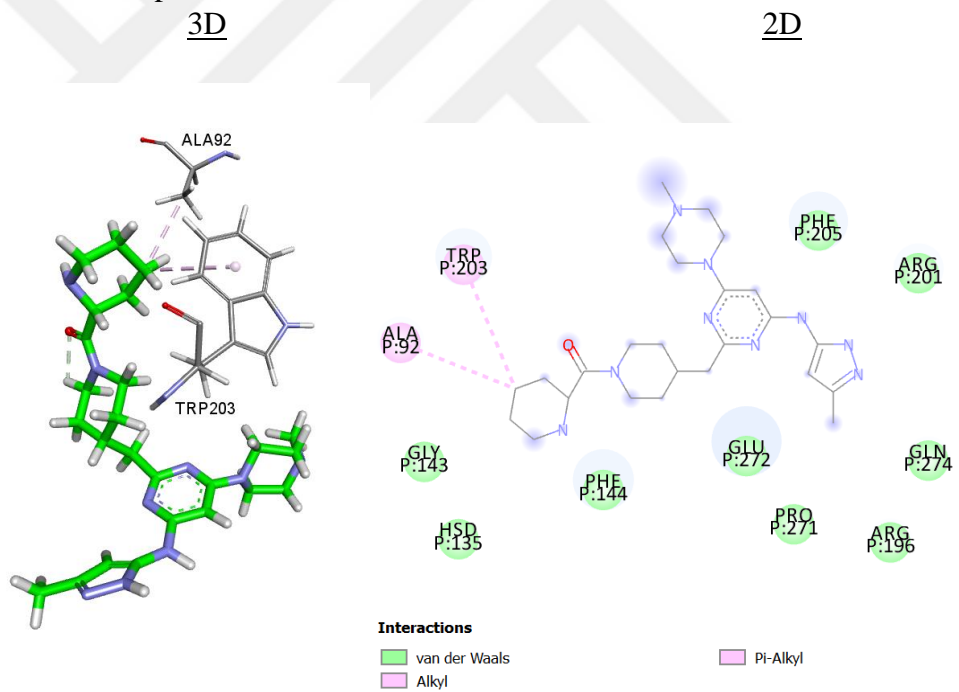
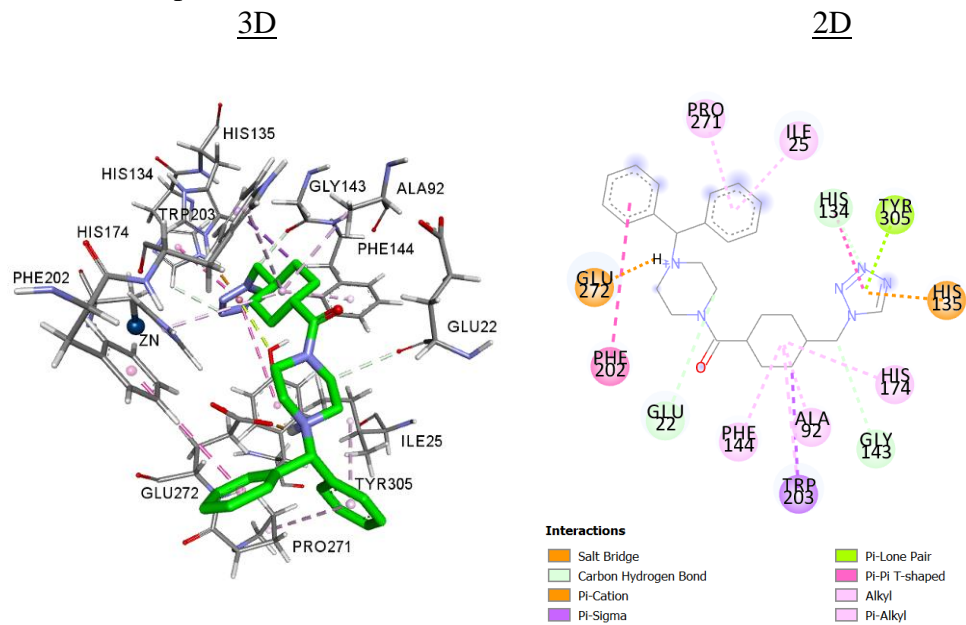


Figure 4.15 Benchmarking of the binding modes of docked (a) and simulated (b) complexes of **HDAC10** and **Targeted_onc758** through their 2D and 3D schemes with 100 ns MD simulation.

a) Docked Complex



b) Simulated Complex

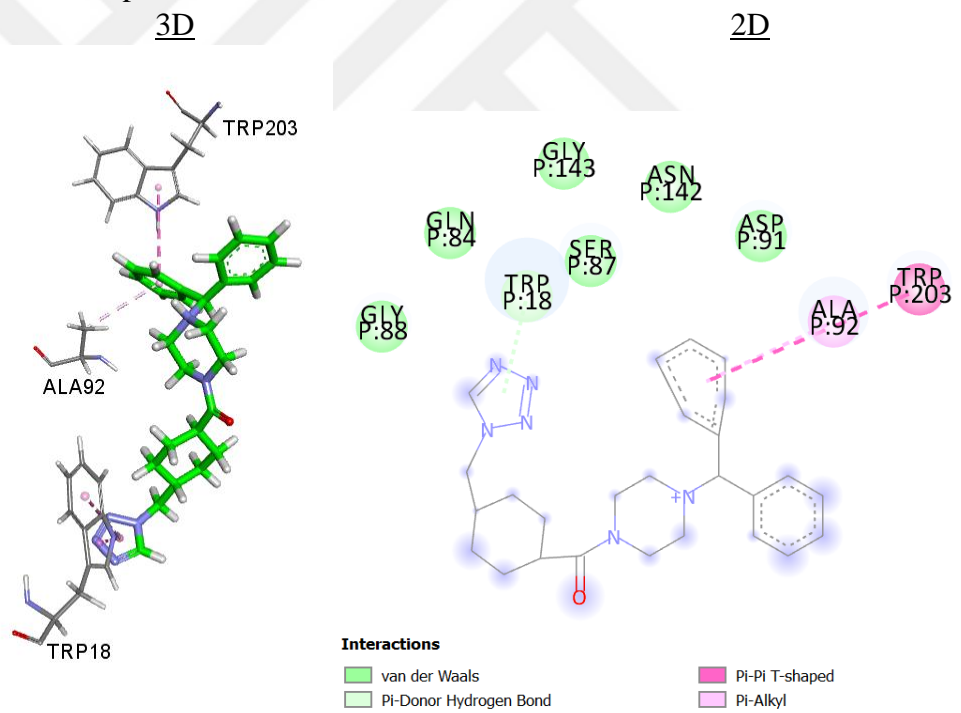


Figure 4.16 Benchmarking of the binding modes of docked (a) and simulated (b) complexes of **HDAC10** and **ZINC000245284480** through their 2D and 3D schemes with 100 ns MD simulation.

RMSD Analysis: The root mean squared deviation graphs of the free HDAC6 enzyme, HDAC6 with TSN and its complex systems with Asinex_imm3320, Nih4_13387, Enzo190, and ZINC000103531486, free form of HDAC10 enzyme, HDAC10 with Rocilinostat and its complex systems with Asinex_imm2279, Targeted_Onc758, and ZINC000245284480 are shown in Figure 4.17. All the studied systems showed a constant equilibrium state throughout the MD simulations. The RMSD of the free HDAC6 enzyme and its known inhibitor TSN slowly and steadily increased from $\sim 2\text{\AA}$ to $\sim 3\text{\AA}$ throughout the whole 100 ns of the MD run. The RMSD of HDAC6 with the Asinex_imm3320 complex rose from $\sim 1.5\text{\AA}$ to $\sim 2.8\text{\AA}$ with the entire MD run and the RMSD remained stable until the end. HDAC6 with Nih4_13387 complex showed a steady RMSD profile in the first 40 ns run with an RMSD average of 2\AA to 2.8\AA , then the systems' RMSD increased up to $\sim 3.2\text{\AA}$ between 50-70 ns and started gradually decreasing around 2.5\AA in 85 ns. After that, the system slowly increased and finally stabilized with an average RMSD of $\sim 2.8\text{\AA}$ after 90 ns of the simulation. HDAC6 with Enzo190 complex showed a stable increase RMSD profile starting from 1.8\AA to 3\AA overtime of the 100 ns MD run. Similarly, the HDAC6_ZINC000103531486 complex showed a steady RMSD profile ranging from 1.5\AA to 3\AA with an equilibrium state until the end of 100 ns. As expected, the apo form of HDAC10 displayed a fluctuating RMSD profile around 2\AA to 7\AA throughout the first 70 ns but reached the equilibration in an average of 5.2\AA until the end of the MD run. HDAC10 with Rocilinostat shows a steady trend between 4\AA to 5\AA in the total simulation time. Only between 10 ns to ~ 25 ns there are some fluctuations seen. HDAC10_Asinex_imm2279 complex showed a balanced RMSD profile around 3\AA to 4.3\AA until the end of the whole MD run. Similarly, the HDAC10_Targeted_Onc758 complex showed a similar trend with the HDAC10_Asinex_imm2279 complex as it rose steadily from $\sim 2.5\text{\AA}$ to 6\AA and stabilized until the end of the simulation.

RMSF Analysis: The root mean squared fluctuation (RMSF) analysis was carried out for both HDAC6 and HDAC10 complex systems and the results are depicted in Figure 4.17. From the RMSF analysis, fluctuating amino acid residues and their movements can be inferred. It can be said that higher RMSF fluctuations occur in highly flexible

loop regions. HDAC6_Asinex_imm3320 complex system showed a lower RMSF profile compared to the system along with the MD simulation as can be seen from their respective RMSD profiles. In the HDAC6_Asinex_imm3320 complex, GLY 203, PRO 268, and LEU 326 amino acid residues were fluctuating because they were located in the loops. The RMSF investigation showed that the HDAC6_Nih4_13387 complex with only two residues namely ASP 204 and PRO 201 visibly fluctuated in the loop regions displayed relatively lower amino acid residues fluctuations of the protein compared to the other complex systems shown in the Figure 4.17 (c) and (d). HDAC6_Enzo190 complex showed amino acid fluctuations in the residues of LEU 15, ASP 204, PRO 268, and LEU 326 as they are all located in the highly movable loop regions. HDAC10_Asinex_imm2279 and HDAC10_Targeted_Onc758 complex showed relatively similar RMSF profiles with their stabilized structures. HDAC10_Asinex_imm2279 complex has ASP 20, THR 363, and CYS 388 fluctuating residues which existed in the loops, and HDAC10_Targeted_Onc758 complex has four amino acid residues fluctuating in the loop regions which are ASP 19, SER 209, VAL 362, and PRO 366 respectively. The movement of the ASP 19 residue is depicted in Figure 4.17 (c) and (d) in detail.

Rg Analysis: The radius of gyration (R_g) profile shows the protein compactness level changing during the MD simulation process. Radius of gyration is one way of representing large conformational ensemble of proteins.

For a given configuration of a protein, the R_g may be calculated as the mass-weighted root mean distance to the center of mass:

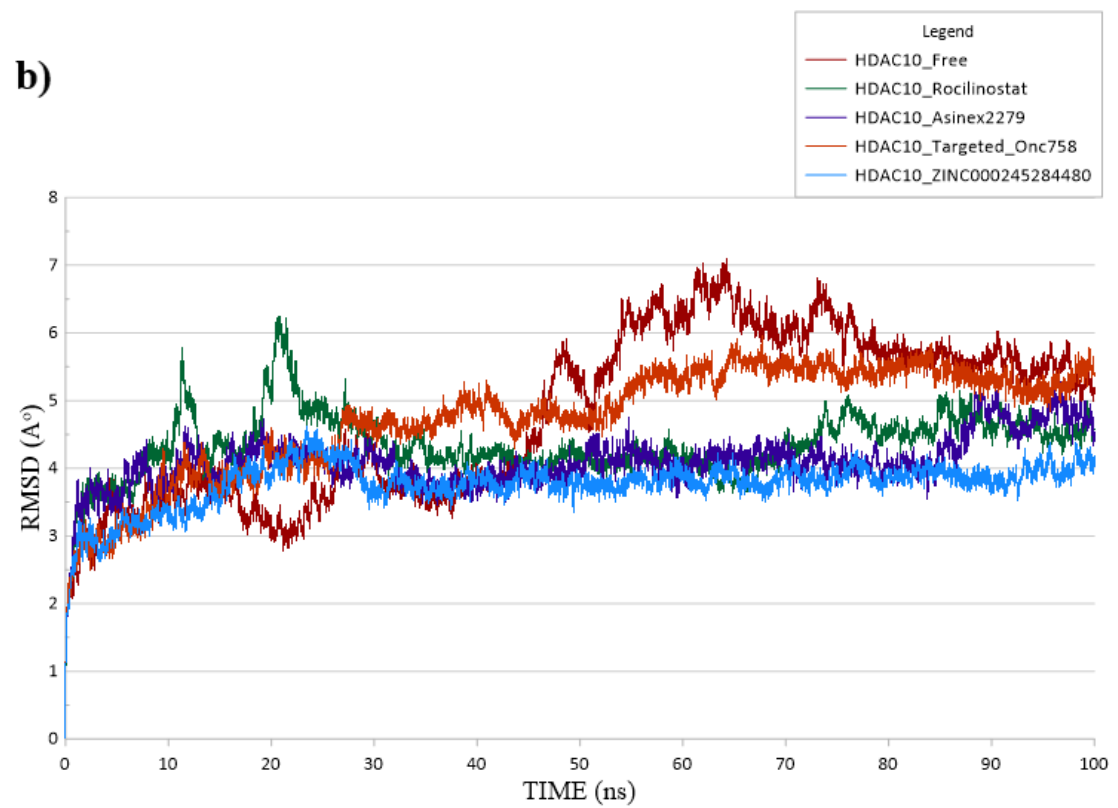
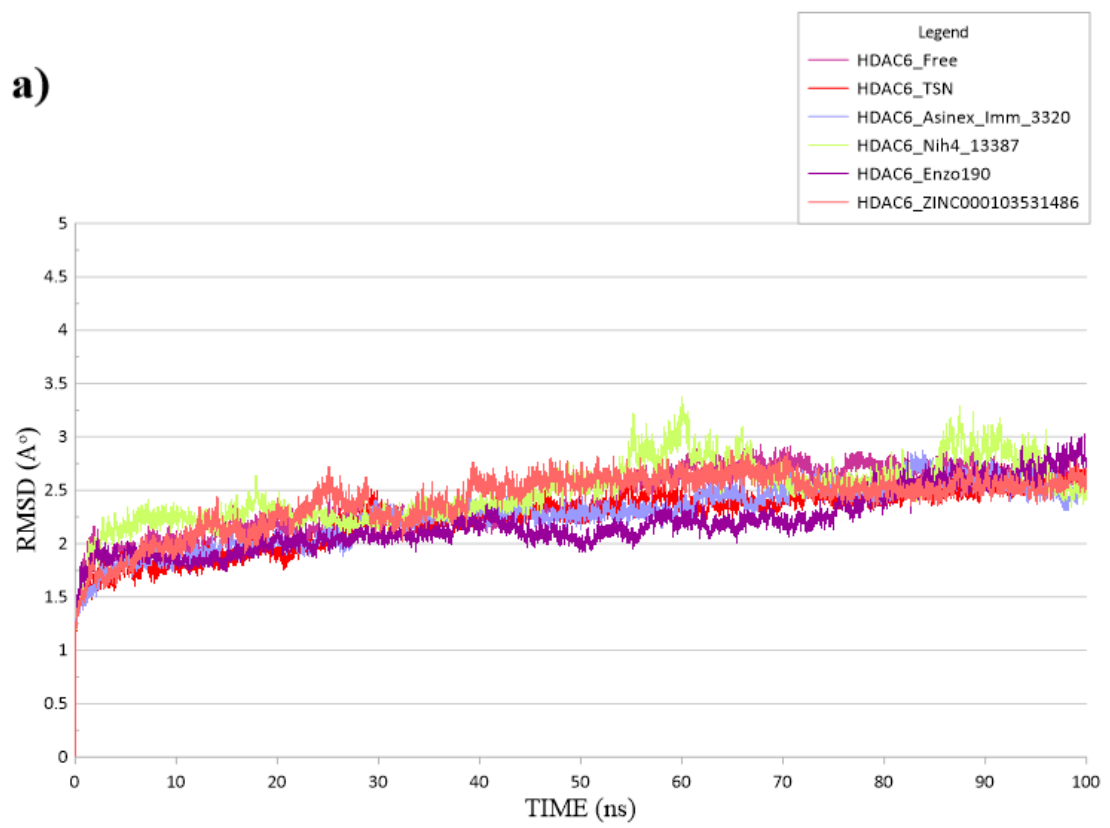
$$R_g = \left(\frac{\sum_i \|\mathbf{r}_i\|^2 m_i}{\sum_i m_i} \right)^{\frac{1}{2}}$$

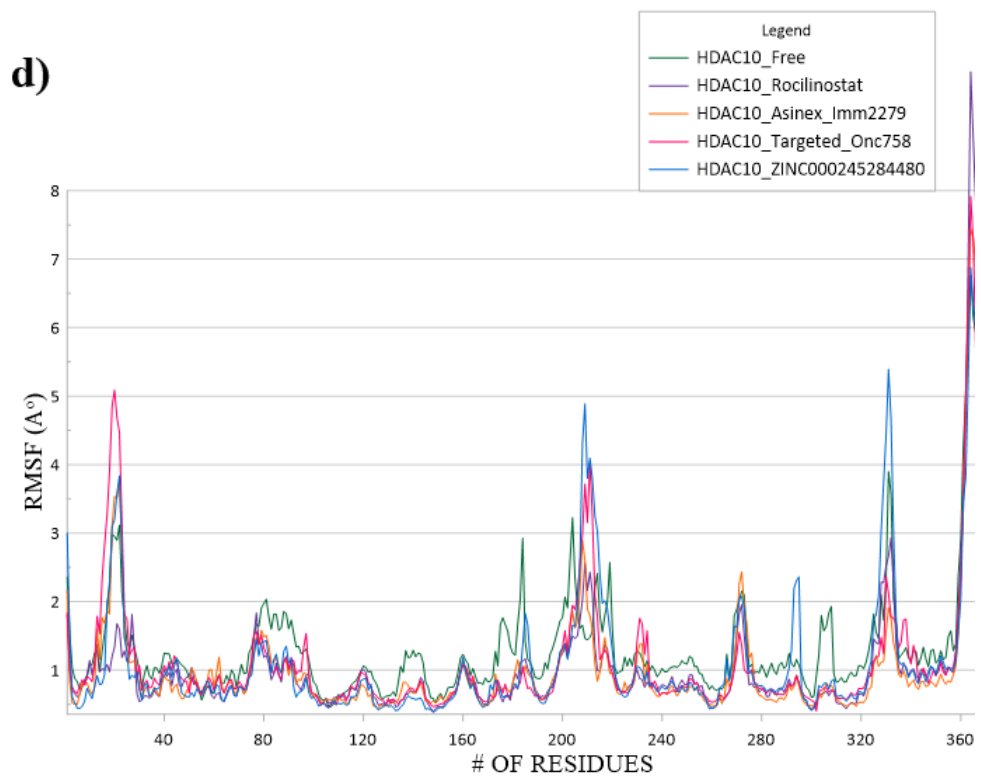
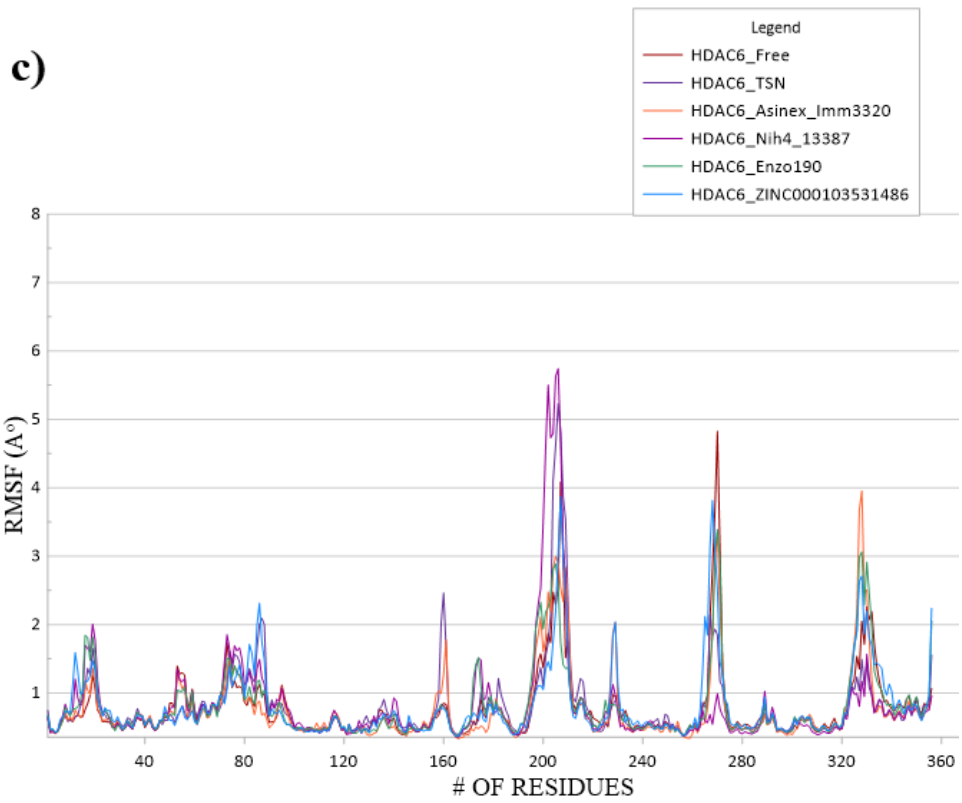
Equation 4.1

where m_i is the mass of atom i and \mathbf{r}_i is the position of atom i with respect to the center of mass of the molecule (Ahmed et al., 2020). In this study, the R_g graphs of HDAC6_Free, HDAC with TSN and its complexes, and HDAC10_Free, HDAC10 with Rocilinostat, and its complexes are plotted in Figure 4.17. All the systems remained

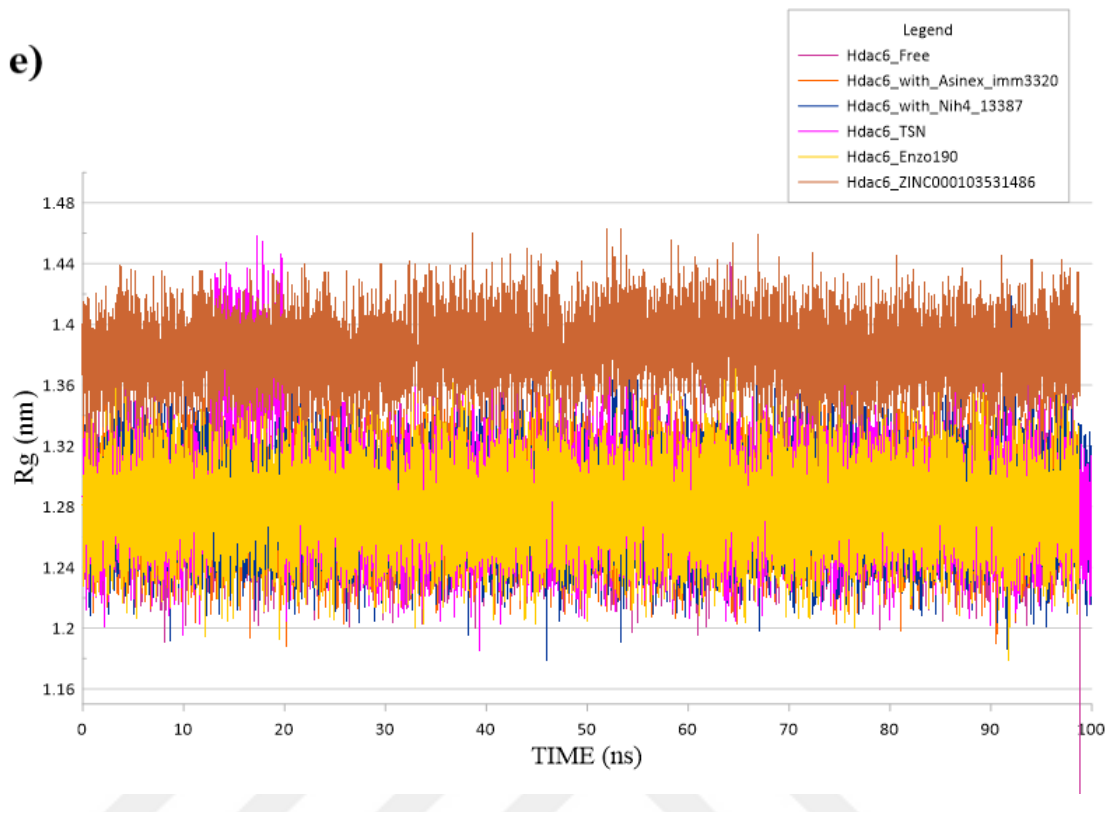
stable in 100 ns MD run. Despite the system HDAC6_TSN which has up to 1.44Å Rg profile between 10ns to 20ns showed higher flexibility among the other systems but this can be considered as a neglectable value since 1.44 Å is still in an acceptable range. Other systems showed relatively lower flexibility with the Rg profile of 1.2Å to 1.48Å throughout the simulation. So, the Rg profiles of the HDAC6 and HDAC10 systems indicate a stable path during the whole MD run.

PE Analysis: The potential energy (PE) profile shows the total energy of the system indicating the physical validity of the simulation performed. The energy graphs of HDAC6, HDAC with TSN and its complexes, and HDAC10, HDAC10 with Rocilinostat and its complexes are plotted in Figure 4.17. All the systems showed the highest binding mode stability over time, unlike HDAC6_ZINC000103531486 has a bit different energy profile but still showing stability. Also, HDAC10 enzyme and its complexes displayed a good stability throughout the simulation, and the ZINC000245284480 complex showed up as the highest stable system among others suggesting that it can have a potential selectivity for HDAC10. So, protein-ligand stability of the all complexes were measured as low and stable during the simulation.

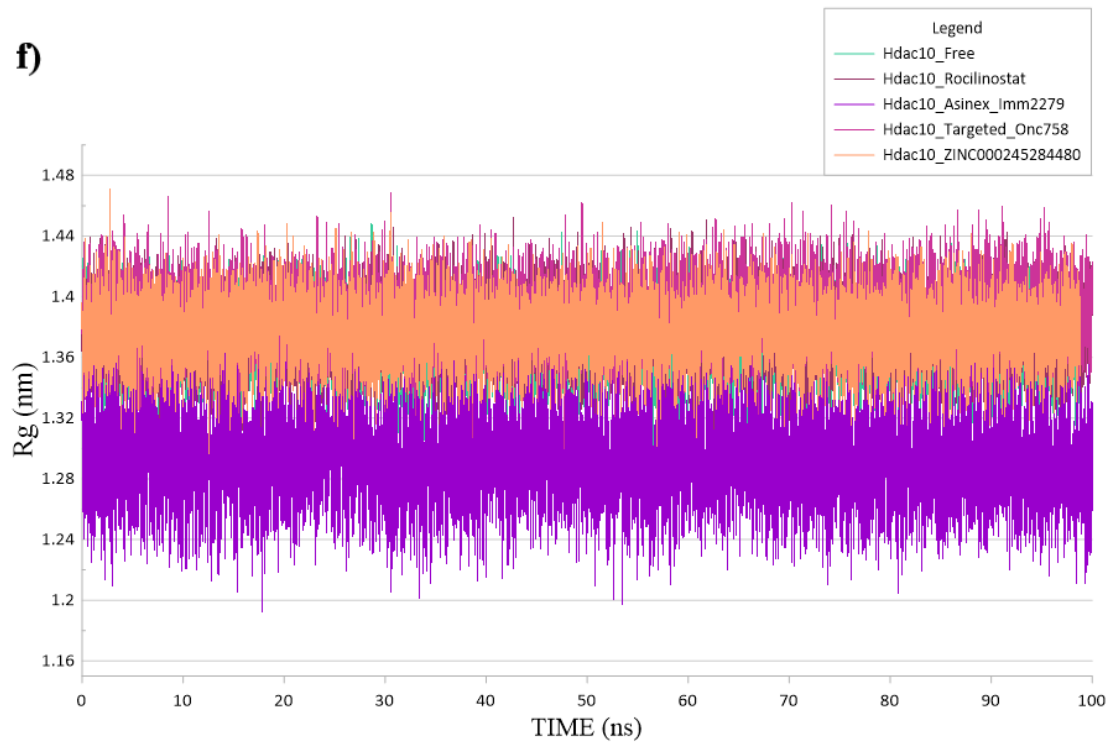




e)



f)



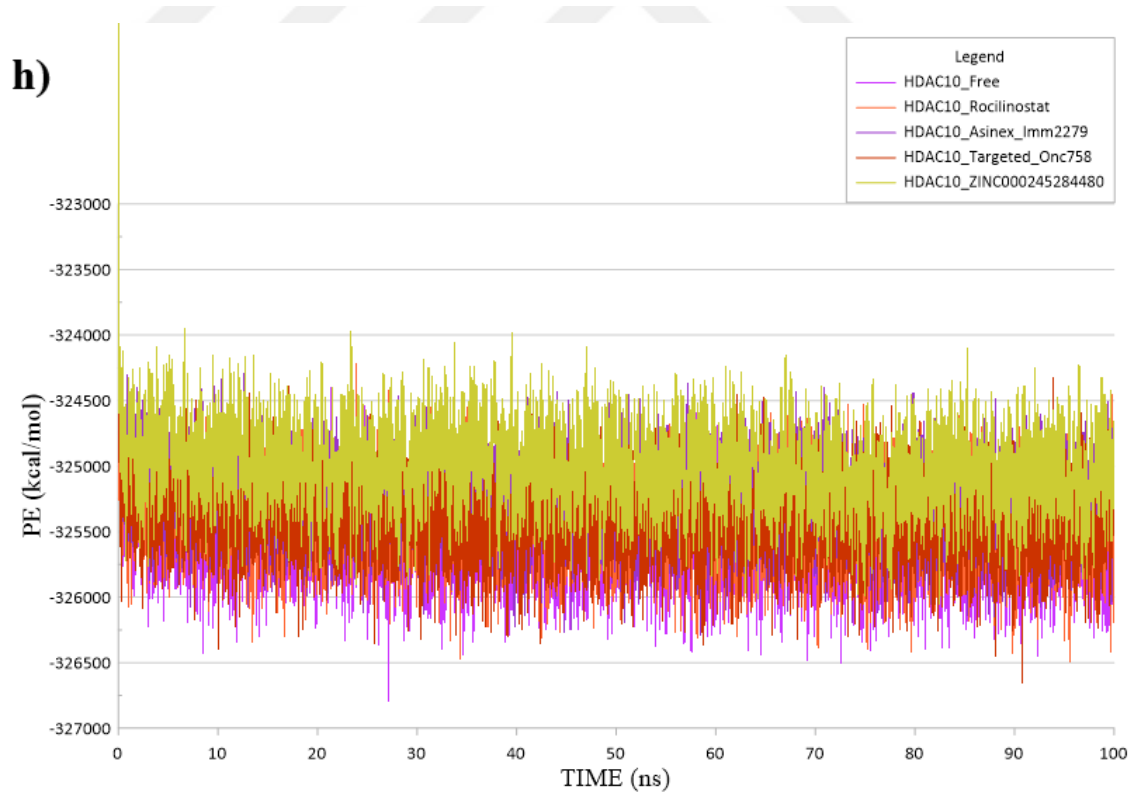
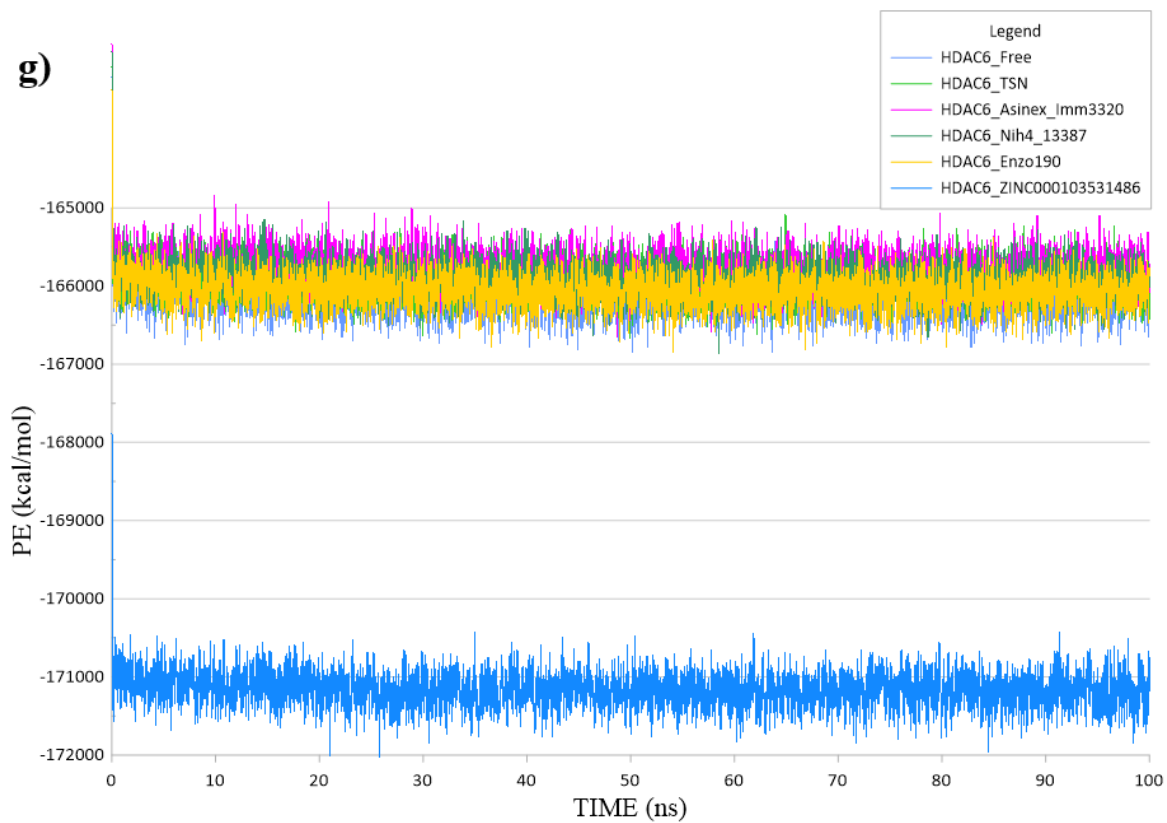


Figure 4. 17 100 ns-MD simulation of Root-mean-squared deviation (RMSD), Root-mean-squared fluctuation (RMSF), Radius of Gyration (Rg) and Potential Energy (PE) profiles of free form of HDAC6 and HDAC10 with their known inhibitors and their complexes. RMSD graphs of HDAC6_free, HDAC6_TSN and with their complexes (a). RMSD graphs of HDAC10_free, HDAC10_Rocilinostat and with their complexes (b). RMSF graphs of HDAC6_free, HDAC6_TSN and with their complexes (c). RMSF graphs of HDAC10_free, HDAC10_Rocilinostat and with their complexes (d). RG graphs of HDAC6_free, HDAC6_TSN and with their complexes (e). RG graphs of HDAC10_free, HDAC10_Rocilinostat and with their complexes (f). Potential energy graphs of HDAC6_free, HDAC6_TSN and with their complexes (g). Potential energy graphs of HDAC10_free, HDAC10_Rocilinostat and with their complexes (h).

5. DISCUSSION

The diversity of the active sites among histone deacetylase protein family including the HDAC 2b class has shown a great importance throughout the studies until today. The diversity within the catalytic channels unveils a significant isoform selectivity within the HDAC class 2b members as well. So, based on this idea structure-based drug design techniques are used to screen more than 2 million drug-like compounds against class IIb HDAC enzymes to investigate the specificity nature of the enzymes.

Compounds Asinex_Imm3320, Nih4_13387, Enzo_190, and ZINC000103531486 showed the highest binding affinity and greater selectivity for HDAC6 whereas, Asinex_Imm2279, Targeted_Onc758, and ZINC000245284480 showed high selectivity for HDAC10. Asinex_Imm3320 and Nih4_13387 has showed the highest selectivity for HDAC6 among the other ligands. On the other hand, Asinex_Imm2279 was found to have the highest binding affinity among all studied compounds for HDAC10 followed by Targeted_Onc758. These compounds spanned perfectly in the binding pocket of HDAC6 and HDAC10 and formed several important interactions with the key residues in the active site including HIS610, HIS 611, HIS 651, TYR 782, PHE 620, PHE 680, GLU 22, TYR 305 and many other residues.

Deep in the catalytic channel, the catalytic Zn^{2+} metal atom was found to be bonded to the carboxylate groups of Compound Asinex_imm3320 compound via a conventional hydrogen bond and a metal-acceptor interaction. This may result in blocking the catalytic site and thus lead to the inhibition of the enzymatic activity. The Asinex_imm2279 compound spanned the deep catalytic tunnel of the active site of HDAC10 and forming conventional hydrogen bonds with GLU 22 and TYR 305 residues, and also a π -sigma bond with the nitrogen at the backbone of the molecule with TRP 203 residue. It can be said that by covering the entrance of the catalytic pocket of HDAC10 by forming bonds with crucial key residues resulted in great binding affinity and high selectivity.

The 7 top-ranked compounds were tested for their drug-likeness. Their ADMET and drug-likeness properties were found to be within the normal range. In addition,

molecular dynamics simulations were carried out to examine the binding affinity of the top-ranked compounds and the protein-ligand structural stability. Throughout the MD simulations, all the examined inhibitors were found to be stable and stayed interacted to their respective proteins at physiological condition. Meanwhile, novel HDAC inhibitors were investigated along with Tubastatin A (TSN) for HDAC6 and Rocilinostat for HDAC10 as well. In this study, all the seven selected compounds with HDAC6 and HDAC10 complex systems, the apo-proteins, and the known-inhibitor-HDACs complexes were subjected to a long 100 ns MD simulation. Analysis of the MD trajectories were found to be satisfied and all other parameters were consistent throughout the simulation including the RMSD, RMSF, Rg and potential energy (PE) profiles.



6. CONCLUSIONS

All the studies to identify potential class IIb HDACs isoform selective inhibitors for cancer treatment were executed in this dissertation. The key amino acid residues which catalyze the action are highly conserved in between all HDACs and this brings specificity to HDACs for their working mechanism among other species. Class IIb HDAC enzymes are zinc-dependent enzymes which are mainly located in the nucleus and the cytoplasm. In the literature, they are described with different types of cancers with the overexpression with their existence. Class IIb HDACs (HDAC6 and HDAC10) also targets other non-histone proteins for inducing cancer tissues invasion and microtubule control. The main goal of this study was to apply an in-silico approach which is structure-based virtual screening to identify promising selective inhibitors for HDAC6 and HDAC10. To reach this aim, several molecular modeling methods and computational approaches were carried out including structural and amino acid sequence alignments, molecular docking, virtual screening, molecular dynamics simulation, physiochemical description, and free binding energy calculations.

Difficulties in obtaining isoform-selectivity established while calculating high amino acid sequence similarity and conserved active sites between class IIb HDACs. High structural resemblance between HDAC6 and HDAC10 revealed a promising challenge in designing specific inhibitors for each isoform.

Up to date, in the literature as well, there are no resolved structures for human HDAC10. For this reason, the 3D structural model of human HDAC10 was obtained from the recent search of our molecular modeling lab group and the X-ray structure of human HDAC6 (5EDU) catalytic domain 2 was downloaded from the PDB website for this study. The libraries consisting of cancer-like compounds with 1.205.135 molecules and a total of 1.050.000 molecules from the ZINC15 database were downloaded for virtual screening using AutoDock 4.2, AuroDockVina (Quick) and GOLD tools. According to the highest binding affinity, the 7 top-ranked compounds (4 for HDAC6 and 3 for HDAC10) were selected as potent and isoform-specific inhibitors. Additionally, these top compounds have shown drug-likeness and physiochemical properties (ADMET) properties that is in a considerable range for further applying 100 ns MD simulations. Later, molecular dynamics simulation was established to evaluate

the structural dynamics and the stability of apo-proteins (proteins alone) of the HDAC6 and HDAC10, the selective inhibitor-protein complexes, and their known inhibitor-protein complexes. All the MD simulations suggested that all studied inhibitors showed stability and remained interacted with the active site of their targets throughout the MD simulation. The RMSD, RMSF, Rg and PE calculations and analysis showed that the stability of the complexes over time was compatible. These findings suggest that the reported inhibitors could be used for further optimization and tested in in vitro studies for designing HDAC6 and HDAC10 isoform-specific inhibitors.



REFERENCES

- A. Ganesan. (2019). Targeting the Zinc-Dependent Histone Deacetylases (HDACs) for Drug Discovery. *Springer*. <https://doi.org/10.1007/7355>
- Abbass, S., Hassan, H., Mohamed, M., Moustafa, G., & Abuo-Rahma, G. (2019). Recent Prospectives of Anticancer Histone Deacetylase Inhibitors. *Journal of Advanced Biomedical and Pharmaceutical Sciences*, 0(0), 0–0. <https://doi.org/10.21608/jabps.2019.14468.1051>
- Abend, A., & Kehat, I. (2015). Histone deacetylases as therapeutic targets - From cancer to cardiac disease. In *Pharmacology and Therapeutics* (Vol. 147). Elsevier B.V. <https://doi.org/10.1016/j.pharmthera.2014.11.003>
- Ahmed, M. C., Crehuet, R., & Lindorff-Larsen, K. (2020). Computing, analyzing, and comparing the radius of gyration and hydrodynamic radius in conformational ensembles of intrinsically disordered proteins. *Methods in Molecular Biology*, 2141, 429–445. https://doi.org/10.1007/978-1-0716-0524-0_21
- Alejandra Hernandez-Santoyo, Aldo Yair Tenorio-Barajas, Victor Altuzar, H. V.-C. and C. M.-B. (2016). Protein-Protein and Protein-Ligand Docking Chapter. In *Protein Engineering - Technology and Application* (Issue tourism, p. 21). <https://doi.org/10.5772/56376>
- Alhossary, A., Handoko, S. D., Mu, Y., & Kwoh, C. K. (2015). Fast, accurate, and reliable molecular docking with QuickVina 2. *Bioinformatics*, 31(13), 2214–2216. <https://doi.org/10.1093/bioinformatics/btv082>
- Allen, M. P. (2004). Introduction to Molecular Dynamics Simulation. *Computational Soft Matter: From Synthetic Polymers to Proteins, Lecture Notes, Norbert Attig, Kurt Binder, Helmut Grubmüller, Kurt Kremer (Eds.), John von Neumann Institute for Computing, Jülich, NIC Series, 23, 1–28.*

- Aminpour, M., Montemagno, C., & Tuszynski, J. A. (2019). An overview of molecular modeling for drug discovery with specific illustrative examples of applications. *Molecules*, 24(9). <https://doi.org/10.3390/molecules24091693>
- Anna E. Lohning, Stephan M. Levonis, B. W.-N. and S. S. S. (2017). *A Practical Guide to Molecular Docking and Homology Modelling for Medicinal Chemists Article*. January, 44–49. <https://doi.org/10.2174/1568026617666170130110827>
- Badalà, F., Nouri-mahdavi, K., & Raoof, D. A. (2008). Recent Advances in Ligand-Based Drug Design: Relevance and Utility. *Computer*, 144(5), 724–732.
- Batool, M., Ahmad, B., & Choi, S. (2019). A structure-based drug discovery paradigm. *International Journal of Molecular Sciences*, 20(11). <https://doi.org/10.3390/ijms20112783>
- Benedetti, R., Conte, M., & Altucci, L. (2015). Targeting Histone Deacetylases in Diseases: Where Are We? *Antioxidants and Redox Signaling*, 23(1), 99–126. <https://doi.org/10.1089/ars.2013.5776>
- Bertino, E. M., & Otterson, G. A. (2011). Romidepsin: A novel histone deacetylase inhibitor for cancer. *Expert Opinion on Investigational Drugs*, 20(8), 1151–1158. <https://doi.org/10.1517/13543784.2011.594437>
- BIOVIA, D. S. (2017). BIOVIA Discovery Studio 2017 R2: A comprehensive predictive science application for the Life Sciences. In *San Diego, CA, USA*.
- Bukhtoyarov, O. V., & Samarin, D. M. (2015). Pathogenesis of Cancer: Cancer Reparative Trap. *Journal of Cancer Therapy*, 06(05), 399–412. <https://doi.org/10.4236/jct.2015.65043>
- Butler, K. V., Kalin, J., Brochier, C., Vistoli, G., Langley, B., & Kozikowski, A. P. (2010). Rational design and simple chemistry yield a superior, neuroprotective HDAC6 inhibitor, tubastatin A. *Journal of the American Chemical Society*,

132(31), 10842–10846. <https://doi.org/10.1021/ja102758v>

Chen, Q. W., Zhu, X. Y., Li, Y. Y., & Meng, Z. Q. (2014). Epigenetic regulation and cancer (review). *Oncology Reports*, 31(2), 523–532.

<https://doi.org/10.3892/or.2013.2913>

Cheng, Y., He, C., Wang, M., Ma, X., Mo, F., Yang, S., Han, J., & Wei, X. (2019). Targeting epigenetic regulators for cancer therapy: Mechanisms and advances in clinical trials. *Signal Transduction and Targeted Therapy*, 4(1).

<https://doi.org/10.1038/s41392-019-0095-0>

Clawson, G. A. (2016). Histone deacetylase inhibitors as cancer therapeutics. *Annals of Translational Medicine*, 4(15), 1–5. <https://doi.org/10.21037/atm.2016.07.22>

Cosenza, M., & Pozzi, S. (2018). The therapeutic strategy of HDAC6 inhibitors in lymphoproliferative disease. *International Journal of Molecular Sciences*, 19(8).

<https://doi.org/10.3390/ijms19082337>

Dar, A. M., & Mir, S. (2017). Molecular Docking: Approaches, Types, Applications and Basic Challenges. *Journal of Analytical & Bioanalytical Techniques*, 08(02), 8–10. <https://doi.org/10.4172/2155-9872.1000356>

Dawood, M., Elbadawi, M., Böckers, M., Bringmann, G., & Efferth, T. (2020). Molecular docking-based virtual drug screening revealing an oxofluorenyl benzamide and a bromonaphthalene sulfonamido hydroxybenzoic acid as HDAC6 inhibitors with cytotoxicity against leukemia cells. *Biomedicine and Pharmacotherapy*, 129(June), 110454.

<https://doi.org/10.1016/j.biopha.2020.110454>

De Ruijter, A. J. M., Van Gennip, A. H., Caron, H. N., Kemp, S., & Van Kuilenburg, A. B. P. (2003). Histone deacetylases (HDACs): Characterization of the classical HDAC family. *Biochemical Journal*, 370(3), 737–749.

<https://doi.org/10.1042/BJ20021321>

- Delcuve, G. P., Khan, D. H., & Davie, J. R. (2013). Roles of histone deacetylases in epigenetic regulation: Emerging paradigms from studies with inhibitors. *Epigenetics and Pathology: Exploring Connections between Genetic Mechanisms and Disease Expression*, 143–171. <https://doi.org/10.1201/b16304>
- Dong, J., Wang, N. N., Yao, Z. J., Zhang, L., Cheng, Y., Ouyang, D., Lu, A. P., & Cao, D. S. (2018). Admetlab: A platform for systematic ADMET evaluation based on a comprehensively collected ADMET database. *Journal of Cheminformatics*, 10(1), 1–11. <https://doi.org/10.1186/s13321-018-0283-x>
- Durrant JD, M. (2011). Molecular dynamics simulations and drug discovery. *BMC Biology*, 9(71). <https://doi.org/10.1186/1741-7007-9-71>
- Elmallah, M. I. Y., & Micheau, O. (2019). Epigenetic regulation of TRAIL signaling: Implication for cancer therapy. *Cancers*, 11(6). <https://doi.org/10.3390/cancers11060850>
- Eslaminejad, M. B., Fani, N., & Shahhoseini, M. (2013). Epigenetic regulation of osteogenic and chondrogenic differentiation of mesenchymal stem cells in culture. *Cell Journal*, 15(1), 1–10.
- Estiu, G., Greenberg, E., Harrison, C. B., Kwiatkowski, N. P., Mazitschek, R., Bradner, J. E., & Wiest, O. (2008). Structural origin of selectivity in class II-selective histone deacetylase inhibitors. *Journal of Medicinal Chemistry*, 51(10), 2898–2906. <https://doi.org/10.1021/jm7015254>
- Ferreira De Freitas, R., Harding, R. J., Franzoni, I., Ravichandran, M., Mann, M. K., Ouyang, H., Lautens, M., Santhakumar, V., Arrowsmith, C. H., & Schapira, M. (2018). Identification and Structure-Activity Relationship of HDAC6 Zinc-Finger Ubiquitin Binding Domain Inhibitors [Research-article]. *Journal of Medicinal Chemistry*, 61(10), 4517–4527. <https://doi.org/10.1021/acs.jmedchem.8b00258>
- Gallinari, P., Di Marco, S., Jones, P., Pallaoro, M., & Steinkühler, C. (2007). HDACs,

histone deacetylation and gene transcription: From molecular biology to cancer therapeutics. *Cell Research*, 17(3), 195–211. <https://doi.org/10.1038/sj.cr.7310149>

Géraldy, M., Morgen, M., Sehr, P., Steimbach, R. R., Moi, D., Ridinger, J., Oehme, I., Witt, O., Malz, M., Nogueira, M. S., Koch, O., Gunkel, N., & Miller, A. K. (2019). Selective Inhibition of Histone Deacetylase 10: Hydrogen Bonding to the Gatekeeper Residue is Implicated. *Journal of Medicinal Chemistry*, 62(9), 4426–4443. <https://doi.org/10.1021/acs.jmedchem.8b01936>

Grant, S., Easley, C., & Kirkpatrick, P. (2007). Vorinostat. *Nature Reviews Drug Discovery*, 6(1), 21–22. <https://doi.org/10.1038/nrd2227>

Gregoretta, I. V., Lee, Y. M., & Goodson, H. V. (2004). Molecular evolution of the histone deacetylase family: Functional implications of phylogenetic analysis. *Journal of Molecular Biology*, 338(1), 17–31. <https://doi.org/10.1016/j.jmb.2004.02.006>

Guan, L., Yang, H., Cai, Y., Sun, L., Di, P., Li, W., Liu, G., & Tang, Y. (2019). ADMET-score-a comprehensive scoring function for evaluation of chemical drug-likeness. *MedChemComm*, 10(1), 148–157. <https://doi.org/10.1039/C8MD00472B>

Guardiola, A. R., & Yao, T. P. (2002). Molecular cloning and characterization of a novel histone deacetylase HDAC10. *Journal of Biological Chemistry*, 277(5), 3350–3356. <https://doi.org/10.1074/jbc.M109861200>

Haberland, M., Montgomery, R. L., & Olson, E. N. (2009). The many roles of histone deacetylases in development and physiology: Implications for disease and therapy. *Nature Reviews Genetics*, 10(1), 32–42. <https://doi.org/10.1038/nrg2485>

Hai, Y., & Christianson, D. W. (2016). Histone deacetylase 6 structure and molecular basis of catalysis and inhibition. *Nature Chemical Biology*, 12(9), 741–747. <https://doi.org/10.1038/nchembio.2134>

- Hai, Y., Shinsky, S. A., Porter, N. J., & Christianson, D. W. (2017). Histone deacetylase 10 structure and molecular function as a polyamine deacetylase. *Nature Communications*, 8(May), 1–9. <https://doi.org/10.1038/ncomms15368>
- Hassell. (2019). Histone Deacetylases and their Inhibitors in Cancer Epigenetics. *Diseases*, 7(4), 57. <https://doi.org/10.3390/diseases7040057>
- Herbst-Gervasoni, C. J., Steimbach, R. R., Morgen, M., Miller, A. K., & Christianson, D. W. (2020). Structural Basis for the Selective Inhibition of HDAC10, the Cytosolic Polyamine Deacetylase. *ACS Chemical Biology*, 15(8), 2154–2163. <https://doi.org/10.1021/acscchembio.0c00362>
- Hollingsworth, S. A., & Dror, R. O. (2018). Molecular Dynamics Simulation for All. *Neuron*, 99(6), 1129–1143. <https://doi.org/10.1016/j.neuron.2018.08.011>
- Hospital, A., Goñi, J. R., Orozco, M., & Gelpí, J. L. (2015). Molecular dynamics simulations: Advances and applications. *Advances and Applications in Bioinformatics and Chemistry*, 8(1), 37–47. <https://doi.org/10.2147/AABC.S70333>
- Hull, E. E., Montgomery, M. R., & Leyva, K. J. (2016). HDAC Inhibitors as Epigenetic Regulators of the Immune System: Impacts on Cancer Therapy and Inflammatory Diseases. *BioMed Research International*, 2016. <https://doi.org/10.1155/2016/8797206>
- Ibrahim Uba, A., & Yelekçi, K. (2019a). Homology modeling of human histone deacetylase 10 and design of potential selective inhibitors. *Journal of Biomolecular Structure and Dynamics*, 37(14), 3627–3636. <https://doi.org/10.1080/07391102.2018.1521747>
- Ibrahim Uba, A., & Yelekçi, K. (2019b). Homology modeling of human histone deacetylase 10 and design of potential selective inhibitors. *Journal of Biomolecular Structure and Dynamics*, 37(14), 3627–3636. <https://doi.org/10.1080/07391102.2018.1521747>

Icardi, L., De Bosscher, K., & Tavernier, J. (2012). The HAT/HDAC interplay: Multilevel control of STAT signaling. *Cytokine and Growth Factor Reviews*, 23(6), 283–291. <https://doi.org/10.1016/j.cytogfr.2012.08.002>

Ikuo Moriguchi et al. (1992). Simple Method of Calculating Octanol/Water Partition Coefficient. *Pharmaceutical Society of Japan*, 40(1), 127–130.

Islam, M. M., Banerjee, T., Packard, C. Z., Kotian, S., Selvendiran, K., Cohn, D. E., & Parvin, J. D. (2017). HDAC10 as a potential therapeutic target in ovarian cancer. *Gynecologic Oncology*, 144(3), 613–620. <https://doi.org/10.1016/j.ygyno.2017.01.009>

Jaenisch, R., & Bird, A. (2003). Epigenetic regulation of gene expression: How the genome integrates intrinsic and environmental signals. *Nature Genetics*, 33(3S), 245–254. <https://doi.org/10.1038/ng1089>

Janke, C., & Montagnac, G. (2017). Causes and Consequences of Microtubule Acetylation. *Current Biology*, 27(23), R1287–R1292. <https://doi.org/10.1016/j.cub.2017.10.044>

Jinhua Tang, H. Y., & Zhuan, and S. (2013). Histone deacetylases as targets for treatment of multiple diseases. *Clin Sci (Lond)*, 124(11), 651–662. <https://doi.org/10.1042/CS20120504>

Jo, S., Kim, T., Iyer, V. G., & Im, W. (2008). CHARMM-GUI: a web-based graphical user interface for CHARMM. *Journal of Computational Chemistry*, 29(11), 1859–1865. <https://doi.org/10.1002/jcc.20945>

Jones, G., Willett, P., Glen, R. C., Leach, A. R., & Taylor, R. (1997). Development and validation of a genetic algorithm for flexible docking. *Journal of Molecular Biology*, 267(3), 727–748. <https://doi.org/10.1006/jmbi.1996.0897>

Jung, M. (2001). Inhibitors of Histone Deacetylase as New Anticancer Agents. In

Current Medicinal Chemistry (Vol. 8, Issue 12, pp. 1505–1511).

<https://doi.org/10.2174/0929867013372058>

Kagohara, L. T., Stein-O'Brien, G. L., Kelley, D., Flam, E., Wick, H. C., Danilova, L. V., Easwaran, H., Favorov, A. V., Qian, J., Gaykalova, D. A., & Fertig, E. J. (2018). Epigenetic regulation of gene expression in cancer: Techniques, resources and analysis. *Briefings in Functional Genomics*, 17(1), 49–63.
<https://doi.org/10.1093/bfpg/elx018>

Kashyap, K., & Kakkar, R. (2020). An insight into selective and potent inhibition of histone deacetylase 8 through induced-fit docking, pharmacophore modeling and QSAR studies. *Journal of Biomolecular Structure and Dynamics*, 38(1), 48–65.
<https://doi.org/10.1080/07391102.2019.1567388>

Kazantsev, A. G., & Thompson, L. M. (2008). Therapeutic application of histone deacetylase inhibitors for central nervous system disorders. *Nature Reviews Drug Discovery*, 7(10), 854–868. <https://doi.org/10.1038/nrd2681>

Kim, D. H., Kim, M., & Kwon, H. J. (2003). Histone deacetylase in carcinogenesis and its inhibitors as anti-cancer agents. *Journal of Biochemistry and Molecular Biology*, 36(1), 110–119. <https://doi.org/10.5483/bmbrep.2003.36.1.110>

Kim, H. J., & Bae, S. C. (2011). Histone deacetylase inhibitors: Molecular mechanisms of action and clinical trials as anti-cancer drugs. *American Journal of Translational Research*, 3(2), 166–179.

Kruger, S., Ilmer, M., Kobold, S., Cadilha, B. L., Endres, S., Ormanns, S., Schuebbe, G., Renz, B. W., D'Haese, J. G., Schloesser, H., Heinemann, V., Subklewe, M., Boeck, S., Werner, J., & Von Bergwelt-Baildon, M. (2019). Advances in cancer immunotherapy 2019 - Latest trends. *Journal of Experimental and Clinical Cancer Research*, 38(1), 1–11. <https://doi.org/10.1186/s13046-019-1266-0>

Laubach, J. P., Moreau, P., San-Miguel, J. F., & Richardson, P. G. (2015). Panobinostat

for the treatment of multiple myeloma. *Clinical Cancer Research*, 21(21), 4767–4773. <https://doi.org/10.1158/1078-0432.CCR-15-0530>

Lee, J., Cheng, X., Swails, J. M., Yeom, M. S., Eastman, P. K., Lemkul, J. A., Wei, S., Buckner, J., Jeong, J. C., Qi, Y., Jo, S., Pande, V. S., Case, D. A., Brooks, C. L., MacKerell, A. D., Klauda, J. B., & Im, W. (2016). CHARMM-GUI Input Generator for NAMD, GROMACS, AMBER, OpenMM, and CHARMM/OpenMM Simulations Using the CHARMM36 Additive Force Field. *Journal of Chemical Theory and Computation*, 12(1), 405–413. <https://doi.org/10.1021/acs.jctc.5b00935>

Li, S., Yang, D., Gao, L., Wang, Y., & Peng, Q. (2020). Epigenetic regulation and mechanobiology. *Biophysics Reports*, 6(2–3), 33–48. <https://doi.org/10.1007/s41048-020-00106-x>

Li, Yingxiu, Shin, D., & Kwon, S. H. (2013). Histone deacetylase 6 plays a role as a distinct regulator of diverse cellular processes. *FEBS Journal*, 280(3), 775–793. <https://doi.org/10.1111/febs.12079>

Li, Yixuan, & Seto, E. (2016). HDACs and HDAC inhibitors in cancer development and therapy. *Cold Spring Harbor Perspectives in Medicine*, 6(10), 1–34. <https://doi.org/10.1101/cshperspect.a026831>

Li, Youxuan, & Woster, P. M. (2015). Discovery of a new class of histone deacetylase inhibitors with a novel zinc binding group. *MedChemComm*, 6(4), 613–618. <https://doi.org/10.1039/c4md00401a>

Lipinski, C. A. (2004). Lead- and drug-like compounds: The rule-of-five revolution. *Drug Discovery Today: Technologies*, 1(4), 337–341. <https://doi.org/10.1016/j.ddtec.2004.11.007>

Lipinski, C. A., Lombardo, F., Dominy, B. W., & Feeney, P. J. (2001). Experimental and computational approaches to estimate solubility and permeability in drug

discovery and development settings. *Advanced Drug Delivery Reviews*, 64(SUPPL.), 4–17. <https://doi.org/10.1016/j.addr.2012.09.019>

Liu, J. R., Yu, C. W., Hung, P. Y., Hsin, L. W., & Chern, J. W. (2019). High-selective HDAC6 inhibitor promotes HDAC6 degradation following autophagy modulation and enhanced antitumor immunity in glioblastoma. *Biochemical Pharmacology*, 163(33), 458–471. <https://doi.org/10.1016/j.bcp.2019.03.023>

Liu, Y., Peng, L., Seto, E., Huang, S., & Qiu, Y. (2012). Modulation of histone deacetylase 6 (HDAC6) nuclear import and tubulin deacetylase activity through acetylation. *Journal of Biological Chemistry*, 287(34), 29168–29174. <https://doi.org/10.1074/jbc.M112.371120>

LoPresti, P. (2020). HDAC6 in Diseases of Cognition and of Neurons. *Cells*, 10(1). <https://doi.org/10.3390/cells10010012>

Macalino, S. J. Y., Gosu, V., Hong, S., & Choi, S. (2015). Role of computer-aided drug design in modern drug discovery. *Archives of Pharmacal Research*, 38(9), 1686–1701. <https://doi.org/10.1007/s12272-015-0640-5>

Mariño-Ramírez, L., Kann, M. G., Shoemaker, B. A., & Landsman, D. (2005). Histone structure and nucleosome stability. *Expert Review of Proteomics*, 2(5), 719–729. <https://doi.org/10.1586/14789450.2.5.719>

Martin, S. A. (2017). *Topoisomerase Inhibitors The DNA mismatch repair pathway Selectively Replicating Oncolytic Aden- oviruses Combined with Chemotherapy , Radiotherapy , or Molecular Target- ed Therapy for Treatment of Human Cancers.*

Mazzocchi, M., Collins, L. M., Sullivan, A. M., & O’Keeffe, G. W. (2020). The class II histone deacetylases as therapeutic targets for Parkinson’s disease. *Neuronal Signaling*, 4(2), 1–9. <https://doi.org/10.1042/ns20200001>

Meng, X. Y., Zhang, H. X., Mezei, M., & Cui, M. (2011). Molecular docking: a

powerful approach for structure-based drug discovery. *Current computer-aided drug design. Current Computer Aided Drug Design*, 7(2), 146–157.

<https://www.ingentaconnect.com/content/ben/cad/2011/00000007/00000002/art00008%0Ahttps://www.ncbi.nlm.nih.gov/pmc/articles/PMC3624763/pdf/nihms412728.pdf>

Meschino, J. P. (2016). How Chemotherapy Drugs Work. *Dynamic Chiropractic Canada*, 3(5), hlm.1-7.

Milazzo, G., Mercatelli, D., Di Muzio, G., Triboli, L., De Rosa, P., Perini, G., & Giorgi, F. M. (2020). Histone deacetylases (HDACs): Evolution, specificity, role in transcriptional complexes, and pharmacological actionability. *Genes*, 11(5). <https://doi.org/10.3390/genes11050556>

Miyake, Y., Keusch, J. J., Wang, L., Saito, M., Hess, D., Wang, X., Melancon, B. J., Helquist, P., Gut, H., & Matthias, P. (2016). deacetylation and its selective inhibition. *Nature Publishing Group, July*. <https://doi.org/10.1038/nchembio.2140>

Moradzadeh, M., Tabarraei, A., & Sadeghnia, H. R. (2015). The Role of Histone Deacetylase (HDAC) as a Biomarker in Cancer. *Journal of Molecular Biomarkers & Diagnosis*, 06(04), 2–6. <https://doi.org/10.4172/2155-9929.1000240>

Morris, G. M., Ruth, H., Lindstrom, W., Sanner, M. F., Belew, R. K., Goodsell, D. S., & Olson, A. J. (2009). Software news and updates AutoDock4 and AutoDockTools4: Automated docking with selective receptor flexibility. *Journal of Computational Chemistry*, 30(16), 2785–2791. <https://doi.org/10.1002/jcc.21256>

Morris, M. J., & Monteggia, L. M. (2013). Unique functional roles for class I and class II histone deacetylases in central nervous system development and function. *International Journal of Developmental Neuroscience*, 31(6), 370–381. <https://doi.org/10.1016/j.ijdevneu.2013.02.005>

Mottamal, M., Zheng, S., Huang, T. L., & Wang, G. (2015). Histone deacetylase

inhibitors in clinical studies as templates for new anticancer agents. *Molecules*, 20(3), 3898–3941. <https://doi.org/10.3390/molecules20033898>

Neves, B. J., Braga, R. C., Melo-Filho, C. C., Moreira-Filho, J. T., Muratov, E. N., & Andrade, C. H. (2018). QSAR-based virtual screening: Advances and applications in drug discovery. *Frontiers in Pharmacology*, 9(NOV), 1–7. <https://doi.org/10.3389/fphar.2018.01275>

Noack, M., Leyk, J., & Richter-Landsberg, C. (2014). HDAC6 inhibition results in tau acetylation and modulates tau phosphorylation and degradation in oligodendrocytes. *Glia*, 62(4), 535–547. <https://doi.org/10.1002/glia.22624>

Ntie-Kang, F., Nyongbela, K. D., Ayimele, G. A., & Shekfeh, S. (2019). “Drug-likeness” Properties of natural compounds. *Physical Sciences Reviews*, 4(11), 1–14. <https://doi.org/10.1515/psr-2018-0169>

Oehme, I., Linke, J. P., Böck, B. C., Milde, T., Lodrini, M., Hartenstein, B., Wiegand, I., Eckert, C., Roth, W., Kool, M., Kaden, S., Gröne, H. J., Schulte, J. H., Lindner, S., Hamacher-Brady, A., Brady, N. R., Deubzer, H. E., & Witt, O. (2013). Histone deacetylase 10 promotes autophagy-mediated cell survival. *Proceedings of the National Academy of Sciences of the United States of America*, 110(28). <https://doi.org/10.1073/pnas.1300113110>

Omotuyi, I. O., & Olusanya, O. (2015). 208 Histone deacetylase (HDAC) I catalytic core Asp-His charge relay system is altered by HDAC inhibitors: atomistic simulation studies. *Journal of Biomolecular Structure and Dynamics*, 33(sup1), 140–140. <https://doi.org/10.1080/07391102.2015.1038139>

Pal, S., Kumar, V., Kundu, B., Bhattacharya, D., Preethy, N., Reddy, M. P., & Talukdar, A. (2019). Ligand-based Pharmacophore Modeling, Virtual Screening and Molecular Docking Studies for Discovery of Potential Topoisomerase I Inhibitors. *Computational and Structural Biotechnology Journal*, 17, 291–310. <https://doi.org/10.1016/j.csbj.2019.02.006>

- Park, J., Terranova-Barberio, M., Zhong, A. Y., Thomas, S., & Munster, P. N. (2017). Clinical applications of histone deacetylase inhibitors. In *Handbook of Epigenetics: The New Molecular and Medical Genetics* (Second Edi, pp. 605–621). Elsevier Inc. <https://doi.org/10.1016/B978-0-12-805388-1.00040-7>
- Park, S. Y., & Kim, J. S. (2020). A short guide to histone deacetylases including recent progress on class II enzymes. *Experimental and Molecular Medicine*, *52*(2), 204–212. <https://doi.org/10.1038/s12276-020-0382-4>
- Patodia, S. (2014). Molecular Dynamics Simulation of Proteins: A Brief Overview. *Journal of Physical Chemistry & Biophysics*, *4*(6), 4–7. <https://doi.org/10.4172/2161-0398.1000166>
- Peng, L., & Seto, E. (2011). Deacetylation of nonhistone proteins by HDACs and the implications in cancer. *Handbook of Experimental Pharmacology*, *206*, 39–56. https://doi.org/10.1007/978-3-642-21631-2_3
- Phillips, J. C., Braun, R., Wang, W., Gumbart, J., Tajkhorshid, E., Villa, E., Chipot, C., Skeel, R. D., Kalé, L., & Schulten, K. (2005). Scalable molecular dynamics with NAMD. *Journal of Computational Chemistry*, *26*(16), 1781–1802. <https://doi.org/10.1002/jcc.20289>
- Plummer, M., de Martel, C., Vignat, J., Ferlay, J., Bray, F., & Franceschi, S. (2016). Global burden of cancers attributable to infections in 2012: a synthetic analysis. *The Lancet Global Health*, *4*(9), e609–e616. [https://doi.org/10.1016/S2214-109X\(16\)30143-7](https://doi.org/10.1016/S2214-109X(16)30143-7)
- Porter, N. J., & Christianson, D. W. (2019). Structure, mechanism, and inhibition of the zinc-dependent histone deacetylases. *Current Opinion in Structural Biology*, *59*, 9–18. <https://doi.org/10.1016/j.sbi.2019.01.004>
- Porter, N. J., Mahendran, A., Breslow, R., & Christianson, D. W. (2017). Unusual zinc-binding mode of HDAC6-selective hydroxamate inhibitors. *Proceedings of the*

National Academy of Sciences of the United States of America, 114(51), 13459–13464. <https://doi.org/10.1073/pnas.1718823114>

Porwal, M., Road, D., & Pradesh, U. (2016). *Patients With Relapsed or Refractory Peripheral T-Cell Lymphoma*. 7(11), 4358–4366. [https://doi.org/10.13040/IJPSR.0975-8232.7\(11\).4358-66](https://doi.org/10.13040/IJPSR.0975-8232.7(11).4358-66)

Prachayasittikul, V., Prathipati, P., Pratiwi, R., Phanus-umporn, C., Malik, A. A., Schaduangrat, N., Seenprachawong, K., Wongchitrat, P., Supokawej, A., Prachayasittikul, V., Wikberg, J. E. S., & Nantasenamat, C. (2017). Exploring the epigenetic drug discovery landscape. *Expert Opinion on Drug Discovery*, 12(4), 345–362. <https://doi.org/10.1080/17460441.2017.1295954>

Pulya, S., Amin, S. A., Adhikari, N., Biswas, S., Jha, T., & Ghosh, B. (2020). HDAC6 as privileged target in drug discovery: A perspective. *Pharmacological Research*, 105274. <https://doi.org/10.1016/j.phrs.2020.105274>

Quispe-Tintaya, W. (2017a). HHS Public Access. *Physiology & Behavior*, 176(3), 139–148. <https://doi.org/10.1016/j.sbi.2019.01.004.Structure>

Quispe-Tintaya, W. (2017b). HHS Public Access. *Physiology & Behavior*, 176(3), 139–148.

Rau, K. M., Kang, H. Y., Cha, T. L., Miller, S. A., & Hung, M. C. (2005). The mechanisms and managements of hormone-therapy resistance in breast and prostate cancers. *Endocrine-Related Cancer*, 12(3), 511–532. <https://doi.org/10.1677/erc.1.01026>

Ridinger, J., Koeneke, E., Kolbinger, F. R., Koerholz, K., Mahboobi, S., Hellweg, L., Gunkel, N., Miller, A. K., Peterziel, H., Schmezer, P., Hamacher-Brady, A., Witt, O., & Oehme, I. (2018). Dual role of HDAC10 in lysosomal exocytosis and DNA repair promotes neuroblastoma chemoresistance. *Scientific Reports*, 8(1), 1–17. <https://doi.org/10.1038/s41598-018-28265-5>

- Sakamoto, K. M., & Aldana-Masangkay, G. I. (2011). The role of HDAC6 in cancer. *Journal of Biomedicine and Biotechnology*, 2011. <https://doi.org/10.1155/2011/875824>
- Salmaso, V., & Moro, S. (2018). Bridging molecular docking to molecular dynamics in exploring ligand-protein recognition process: An overview. *Frontiers in Pharmacology*, 9(AUG), 1–16. <https://doi.org/10.3389/fphar.2018.00923>
- Saraswati, A. P., Relitti, N., Brindisi, M., Osko, J. D., Chemi, G., Federico, S., Grillo, A., Brogi, S., McCabe, N. H., Turkington, R. C., Ibrahim, O., O'Sullivan, J., Lamponi, S., Ghanim, M., Kelly, V. P., Zisterer, D., Amet, R., Hannon Barroeta, P., Vanni, F., ... Campiani, G. (2020). Spiroindoline-Capped Selective HDAC6 Inhibitors: Design, Synthesis, Structural Analysis, and Biological Evaluation. *ACS Medicinal Chemistry Letters*, 8. <https://doi.org/10.1021/acsmchemlett.0c00395>
- Schirmacher, V. (2019). From chemotherapy to biological therapy: A review of novel concepts to reduce the side effects of systemic cancer treatment (Review). *International Journal of Oncology*, 54(2), 407–419. <https://doi.org/10.3892/ijo.2018.4661>
- Seto, E., & Yoshida, M. (2014). Erasers of histone acetylation: The histone deacetylase enzymes. *Cold Spring Harbor Perspectives in Biology*, 6(4). <https://doi.org/10.1101/cshperspect.a018713>
- Shukla, S., & Tekwani, B. L. (2020). Histone Deacetylases Inhibitors in Neurodegenerative Diseases, Neuroprotection and Neuronal Differentiation. *Frontiers in Pharmacology*, 11(April), 1–20. <https://doi.org/10.3389/fphar.2020.00537>
- Simões-Pires, C., Zwick, V., Nurisso, A., Schenker, E., Carrupt, P. A., & Cuendet, M. (2013). HDAC6 as a target for neurodegenerative diseases: What makes it different from the other HDACs? *Molecular Neurodegeneration*, 8(1). <https://doi.org/10.1186/1750-1326-8-7>

- Singh, A. K., Bishayee, A., & Pandey, A. K. (2018). Targeting histone deacetylases with natural and synthetic agents: An emerging anticancer strategy. In *Nutrients* (Vol. 10, Issue 6). <https://doi.org/10.3390/nu10060731>
- Smith, K. T., & Workman, J. L. (2009). Introducing the acetylome. *Nature Biotechnology*, 27(10), 917–919. <https://doi.org/10.1038/nbt1009-917>
- Sterling, T., & Irwin, J. J. (2015). ZINC 15 - Ligand Discovery for Everyone. *Journal of Chemical Information and Modeling*, 55(11), 2324–2337. <https://doi.org/10.1021/acs.jcim.5b00559>
- Surabhi, B. K. S. (2018). Computer-aided drug design: An overview. *Methods in Molecular Biology*, 1762(5), 1–19. <https://doi.org/10.22270/jddt.v8i5.1894>
- Tang et al., 2005. (2014). Histone deacetylase inhibitor (HDACI) mechanisms of action: emerging insights. *Bone*, 143(3), 323–336. <https://doi.org/10.1016/j.pharmthera.2014.04.004.Histone>
- Thaler, F., & Mercurio, C. (2014). Towards selective inhibition of histone deacetylase isoforms: What has been achieved, where we are and what will be next. *ChemMedChem*, 9(3), 523–536. <https://doi.org/10.1002/cmdc.201300413>
- Thomas, E. A., & D’Mello, S. R. (2018). Complex neuroprotective and neurotoxic effects of histone deacetylases. *Journal of Neurochemistry*, 145(2), 96–110. <https://doi.org/10.1111/jnc.14309>
- Tong, J. J., Liu, J., Bertos, N. R., & Yang, X. J. (2002). Identification of HDAC10, a novel class II human histone deacetylase containing a leucine-rich domain. *Nucleic Acids Research*, 30(5), 1114–1123. <https://doi.org/10.1093/nar/30.5.1114>
- Trott, O., & Olson, A. J. (2010). AutoDock Vina: improving the speed and accuracy of docking with a new scoring function, efficient optimization, and multithreading. *Journal of Computational Chemistry*, 31(2), 455–461.

<https://doi.org/10.1002/jcc.21334>

- Uba, A. I., & Yelekçi, K. (2018). Identification of potential isoform-selective histone deacetylase inhibitors for cancer therapy: A combined approach of structure-based virtual screening, admet prediction and molecular dynamics simulation assay. *Journal of Biomolecular Structure and Dynamics*, 36(12), 3231–3245. <https://doi.org/10.1080/07391102.2017.1384402>
- Uba, A. I., & Yelekçi, K. (2020). Crystallographic structure versus homology model: a case study of molecular dynamics simulation of human and zebrafish histone deacetylase 10. *Journal of Biomolecular Structure and Dynamics*, 38(15), 4397–4406. <https://doi.org/10.1080/07391102.2019.1691658>
- Villagra, A. and S. E. (2016). *Histone Deacetylase Enzymes of Epigenetics , Part A Current Challenges in Personalized Cancer Medicine Recent Advances in Cancer Therapeutics Clinical Applications of Histone Deacetylase Inhibitors.*
- Wang, D. (2009). *Computational studies on the Histone Deacetylases and the Design of Selective Histone Deacetylase Inhibitors.* 9(3), 241–256.
- Wang, X., Song, K., Li, L., & Chen, L. (2018). Structure-Based Drug Design Strategies and Challenges. *Current Topics in Medicinal Chemistry*, 18(12), 998–1006. <https://doi.org/10.2174/1568026618666180813152921>
- Yadav, R., Mishra, P., & Yadav, D. (2019). Histone deacetylase inhibitors: A prospect in drug discovery. *Turkish Journal of Pharmaceutical Sciences*, 16(1), 101–114. <https://doi.org/10.4274/tjps.75047>
- Yang, F., Zhao, N., Ge, D., & Chen, Y. (2019). Next-generation of selective histone deacetylase inhibitors. *RSC Advances*, 9(34), 19571–19583. <https://doi.org/10.1039/c9ra02985k>
- Yang, P. (2013). HDAC6: Physiological function and its selective inhibitors for cancer

treatment. *Drug Discoveries & Therapeutics*, 7(6), 233–242.
<https://doi.org/10.5582/ddt.2013.v7.6.233>

Zhang, L., Zhang, J., Jiang, Q., Zhang, L., & Song, W. (2018). Zinc binding groups for histone deacetylase inhibitors. *Journal of Enzyme Inhibition and Medicinal Chemistry*, 33(1), 714–721. <https://doi.org/10.1080/14756366.2017.1417274>

Zhang, X., Yang, J., Wang, H., Guo, R., Yin, Y., Zhang, D., Zhang, Q., Wang, H., Zhou, Z., Chen, L., Zhou, J., & Liu, L. (2017). Overexpression of Hdac6 extends reproductive lifespan in mice. *Protein and Cell*, 8(5), 360–364.
<https://doi.org/10.1007/s13238-017-0375-9>

Zilberman, Y., Ballestrem, C., Carramusa, L., Mazitschek, R., Khochbin, S., & Bershadsky, A. (2009). Regulation of microtubule dynamics by inhibition of the tubulin deacetylase HDAC6. *Journal of Cell Science*, 122(19), 3531–3541.
<https://doi.org/10.1242/jcs.046813>

CURRICULUM VITAE

Personal Information

Name Surname : Naz Mina Mert

Education

Undergraduate Education : Bachelor of Molecular Biology, Genetics and Bioengineering, Sabanci University, Turkey, September 2010 – June 2016.

Graduate Education : Master of Science degree in Computational Biology and Bioinformatics, Kadir Has University, Turkey, January 2019 – June 2021.

Foreign Language Skills : Turkish (native), English, German (Intermediate).

Publications:

1. Journal Article: Journal of Molecular Catalysis B: Enzymatic, Vol.133, 2016 (SCI) “Mağaralardan İzole Edilen Gram Negatif Bakterilerde Beta Laktamaz Gen Varlığının PZR Yöntemi İle Araştırılması”. **N.M. Mert**, E. F. Tüfekci, A. Reis. **Poster presentation** at 37rd Turkish Microbiology Congress in Antalya, Turkey, 16-20 November 2016